Sommario

Una delle sfide più importanti della cosmologia riguarda la comprensione della formazione e dell'evoluzione delle strutture. Questi processi fisici ci forniscono informazioni fondamentali sulla natura del nostro Universo. L'analisi della crescita delle perturbazioni di densità e di velocità ci offre un'importante opportunitá per quantificare con più accuratezza la percentuale di materia oscura o comprendere le cause che guidano l'espansione accelerata dell'Universo (il cosiddetto problema dell'Energia Oscura).

A grandi scale la crescita delle fluttuazioni può essere descritta con la teoria delle perturbazioni lineari. I risultati a queste scale sono stati largamente confermati dalla simulazioni numeriche e utilizzati nell'analisi dei dati reali.

Le future osservazioni di galassie ci permetteranno di porre dei vincoli sulla crescita delle perturbazioni con una precisione mai raggiunta prima. Inoltre, informazioni fisiche rilevanti sono presenti a scale più piccole di O(100 Mpc), dove le strutture sono molto piú raggruppate e la teoria delle perturbazioni lineare non è più valida.

Le tecniche più utilizzate per affrontare il problema della formazione delle strutture sono le simulazioni ad N-corpi, anche se mostrano alcuni inconvenienti. Infatti, le simulazioni rendono più difficile la comprensione della fisica rispetto all'approccio analitico e semi-analitico. Inoltre le simulazioni sono limitate dal lungo tempo di calcolo che caratterizza questi studi.

Date le precedenti motivazioni, differenti approcci semi-analitici al problema sono apparsi negli ultimi anni. Essi sono basati sulla possibilità di riformulare la serie di perturbazioni cosmologiche in maniera appropriata. La maggior parte di queste nuove teorie riorganizza l'espansione in serie ridefinendo le grandezze fondamentali dello sviluppo perturbativo. In particolare il *propagatore non lineare* assume un ruolo fondamentale ed è stato calcolato analiticamente con approcci differenti. Esso rappresenta il cross-correlatore tra le perturbazioni finali e iniziali di densità, o di velocità.

L'obiettivo principale di questa tesi è quello di andare oltre le approssimazioni note relative al calcolo del propagatore non lineare facendo uso delle equazioni *esatte* di evoluzione per il propagatore. Abbiamo sviluppato e motivato un metodo di approssimazione analitico che ci ha permesso di includere una più ampia classe di correzioni perturbative che sono state trascurate in altre risommazioni analitiche. In particolare, questo metodo ci permette di considerare le correzioni date da un generico spettro di potenza non lineare. Inoltre abbiamo calcolato il propagatore non lineare considerando due differenti approssimazioni per lo spettro di potenza esatto. Questo problema è stato trattato sia con tecniche analitiche che numeriche. Come risultato generale, abbiamo trovato che gli approcci predenti portano ad un

risultato errato per quanto riguarda il segno delle correzioni del propagatore. Questo chiarisce un problema controverso e suggerisce che sono necessari ulteriori confronti con le simulazioni a N-corpi. Abbiamo trovato che le nuove correzioni sono significative alle scale rilevanti e quindi non possono essere trascurate in uno schema di risommazione che mira a raggiungere un'accuratezza compatibile con le future osservazioni astrofisiche. Inoltre proponiamo un metodo per calcolare lo spettro di potenza tenendo conto di questi risultati.

Abstract

One of the most interesting challenges of present cosmology concerns the understanding of structure formation and evolution. This physical process encodes fundamental information about the nature of our Universe. The analysis of the growth of density and velocity perturbations gives us an excellent opportunity to address basic questions such as the amount of dark matter or the reason for the present accelerated expansion of the Universe (known as the Dark Energy problem).

On large scales the growth of perturbations can be described by linear perturbation theory. The results on these scales have been largely confirmed by numerical simulations and employed in real data analysis.

Future galaxy surveys will be able to give constraints on the perturbations growth with unprecedent precision. Moreover relevant physical information is encoded in scales smaller than O(100 Mpc), where where the structures are more clustered and linear perturbation theory breaks down. Higher orders in the perturbative expansion are not manifestly suppressed by a small expansion parameter, so that their use depends on the scale, redshift, and on features of initial conditions such as the shape of the primordial power spectrum and of the other statistical correlators (bispectrum, trispectrum, etc.).

The main implemented tools to face the problem of nonlinear structure formation are the N-body simulations, even though they show inconveniences. Indeed, simulations give less physical insight with respect to analytical or semi-analytical approach. Furthermore simulations are limited by the long computational time involved.

Given the motivations above, different semi-analytical approaches to the problem have appeared in the last years. These are based on the possibility of recasting the cosmological perturbation series in an appropriate way. Most of these new theories reorganize the series expansion by redefining the building blocks of the perturbative expansion. In particular the *nonlinear propagator* gains a fundamental role and it has been analytically computed by means of different approximations. It represents the cross-correlation between the final density, or velocity, perturbations and the initial ones.

The main purpose of this thesis is to go beyond the known nonlinear propagator approximations leveraging on the *exact* evolution equations for the propagator which we derive. We analytically develop a well motivated approximation scheme by including a larger class of perturbative corrections which are neglected in other analytic re-summations. More specifically, this method allows us to take into account also the corrections given by a generic non linear matter power spectrum. Furthermore we compute the non linear propagator considering two different approximations for the full nonlinear power spectra. This problem has been addressed both with analytic and numerical techniques. As a general result we find that the precedent

approaches lead to a wrong prediction on the sign of the propagator corrections. This clarifies a controversial problem and points out that further comparisons with N-body simulations are necessary. We find that the new corrections are significant at the relevant scales and therefore cannot be neglected in a re-summation scheme aiming at an accuracy compatible with future generation galaxy surveys. Furthermore we propose a method to implement the power spectrum computation taking into account this results.

Contents

Chapter 1

Gravitational instabilities: Eulerian dynamics

One of the main goals of Cosmology is the understanding of the process of formation of large-scale structures. It is widely accepted that the baryonic mass of the universe is just a small fraction of the total mass, while the main part of it is a form of non relativistic and non collisional matter called *cold dark matter* (CDM). When, after the radiation era, CDM becomes the dominant form of energy in the universe, the primordial density fluctuations originated during inflation grow by gravitational interaction. Cosmic Microwave Background (CMB) measurements [1] show that primordial fluctuations are very small ($\delta\rho/\rho \simeq \mathcal{O}(10^{-5})$), therefore perturbation theory is a very effective tool in this context. However, gravitational instabilities make perturbations larger and larger as the redshift and the scale decrease, hence the perturbation theory starts to break down in the regimes relevant to the description of the large scale structure of the universe in recent epochs.

The development of the gravitational instabilities can be described by means of the Vlasov equation. While the solution of this non-local partial derivative differential equation of a distribution function depending on seven variables is a prohibitive task, a more manageable approach consists in taking the first few moments of the Vlasov equation, and to restrict to a few equations describing a Newtonian fluid in a Eulerian frame(for a review see [2]). In this chapter we will explain the basis of

the cosmological perturbation theory (PT) applied to the Eulerian equations.

1.1 Dark matter evolution

A widely accepted method to study the dynamics of the dark matter fluctuations at large scale is to consider the dark matter density field $\rho(\mathbf{r}, t)$, its velocity fields $\mathbf{v}(\mathbf{r}, t)$ and the Newtonian potential ϕ. We assume that the matter interact only gravitationally (pressureless fluid) and that the velocities are not relativistic. As usual we neglect the stress-tensor at large scale, thus working in the so-called "single stream approximation" where there are no deviations from a coherent fluid flow. We consider also scales much smaller than the Hubble radius. In this context, General Relativity studies allow us to justify a Newtonian treatment, indeed the differences between the two approaches are negligible.

The Vlasov equation would be the appropriate tool to describe the full dynamics of the fluid, however, taking advantage of single stream approximation and by taking the moments of the Vlasov equation one gets: the continuity equation

$$\frac{\partial \rho}{\partial t} + \nabla_{\mathbf{r}} \cdot (\rho\, \mathbf{v}) = 0\,, \tag{1.1}$$

describing the conservation of the mass, the Euler equation

$$\frac{\partial \mathbf{v}}{\partial t} + (\mathbf{v} \cdot \nabla_{\mathbf{r}})\mathbf{v} = -\nabla\phi\,, \tag{1.2}$$

describing the conservation of the momentum, and the Poisson equation,

$$\nabla^2_{\mathbf{r}}\phi = 4\pi G\rho\,. \tag{1.3}$$

In order to consider the departures from the homogeneous Hubble flow, we will write the equations in comoving coordinate $\mathbf{r} = a(\tau)\mathbf{x}$, where the conformal time τ is defined as $\mathrm{d}t = a(\tau)\mathrm{d}\tau$ (t: cosmic time) and $a(\tau)$ is the cosmological scale factor. The previous equations are valid in a homogeneous and isotropic background

universe, witch evolves according to Friedmann equations:

$$\begin{aligned}
&\frac{\partial \mathcal{H}(\tau)}{\partial \tau} = -\frac{\Omega_m(\tau)}{2}\mathcal{H}^2(\tau) + \frac{\Lambda}{3}a^2(\tau) \equiv \left(\Omega_\Lambda(\tau) - \frac{\Omega_m(\tau)}{2}\right)\mathcal{H}^2(\tau)\,, \\
&(\Omega_{tot}(\tau) - 1)\mathcal{H}^2(\tau) = k\,,
\end{aligned} \tag{1.4}$$

where $\mathcal{H} \equiv \mathrm{d}\ln a/\mathrm{d}t = \mathcal{H}a$ is the conformal expansion rate, H is the Hubble constant, Ω_m is the ratio of matter density to critical density, Λ is the cosmological constant and $k = -1, 0, 1$ for $\Omega_{tot} < 1$, $\Omega_{tot} = 1$ and $\Omega_{tot} > 1$ respectively ($\Omega_{tot} \equiv \Omega_m + \Omega_\Lambda$). Note that Ω_m and Ω_Λ are time dependent.

We define the dark matter density contrast $\delta(\mathbf{x}, \tau)$

$$\rho(\mathbf{x}, \tau) \equiv \bar{\rho}(\tau)[1 + \delta(\mathbf{x}, \tau)] \tag{1.5}$$

and the peculiar velocity

$$\mathbf{v}(\mathbf{x}, \tau) \equiv \mathcal{H}(\tau)\mathbf{x} + \mathbf{v}_p(\mathbf{x}, \tau) \tag{1.6}$$

of the fluid, where the first term expresses the contribution from the Hubble flow and the second is known as peculiar velocity of the fluid $\mathbf{v}_p$. From the continuity, Euler and Poisson equations it is possible to find out the equations describing the dynamics of the density contrast and peculiar velocity:

$$\begin{aligned}
&\frac{\partial \delta(\mathbf{x}, \tau)}{\partial \tau} + \nabla \cdot [(1 + \delta(\mathbf{x}, \tau))\mathbf{v}_p(\mathbf{x}, \tau)] = 0\,, \\
&\frac{\partial \mathbf{v}_p(\mathbf{x}, \tau)}{\mathrm{d}\tau} + \mathcal{H}(\tau)\mathbf{v}_p(\mathbf{x}, \tau) + (\mathbf{v}_p(\mathbf{x}, \tau) \cdot \nabla)\mathbf{v}_p(\mathbf{x}, \tau) = -\nabla\Phi(\mathbf{x}, \tau)\,, \\
&\nabla^2\Phi(\mathbf{x}, \tau) = \frac{3}{2}\mathcal{H}^2(\tau)\Omega_m(\tau)\delta(\mathbf{x}, \tau)\,,
\end{aligned} \tag{1.7}$$

where Φ is sourced only by density fluctuations and it is defined by

$$\Phi(\mathbf{x}, \tau) = \frac{1}{2}\frac{\partial \mathcal{H}}{\partial \tau}x^2 + \phi(\mathbf{x}, \tau)\,. \tag{1.8}$$

1.2 Linear Perturbation Theory

At large scales the universe is expected to be smooth and thus the perturbation fields can be assumed to be small compared to $\bar{\rho}$ and to the Hubble flow. Hence we can linearize the eq. (1.7) to obtain:

$$\begin{aligned} &\frac{\partial \delta(\mathbf{x},\tau)}{\partial \tau} + \theta(\mathbf{x},\tau) = 0\,, \\ &\frac{\partial \mathbf{v}_p(\mathbf{x},\tau)}{\partial \tau} + \mathcal{H}(\tau)\mathbf{v}_p(\mathbf{x},\tau) = -\nabla\Phi(\mathbf{x},\tau)\,, \end{aligned} \tag{1.9}$$

where $\theta(\mathbf{x},\tau) \equiv \nabla \cdot \mathbf{v}_p(\mathbf{x},\tau)$ is the divergence of the velocity field. As any vector field, the velocity is completely described by its divergence and its vorticity $\mathbf{w}(\mathbf{x},\tau) \equiv \nabla \times \mathbf{v}_p(\mathbf{x},\tau)$. Thus from the second eq. of (1.9) we get:

$$\frac{\partial \theta(\mathbf{x},\tau)}{\partial \tau} + \mathcal{H}\theta(\mathbf{x},\tau) + \frac{3}{2}\Omega_m(\tau)\mathcal{H}^2(\tau)\delta(\mathbf{x},\tau) = 0\,, \tag{1.10}$$

$$\frac{\mathbf{w}(\mathbf{x},\tau)}{\partial \tau} + \mathcal{H}(\tau)\mathbf{w}(\mathbf{x},\tau) = 0. \tag{1.11}$$

Equation (1.11) gives $\mathbf{w}(\tau) \propto a^{-1}$: in the linear regime any vorticity decays away due to the expansion of the universe. Hence we can neglect the vorticity and study only the equations for the velocity divergence and density contrast. In order to do that we write $\delta(\mathbf{x},\tau) = D_1(\tau)\delta(\mathbf{x},0)$ where $D_1(\tau)$ is called the linear growth factor. We take the time derivative of eq. (1.10):

$$\frac{\mathrm{d}^2 D_1(\tau)}{\mathrm{d}\tau^2} + \mathcal{H}(\tau)\frac{\mathrm{d}D_1(\tau)}{\mathrm{d}\tau} = \frac{3}{2}\Omega_m(\tau)\mathcal{H}^2(\tau)D_1(\tau)\,. \tag{1.12}$$

A generic solution for the matter perturbation is

$$\delta(\mathbf{x},\tau) = D_1^+(\tau)A(\mathbf{x}) + D_1^-(\tau)B(\mathbf{x})\,, \tag{1.13}$$

where $A(\mathbf{x})$ and $B(\mathbf{x})$ are two arbitrarily functions of position describing the initial density field configuration, D_1^+ is the fastest growing mode and D_1^- is the slowest

one. The velocity divergence is given by

$$\theta(\mathbf{x},\tau) = -\mathcal{H}(\tau)[f(\Omega_m,\Omega_\Lambda)A(\mathbf{x}) + g(\Omega_m,\Omega_\Lambda)B(\mathbf{x})]\,,$$
$$f(\Omega_m,\Omega_\Lambda) \equiv \frac{\mathrm{d}\ln D_1^+}{\mathrm{d}\ln a} = \frac{1}{\mathcal{H}}\frac{\mathrm{d}\ln D_1^+}{\mathrm{d}\tau}\,, \qquad g(\Omega_m,\Omega_\Lambda) \equiv \frac{1}{\mathcal{H}}\frac{\mathrm{d}\ln D_1^-}{\mathrm{d}\tau}\,. \quad (1.14)$$

The linear growth factor depends on cosmology through the Friedmann equations. In the case of matter dominated universe with $\Omega_m = 1$ and $\Omega_\Lambda = 0$ we have

$$D_1^+(\tau) = a\,, \qquad D_1^-(\tau) = a^{-3/2}\,. \quad (1.15)$$

In a ΛCDM cosmology the linear growth factor admit the integral representation [3]

$$D_1^+(\tau) = a^3 H(a)\frac{5\Omega_m}{2}\int_0^a \frac{\mathrm{d}a'}{a'^3 H^3(a')}\,. \quad (1.16)$$

1.3 Non-linear Perturbation Theory

In this section we want to study the perturbations going beyond the linear approximation. In general it is not an easy task but it is important to understand the physics in the mildly nonlinear regime (between large and small scales). In order to do that we must address the problem of the vorticity degree of freedom. From eq. (1.7) we can write the vorticity equation of motion (pressureless perfect fluid)

$$\frac{\partial \mathbf{w}(\mathbf{x},\tau)}{\partial\tau} + \mathcal{H}(\tau)\mathbf{w}(\mathbf{x},\tau) - \nabla\times[\mathbf{v}_p(\mathbf{x},\tau)\times\mathbf{w}(\mathbf{x},\tau)] = 0\,. \quad (1.17)$$

Thus if the primordial vorticity vanishes it remains zero at all times. If initial vorticity is not zero it can be amplified nonlinearly throw the third term of Eq. (1.17). So if we assume that the stress tensor and the initial vorticity vanish then we can consider only the velocity divergence and neglect the vorticity. This is true at enough large scales, indeed at small scales we have the breakdown of the PT due to the multi-streaming behavior of the fluid.

The assumption of the Perturbation Theory is that it is possible to expand the density and the velocity fields about the linear solutions, effectively treating the

variance of the linear fluctuations as a small parameter. Linear solutions correspond to simple (time dependent) scaling of the initial density field; thus we can write

$$\delta(\mathbf{x},\tau) = \sum_{n=1}^{\infty} \delta^n(\mathbf{x},\tau)\,, \qquad \theta(\mathbf{x},\tau) = \sum_{n=1}^{\infty} \theta^n(\mathbf{x},\tau)\,, \tag{1.18}$$

where δ^1 and θ^1 are linear in the initial density field, δ^2 and θ^2 are quadratic in the initial density field, and so on.

1.3.1 Going to Fourier space

It is natural to study the non linearities in Fourier space. One prefers to work in this space because in the linear regime (at large scale) each Fourier mode evolve independently conserving the primordial statistics, while nonlinear correction will induce coupling of different k-modes (at smaller scales). The Fourier transform is defined in the subsequent way

$$\tilde{A}(\mathbf{k},\tau) = \int \frac{\mathrm{d}^3\mathbf{x}}{(2\pi)^3} \exp(-\mathrm{i}\mathbf{k}\cdot\mathbf{x}) A(\mathbf{x},\tau). \tag{1.19}$$

Fourier transforming the equations of motion (neglecting the vorticity) we get[1]

$$\begin{aligned} &\frac{\partial\delta(\mathbf{k},\tau)}{\partial\tau} + \tilde{\theta}(\mathbf{k},\tau) = -\int \mathrm{d}^3\mathbf{q}\,\mathrm{d}^3\mathbf{p}\,\delta_D(\mathbf{k}-\mathbf{q}-\mathbf{q})\alpha(\mathbf{q},\mathbf{p})\tilde{\theta}(\mathbf{q},\tau)\tilde{\delta}(\mathbf{p},\tau)\,, \\ &\frac{\partial\theta(\mathbf{k},\tau)}{\partial\tau} + \mathcal{H}(\tau)\tilde{\theta}(\mathbf{k},\tau) + \frac{3}{2}\Omega_m\mathcal{H}^2(\tau)\tilde{\delta}(\mathbf{k},\tau) = -\int \mathrm{d}^3\mathbf{q}\,\mathrm{d}^3\mathbf{p}\,\delta_D(\mathbf{k}-\mathbf{q}-\mathbf{q}) \\ &\qquad\qquad \times\beta(\mathbf{q},\mathbf{p})\tilde{\theta}(\mathbf{q},\mathbf{p})\tilde{\theta}(\mathbf{q},\tau)\tilde{\theta}(\mathbf{q},\tau) \end{aligned} \tag{1.20}$$

The non linear interactions are written in the RHS of the equations and are expressed by the α and β functions that give us the mode coupling:

$$\alpha(\mathbf{q},\mathbf{p}) \equiv \frac{(\mathbf{q}+\mathbf{p})\cdot\mathbf{q}}{q^2} \qquad\qquad \beta(\mathbf{q},\mathbf{p}) \equiv \frac{(\mathbf{q}+\mathbf{p})^2(\mathbf{q}\cdot\mathbf{p})}{2q^2p^2}\,. \tag{1.21}$$

[1] In the following, for simplicity, we omit the tilde symbol.

Setting $\alpha = \beta = 0$ we achieve the linear perturbation theory. Therefore the equations of motion can be easily solved and in the Einstein-de Sitter cosmology they read

$$\begin{aligned} &\delta(\mathbf{k},\tau) = \delta(\mathbf{k},0)a^m(\tau), \\ &\theta(\mathbf{k},\tau) = -\mathcal{H}(\tau)\, m\, \delta(\mathbf{k},\tau) \qquad\qquad (m = 1, -3/2)\,, \end{aligned} \tag{1.22}$$

where for $(m = 1)$ we have the growing mode and for $(m = -3/2)$ we have the decaying mode.

Einsten-de Sitter cosmology

If the universe is matter dominated, $\Omega_m = 1$ and $\Omega_\Lambda = 0$, then we can formally solve the non linear equations of motion with the following perturbative expansion [4, 5]

$$\delta(\mathbf{k},\tau) = \sum_{n=1}^{\infty} a^n(\tau)\delta_n(\mathbf{k})\,, \qquad\qquad \theta(\mathbf{k},\tau) = -\mathcal{H}(\tau)\sum_{n=1}^{\infty} a^n(\tau)\theta_n(\mathbf{k})\,, \tag{1.23}$$

where we are taking into account only the fastest growing mode. For $n = 1$ we retrieve the linear growing mode $\delta^{(1)} = a(\tau)\delta_1(\mathbf{k})$, that completely characterize the linear perturbations since $\theta_1(\mathbf{k}) = \delta_1(\mathbf{k})$ from the continuity equation. The previous expansions allow one to determine $\delta_n(\mathbf{k})$ and $\theta_n(\mathbf{k})$ in terms of linear solutions.

$$\begin{aligned} \delta_n(\mathbf{k}) &= \int \mathrm{d}^3\mathbf{q}_1 \ldots \int \mathrm{d}^3\mathbf{q}_n \delta_D(\mathbf{k} - \mathbf{q}_{1\ldots n}) F_n(\mathbf{q}_1 \ldots \mathbf{q}_n)\delta_0(\mathbf{q}_1)\ldots\delta_0(\mathbf{q}_n)\,, \\ \theta_n(\mathbf{k}) &= \int \mathrm{d}^3\mathbf{q}_1 \ldots \int \mathrm{d}^3\mathbf{q}_n \delta_D(\mathbf{k} - \mathbf{q}_{1\ldots n}) G_n(\mathbf{q}_1 \ldots \mathbf{q}_n)\delta_0(\mathbf{q}_1)\ldots\delta_0(\mathbf{q}_n), \end{aligned} \tag{1.24}$$

where F_n and G_n are homogeneous functions of the wave vectors $\{\mathbf{q}_1, \ldots, \mathbf{q}_n\}$ with degree zero. They are constructed from the fundamental mode coupling functions according to the recursions relations [4]

$$F_n(\mathbf{q}_1, \ldots, \mathbf{q}_n) = \sum_{m=1}^{n-1} \frac{G_m(\mathbf{q}_1, \ldots, \mathbf{q}_m)}{(2n+3)(n-1)} \left[(2n+1)\alpha(\mathbf{k}_1, \mathbf{k}_2) F_{n-m}(\mathbf{q}_{m+1}, \ldots, \mathbf{q}_n)\right.$$

$$
\begin{aligned}
&+2\beta(\mathbf{k}_1,\mathbf{k}_2)G_{n-m}(\mathbf{q}_{m+1,\ldots,\mathbf{q}_n})]\ ,\\
G_n(\mathbf{q}_1,\ldots,\mathbf{q}_n) &= \sum_{m=1}^{n-1}\frac{G_m(\mathbf{q}_1,\ldots,\mathbf{q}_m)}{(2n+3)(n-1)}\,[3\alpha(\mathbf{k}_1,\mathbf{k}_2)F_{n-m}(\mathbf{q}_{m+1},\ldots,\mathbf{q}_n)\\
&+2n\beta(\mathbf{k}_1,\mathbf{k}_2)G_{n-m}(\mathbf{q}_{m+1},\ldots,\mathbf{q}_n)]\ ,
\end{aligned}
\tag{1.25}
$$

where $\mathbf{k}_1 \equiv \mathbf{q}_1 + \cdots + \mathbf{q}_m$, $\mathbf{k}_2 \equiv \mathbf{q}_{m+1} + \cdots + \mathbf{q}_n$, $\mathbf{k} \equiv \mathbf{k}_1 + \mathbf{k}_2$, and $F_1 = G_1 \equiv 1$ and $\delta_1(\mathbf{k}) = \theta_1(\mathbf{k}) = \delta_0(\mathbf{k})$ are the initial perturbations.

Arbitrary cosmology: approximate solutions

With a simple approximation it is possible to get a separable solution also in a general ΛCDM cosmology [6]. In this way we have that the information about the cosmological parameters Ω_m and Ω_Λ are encoded in the linear grow factor, $D_1(\tau)$.

In linear PT, the growing mode solution to the equations of motion reads

$$
\begin{aligned}
\delta(\mathbf{k},\tau) &= D_1(\tau)\delta_1(\mathbf{k})\,,\\
\theta(\mathbf{k},\tau) &= -\mathcal{H}(\tau)f(\Omega_m,\Omega_\Lambda)D_1(\tau)\delta_1(\mathbf{k})\,.
\end{aligned}
\tag{1.26}
$$

We look for separable solutions of the form

$$
\begin{aligned}
\delta(\mathbf{k},\tau) &= \sum_{n=1}^{\infty} D_n(\tau)\delta_n(\mathbf{k})\,,\\
\theta(\mathbf{k},\tau) &= \mathcal{H}(\tau)f(\Omega_m,\Omega_\Lambda)\sum_{n=1}^{\infty} E_n(\tau)\theta_n(\mathbf{k})\,.
\end{aligned}
\tag{1.27}
$$

From equations of motion we get

$$
\begin{aligned}
\frac{\mathrm{d}D_n}{\mathrm{d}\log D_1}\delta_n - E_n\theta_n &= \int \mathrm{d}^3\mathbf{q}\,\mathrm{d}^3\mathbf{p}\,\delta_D(\mathbf{k}-\mathbf{q}-\mathbf{p})\alpha(\mathbf{k},\mathbf{q})\\
&\quad\times\sum_{m=1}^{n-1} D_{n-m}E_m\theta_m(\mathbf{q})\delta_{n-m}(\mathbf{p})\,,\\
\frac{\mathrm{d}E_n}{\mathrm{d}\log D_1}\theta_n + \left(\frac{3\Omega_m}{2f^2}-1\right)E_n\theta_n - \frac{3\Omega_m}{2f^2}D_n\delta_n &
\end{aligned}
$$

$$= \int \mathrm{d}^3\mathbf{q}\mathrm{d}^3\mathbf{p}\delta_D(\mathbf{k}-\mathbf{q}-\mathbf{p})\beta(\mathbf{k},\mathbf{q},\mathbf{p})\sum_{m=1}^{n-1} E_{n-m}E_m\theta_m(\mathbf{q})\theta_{n-m}(\mathbf{p})\,. \qquad (1.28)$$

It is easy to check that if $f(\Omega_m,\Omega_\Lambda)=\Omega_m^{1/2}$ then the system of equations become separable, with $D_n=E_n=(D_1)^n$. In fact, the recursion relations then reduce to the standard Einstein-de Sitter case (eq. (1.25)). Hence $\Omega_m/f^2=1$ leads to separability of the PT solutions to any order.

As it was shown in Section 1.2 in the ΛCDM cosmology the growth factor can be written in the integral representation (1.16). In general it is not possible to solve analytically for $D_1(\tau)$ but it can be approximated by [7]

$$D_1(\tau)\approx\left(\frac{5}{2}\right)\frac{a\Omega_m}{\Omega_m^{4/7}-\Omega_\Lambda+(1+\Omega_m/2)(1+\Omega_\Lambda/70)}\,. \qquad (1.29)$$

Taking into account that $\Omega_m+\Omega_\Lambda=1$ we get

$$f(\Omega_m,1-\Omega_m)\approx\Omega_m^{5/9}\,. \qquad (1.30)$$

Therefore $f(\Omega_m,1-\Omega_m)\approx\Omega_m^{1/2}$ is actually a very good approximation.

1.4 The statistical description

The time scale for cosmological evolution is so much longer than that over which we can make observations, that it is non possible to follow evolution of a single system. We observe through our past light cone different objects at different times of their evolution. Hence the evolution of structure must be tested statistically.

For the theoretical cosmology the goal is to make statistical predictions, which in turn depend on the statistical properties of the primordial perturbations leading to the formation of the large-scale structures. The statistical characterization of the fields is generally done using N-point correlation functions, or their Fourier space counterparts. In the case of Gaussian statistics initial conditions, before the matter gravitational clustering, all the information is encoded in the two point correlation function (Wick's theorem). The subsequent time evolution does generate

non-Gaussinities, this happens gradually from small to larger scale. The study of that non-Gaussian features at intermediate scale ($k \approx 20\,h^{-1}$Mpc) is an important goal of the present and future years.

1.4.1 Correlation functions

In order to study the relevant physical quantities one must characterize the statistical properties of the fields of interest (density field, velocity divergence, ...). We will assume that the cosmic fields are statistically homogeneous and isotropic, as predicted by most of the cosmological theories. The validity of this assumption can and should be tested against the observational data.

Power spectrum definition and higher order correlators

The two-point correlation function is defined as the joint ensemble average of the density field at two different location

$$\xi(r) = \langle \delta(\mathbf{x})\delta(\mathbf{x}+\mathbf{r})\rangle\,, \tag{1.31}$$

which depends only on the norm of the $\mathbf{r}$ due to statistical homogeneity and isotropy. The density contrast is usually written in terms of its Fourier components,

$$\delta(\mathbf{x}) = \int \mathrm{d}^3\mathbf{k}\,\delta(\mathbf{k})\exp(\mathrm{i}\mathbf{k}\cdot\mathbf{x})\,. \tag{1.32}$$

In Fourier space, taking into account the homogeneity and isotropy of the space, the correlator reads

$$\langle \delta(\mathbf{k})\delta(\mathbf{k})'\rangle = \delta_D(\mathbf{k}+\mathbf{k}')\int \frac{\mathrm{d}^3\mathbf{r}}{(2\pi)^3}\xi(r)\exp(\mathrm{i}\mathbf{k}\cdot\mathbf{r}) \equiv \delta_D(\mathbf{k}+\mathbf{k}')P(k)\,, \tag{1.33}$$

where $P(k)$ is by definition the density power spectrum. Hence we have

$$\xi(r) = \int \mathrm{d}^3\mathbf{k}\,P(k)\exp(\mathrm{i}\mathbf{k}\cdot\mathbf{r})\,. \tag{1.34}$$

The power spectrum gains a fundamental role due to the Wick's theorem. In the case of Gaussian fields it states that any ensemble average of variables can then be obtained by product of ensemble average of pairs,

$$\begin{aligned}\langle\delta(\mathbf{k}_1)\dots\delta(\mathbf{k}_{2p+1})\rangle &= 0\,,\\ \langle\delta(\mathbf{k}_1)\dots\delta(\mathbf{k}_{2p})\rangle &= \sum_{\text{all pair associations}}\ \prod_{\text{p pairs (i,j)}}\langle\delta(\mathbf{k}_i)\delta(\mathbf{k}_j)\rangle\,. \end{aligned}\tag{1.35}$$

Hence the statistical properties of the random variable $\delta(\mathbf{x})$ are then entirely determined by the shape and normalization of $P_0(k)$.

In general (for any statistics) it is possible to define higher-order correlation functions. They are defined as the connected part (denoted with subscript c) of the joint ensemble average of the density in an arbitrarily number of locations. They can be formally written as

$$\begin{aligned}\xi_N(\mathbf{x}_i,\dots,\mathbf{x}_N) &= \langle\delta(\mathbf{x}_1),\dots,\delta(\mathbf{x}_N)\rangle_c\\ &\equiv \langle\delta(\mathbf{x}_1),\dots,\delta(\mathbf{x}_N)\rangle - \sum_{\mathscr{S}\in\mathscr{P}\{\mathbf{x}_1,\dots,\mathbf{x}_N\}}\ \prod_{s_i\in\mathscr{S}}\xi_{\#s_i}(\mathbf{x}_{s_i(1)},\dots,\mathbf{x}_{s_i(\#s_i)})\,,\end{aligned}\tag{1.36}$$

where the sum is made over the proper partitions (any partition except set itself) of $\{\mathbf{x}_1,\dots,\mathbf{x}_N\}$ and s_i is a subset of $\{\mathbf{x}_1,\dots,\mathbf{x}_N\}$ contained in partition $\mathscr{P}$. If $\langle\delta(\mathbf{x})\rangle = 0$ only partitions that contain no singlets contribute.

In case of a Gaussian field, all connected correlation functions are zero except the two-point one. The connected part has the important property that it vanishes when one or more points are separated by infinite separation. Furthermore it provides a useful way of characterizing the statistical properties since each connected correlation provides independent information.

In Fourier space, cause of the space homogeneity, the connected correlators are always proportional to $\delta_D(\mathbf{k}_1+\cdots,\mathbf{k}_N)$. So we define $P_N(\mathbf{k}_1,\cdots,\mathbf{k}_N)$ with this equation:

$$\langle\delta(\mathbf{k}_1),\dots,\delta(\mathbf{k}_N)\rangle_c \equiv \delta_D(\mathbf{k}_1+\cdots,\mathbf{k}_N)P_N(\mathbf{k}_1,\cdots,\mathbf{k}_N)\,.\tag{1.37}$$

1.5 From dynamics to statistics

We are going to explain how the results about the time evolution of density and velocity fields can be used to understand the evolution of their statistical properties (described by the correlation functions). In this thesis we will assume Gaussian initial conditions. Therefore all the non-Gaussian features will only arise, gradually from small to larger scales, from the non-linear dynamics of the system.

In order to compute the connected correlators one needs to consider the perturbative expansion given by eq. (1.23) and (1.24). Hence it arises an infinite number of contributions. In general a connected p-correlator function computed at the leading order ("tree level") requires from fist to $(p-1)$th order of PT [8]. The next to leading order contributions ("one-loop" corrections) require from first to $(p+1)$th order in PT and so on [9]. In principle one can compute all the correlation functions, however in this thesis we will mainly focus on the power spectrum which is the Fourier transform of the two point correlation function.

1.5.1 Tree-level and one-loop power spectrum

We focus our attention on the time evolution of the power spectrum. Since we are dealing with 2th order correlator to compute the leading order we need only the linear PT. In the linear regime the evolution of the density and velocity field is given by a simple time-dependent scaling of the initial distribution,

$$P_L(k,\tau) = [D_1(\tau)]^2 \, P^0(k) \tag{1.38}$$

where $D_1(\tau)$ is the growing part of the linear growth factor and $P^0(k)$ is the initial power spectrum.

The next to leading corrections are called one-loop corrections to power spectrum [10, 11, 12, 13, 14, 15, 5, 16, 17, 18].[2] Usually the power spectrum up to one-loop

[2]Multi-loop corrections to the power spectrum were considered in [19]

corrections is written in the following way [3]

$$P(k,\tau) = D_1(\tau)^2 P^0(k) + D_1(\tau)^4 \left[P_{13}(k) + P_{22}(k)\right] + \cdots , \tag{1.39}$$

where the first element on the RHS is the linear power spectrum while the second and third represent the one-loop corrections. $P_{13}(k)$ and $P_{22}(k)$ are defined as following

$$\begin{aligned} P_{22}(k) &\equiv \int \left[F_2(\mathbf{k}-\mathbf{q},\mathbf{q})\right]^2 P^0(|\mathbf{k}-\mathbf{q}|) P^0(q) \mathrm{d}^3\mathbf{q}\,, \\ P_{13}(k) &\equiv \int F_3(\mathbf{k},\mathbf{q},-\mathbf{q}) P^0(k) P^0(q) \mathrm{d}^3\mathbf{q}\,. \end{aligned} \tag{1.40}$$

where the F_n are defined by Eq. (1.25). Here P_{ij} denotes the amplitude given by a connected diagram representing the contribution from $\langle \delta_i \delta_j \rangle_c$ to the power spectrum. We have assumed Gaussian initial condition, for which P_{ij} vanish if $i+j$ is odd. Note the different structure of the two contributions, P_{22} is positive defined and describe the effects of mode coupling with wave-vector $\mathbf{k}-\mathbf{q}$ and $\mathbf{q}$. On the other hand P_{13} is negative and does not describe mode-coupling, i.e. it is proportional to $P^0(k)$. This term can be interpreted as the non-linear correction to the standard $a(\tau)$ linear growth as we will explain in the next chapter. When we use perturbation theory we expand the density and velocity field in terms of the linear amplitude of the fluctuations. At large scale it works and is well justified because the perturbations became small. In the weakly non linear regime PT is no more well defined because the expansion parameter becomes of order of unity or larger. Hence one needs to sum up the corrections to all order in perturbation theory. Hence we need some kind of resummation schemes that allows us to resum infinite classes of perturbative corrections. In the next chapter we will address this really interesting topic.

[3] P_0 is usually called P_{11} in this context.

Chapter 2

Eulerian theory: new field theoretical approaches

As has been mentioned in the previous chapter, when we deal with the weakly non linear regime, cosmological perturbation theory starts to beak down. This happens when we approach to small scale and/or small redshift. Hence it becomes more and more important to find out new methods to reorganize the perturbative expansion in order to compute the correlation functions in this regime. Crocce and Scoccimarro [20], taking advantage from knowledge developed in the turbulence theory of the fluids, have proposed a different formulation of the PT where the series of perturbative corrections is no more treated in the ordinary naive way. They introduced in this context standard tools of field theory as Feynman diagrams and the Dyson equation for the correlators. They called this new approach "Renormalized Perturbation Theory" (RPT).

In the following years alternative techniques have been proposed [21, 22, 23, 24, 25, 26, 27, 28, 29, 30, 31, 32, 33, 34, 35, 36]. These new methods are very useful in order to address the computation of the correlators in the weakly non linear regime. In this chapter we will review these new formulations. We will mainly focus on the path integral approach to the problem, however we will shortly introduce the alternative re-summation schemes proposed in the last years.

2.1 Eulerian theory in a compact form

In order to give the new formulation previously mentioned it is worthwhile to rewrite the equations of motion (1.20) in a compact form [20]. First, we introduce the doublet φ_a $(a = 1, 2)$, given by

$$\begin{pmatrix} \varphi_1(\mathbf{k}, \eta) \\ \varphi_2(\mathbf{k}, \eta) \end{pmatrix} \equiv e^{-\eta} \begin{pmatrix} \delta(\mathbf{k}, \eta) \\ -\theta(\mathbf{k}, \eta)/\mathcal{H} \end{pmatrix} , \tag{2.1}$$

where the time variable has been replaced by a new variable that corresponds to the number of e-folds of the scale factor,

$$\eta \equiv \log \frac{a}{a_{in}} ,$$

a_{in} being the scale factor at a conveniently remote epoch, where all the relevant scales are well inside the linear regime. For simplicity we will consider an Einstein-de Sitter universe first. The linear growing mode corresponds to $\varphi_a = \text{const}$.

Then, we define a *vertex* function, $\gamma_{abc}(\mathbf{k}, \mathbf{p}, \mathbf{q})$ $(a, b, c, = 1, 2)$ given by

$$\begin{aligned} \gamma_{112}(\mathbf{k},\, \mathbf{p},\, \mathbf{q}) &= \frac{1}{2}\, \delta_D(\mathbf{k} + \mathbf{p} + \mathbf{q})\, \alpha(\mathbf{p}, \mathbf{q}) , \\ \gamma_{121}(\mathbf{k},\, \mathbf{p},\, \mathbf{q}) &= \frac{1}{2}\, \delta_D(\mathbf{k} + \mathbf{p} + \mathbf{q})\, \alpha(\mathbf{q}, \mathbf{p}) \\ \gamma_{222}(\mathbf{k},\, \mathbf{p},\, \mathbf{q}) &= \delta_D(\mathbf{k} + \mathbf{p} + \mathbf{q})\, \beta(\mathbf{p}, \mathbf{q}) \end{aligned} \tag{2.2}$$

and zero otherwise. It is symmetric:

$$\gamma_{abc}(\mathbf{k},\, \mathbf{p},\, \mathbf{q}) = \gamma_{acb}(\mathbf{k},\, \mathbf{q},\, \mathbf{p}) . \tag{2.3}$$

With these new definitions the two equations (1.20) can be rewritten as

$$(\delta_{ab}\partial_\eta + \Omega_{ab})\, \varphi_b(\mathbf{k}, \eta) = e^{\eta} \gamma_{abc}(\mathbf{k},\, -\mathbf{p},\, -\mathbf{q}) \varphi_b(\mathbf{p}, \eta)\, \varphi_c(\mathbf{q}, \eta) , \tag{2.4}$$

where

$$\mathbf{\Omega} = \begin{pmatrix} 1 & -1 \\ -3/2 & 3/2 \end{pmatrix},$$

and repeated indices/momenta are summed/integrated over.

We define now the linear retarded *propagator* as the operator giving the evolution of the field φ_a from η_b to η_a in the linear approximation (obtained in the $e^\eta\,\gamma_{abc} \to 0$ limit),

$$\varphi_a^0(\mathbf{k},\eta_a) = g_{ab}(\eta_a,\eta_b)\varphi_b^0(\mathbf{k},\eta_b)\,, \qquad (\eta_a > \eta_b) \tag{2.5}$$

where the subscript "0" indicates solutions of the linear equations.

The propagator $g_{ab}(\eta_a,\eta_b)$ can be explicitly computed by solving the equation

$$(\delta_{ab}\partial_{\eta_a} + \Omega_{ab})\, g_{bc}(\eta_a,\eta_b) = \delta_{ac}\,\delta_D(\eta_a-\eta_b)\,, \tag{2.6}$$

with causal boundary conditions, getting,

$$g_{ab}(\eta_a,\eta_b) = \left[\mathbf{B} + \mathbf{A}\, e^{-5/2(\eta_a-\eta_b)}\right]_{ab} \theta(\eta_a-\eta_b)\,, \tag{2.7}$$

with θ the step-function, and

$$\mathbf{B} = \frac{1}{5}\begin{pmatrix} 3 & 2 \\ 3 & 2 \end{pmatrix} \qquad \text{and} \qquad \mathbf{A} = \frac{1}{5}\begin{pmatrix} 2 & -2 \\ -3 & 3 \end{pmatrix}. \tag{2.8}$$

The linear propagator is the Green's function of the linearized version of eq. (2.4) and describes the standard linear evolution of density and velocity fields from any configuration of initial perturbations. The growing ($\varphi_a \propto$ const.) and the decaying ($\varphi_a \propto \exp(-5/2\eta_a)$) modes can be selected by considering initial fields φ_a proportional to

$$u_a = \begin{pmatrix} 1 \\ 1 \end{pmatrix} \qquad \text{and} \qquad v_a = \begin{pmatrix} 1 \\ -3/2 \end{pmatrix}, \tag{2.9}$$

respectively. The formal solution of eq. (2.4) is the following

$$\varphi_a(\mathbf{k},\eta_a) = g_{ab}(\eta_a,0)\varphi_b^0(\mathbf{k},0) + \int_0^{\eta_a} \mathrm{d}s\, e^s g_{ab}(\eta_a,s)\gamma_{bcd}(\mathbf{k},-\mathbf{p},-\mathbf{q})\varphi_c(\mathbf{p},s)\varphi_d(\mathbf{q},s)\,. \tag{2.10}$$

By means of this equation we can write an explicit expression for $\varphi_a(\mathbf{k},\eta_a)$ expanding the solution in this way

$$\varphi_a(\mathbf{k},\eta_a) = \sum_{n=1}^{\infty} \varphi_a^{(n)}(\mathbf{k},\eta_a)\,, \tag{2.11}$$

with (as in (1.24))

$$\varphi_a^{(n)}(\mathbf{k},\eta_a) = \int \mathrm{d}^3\mathbf{k}_1\cdots\mathrm{d}^3\mathbf{k}_n\delta_D(\mathbf{k}-\mathbf{k}_{1\ldots n})\mathcal{F}_a^{(n)}(\mathbf{k}_1,\ldots,\mathbf{k}_n;\eta_a)\delta_0(\mathbf{k}_1)\cdots\delta_0(\mathbf{k}_n) \tag{2.12}$$

where δ_0 is the density contrast initial condition and $\mathbf{k}_{1\ldots n}\equiv\mathbf{k}_1+\cdots\mathbf{k}_n$. Replacing (2.10) and (2.12) in (2.10) we find the recursion relations satisfied by the kernels

$$\mathcal{F}^{(n)}(\mathbf{k}_1,\ldots,\mathbf{k}_n;\eta_a)\delta_D(\mathbf{k}-\mathbf{k}_{1\ldots n}) = \left[\sum_{m=1}^{n-1}\int_0^{\eta_a} \mathrm{d}s\; e^s\; g_{ab}(\eta,s)\gamma_{bcd}(\mathbf{k},\mathbf{k}_{1\ldots m},\mathbf{k}_{m+1\ldots n})\right.$$
$$\left.\times\mathcal{F}_c^{(m)}(\mathbf{k}_1,\ldots,\mathbf{k}_m;s)\mathcal{F}_d^{(n-m)}(\mathbf{k}_{m+1},\ldots,\mathbf{k}_n;s)\right]_{\text{symmetrized}}\,, \tag{2.13}$$

where the RHS has to be symmetrized under interchange of any two wave vectors. For $n=1$, $\mathcal{F}^{(1)}(\eta_a) = g(\eta_a,\eta_b)u_b$. The standard perturbation theory recursion relations are recovered in the limit in which the initial conditions are imposed in the infinite past $\eta_b\to-\infty$. Otherwise these recursion relations give the full time dependence of the PT solutions.

2.2 Path integral representation: dynamics and statistics

What we are interested in are the statistical quantities characterizing the large scale structures of the universe. The statistics of primordial cosmic fields $\varphi(k,0)$ is

determined by the initial probability functional $W[\varphi_a(k,0)]$. To calculate desired quantities, we need to solve the nonlinear evolution equations and obtain the solution as a function of the initial fields. Namely, we need a theoretical tool which consents us to consider both the statistics and the dynamics of the physical system: it is the path-integral.

We will explain the path-integral formulation of cosmological perturbation theory introduced in [24]. The same approach with non Gaussian initial conditions is explained in [37]. This techniques allow us to apply methods familiar in quantum field theory to construct generating functionals for quantities like the power-spectrum, bispectrum, propagator and any other object of interest. The starting point is to write down an action giving the equation of motion (2.4) at its extrema. One can realize that a new, auxiliary, doublet field χ_a has to be introduced to this aim, and that the action is given by

$$\begin{aligned} S &= \int d\eta \left[\chi_a(-\mathbf{k},\eta)\left(\delta_{ab}\partial_\eta + \Omega_{ab}\right)\varphi_b(\mathbf{k},\eta)\right. \\ &\quad \left. - e^{\eta}\gamma_{abc}(-\mathbf{k},-\mathbf{p},-\mathbf{q})\chi_a(\mathbf{k},\eta)\varphi_b(\mathbf{p},\eta)\varphi_c(\mathbf{q},\eta)\right] . \end{aligned} \tag{2.14}$$

The introduction of the auxiliary field χ_a is required by the bilinear term being first order in the 'time' derivative ∂_η. Indeed, a term of the form $\varphi_a\partial_\eta\varphi_a$ would vanish upon integration by parts. Using equation (2.6), the bilinear part in the first line of the action can be also written as

$$S_2 = \int d\eta_a\, d\eta_b\, \chi_a(-\mathbf{k},\eta_a) g^{-1}_{ab}(\eta_a,\eta_b)\varphi_b(\mathbf{k},\eta_b)\,. \tag{2.15}$$

To find out the equations of motion for φ we need to vary the action (2.14) with respect to χ_a, it gives precisely eq. (2.4), while varying with respect to φ_a gives an equation solved by $\chi_a = 0$. The χ_a field allows us to write the action above, moreover more physically, it is related to the statistics of initial conditions, as we will see below. In the following, in order to simplify the notation, we will write the momentum dependence just when it is not trivial.

Being the system classical, the probability of having a field $\varphi_a(\eta_f)$ at time η_f, starting with an initial condition $\varphi_a(0)$ is different than zero only when the final

point lies on the classical path. This drives us toward a (functional) delta function:

$$P[\varphi_a(\eta_f);\, \varphi_a(0)] = \delta\left[\varphi_a(\eta_f) - \bar{\varphi}_a[\eta_f;\, \varphi_a(0)]\right] , \tag{2.16}$$

where $\bar{\varphi}_a[\eta_f;\, \varphi_a(0)]$ is the solution to the equation of motion (2.4) with initial condition $\varphi_a(0)$. Now we want to rewrite the previous result as a path integral over all the possible trajectories in phase space $\varphi_a(\eta)$, where the only path which contributes is the classical one. This can be realized via a suitable functional Dirac delta, i.e.:

$$P[\varphi_a(\eta_f);\, \varphi_a(0)] = \int \mathcal{D}''\varphi_a\, \delta\left[\varphi_a(\eta) - \bar{\varphi}_a[\eta;\, \varphi_a(0)]\right] , \tag{2.17}$$

where the double prime on the measure of φ_a means that it is kept fixed at the two extrema $\eta = 0$ and $\eta = \eta_f$. In the action (2.14) the χ_a field enters linearly, thus the delta function can be written in the subsequent way:

$$P[\varphi_a(\eta_f);\, \varphi_a(0)] = \mathcal{N} \int \mathcal{D}''\varphi_a\, \mathcal{D}\chi_b\, e^{iS} . \tag{2.18}$$

In the following, the field-independent normalization $\mathcal{N}$ will be set to unity.

We then define a generating functional by following the standard procedure, *i.e.* by introducing sources for φ_a and χ_b and by summing over all the possible final states, *i.e.*,

$$\begin{aligned} Z[J_a,\, K_b;\, \varphi_a(0)] \equiv & \int \mathcal{D}\varphi_a(\eta_f) \int \mathcal{D}''\varphi_a \mathcal{D}\,\chi_b \,\times \\ & \exp\left\{ i \int_0^{\eta_f} d\eta\, \chi_a(\delta_{ab}\partial_\eta + \Omega_{ab})\varphi_b - e^\eta\, \gamma_{abc}\chi_a\varphi_b\varphi_c + J_a\varphi_a + K_a\chi_a \right\} . \end{aligned} \tag{2.19}$$

As mentioned above, in order to go from dynamic to statistical description, we average the generating functional taking into account the initial probability functional for the physical fields $\varphi_a(0)$,

$$Z[J_a,\, K_b;\, C's] = \int \mathcal{D}\varphi_a(0)\, W[\varphi_a(0),\, C's]\, Z[J_a,\, K_b;\, \varphi_a(0)] . \tag{2.20}$$

In general, the initial weight can be expressed in terms of the initial n-point corre-

lations as

$$W[\varphi_a(0),\, C's] = \exp\{-\varphi_a(\mathbf{k},\,0)C_a(\mathbf{k}) - \varphi_a(\mathbf{k}_1,\,0)C_{ab}(\mathbf{k}_1,\,\mathbf{k}_2)\varphi_b(\mathbf{k}_2,\,0) + \varphi_a(\mathbf{k}_1,\,0)\varphi_b(\mathbf{k}_2,\,0)\varphi_c(\mathbf{k}_3,\,0)C_{abc}(\mathbf{k}_1,\,\mathbf{k}_2,\,\mathbf{k}_3) + \cdots\}\,. \tag{2.21}$$

In the case of Gaussian initial conditions, the only non-zero initial correlation is the quadratic one, and the weight function reduces to the form

$$W[\varphi_a(0),\, C_{ab}] = \exp\left\{-\frac{1}{2}\varphi_a(\mathbf{k},\,0)C_{ab}(k)\varphi_b(-\mathbf{k},\,0)\right\}, \tag{2.22}$$

where the covariance matrix $C_{ab}(k)$ is determined by the condition that

$$\mathbf{C}^{-1}_{ab}(k) = P^0_{ab}(k) \equiv w_a w_b P^0(k)\,, \tag{2.23}$$

with $P^0(k)$ the initial power-spectrum and the two-component vector w_a is a combination of u_a and v_a in equation (2.9) describing the initial mixture of growing and decaying modes [20]. In the following, we will restrict the initial conditions to the Gaussian case, Eq. (2.22).

In the following we will show how to find out the correlators from the generating functional. As usual we start by studying the linear theory, $e^\eta\gamma_{abc} \to 0$, corresponds to the tree-level of PT. In this limit the path integral can be explicitly computed. Performing first the χ_a integral, and then the $\int \mathcal{D}\varphi_a(\eta_f)\mathcal{D}''\varphi_a$ ones [1], we obtain

$$Z_0[J_a,\, K_b;\, P^0] = \int \mathcal{D}\varphi_a(0)\, \exp\left\{-\frac{1}{2}\varphi_a(\mathbf{k},\,0)\,(\mathbf{P^{0\,-1}})_{ab}(k)\,\varphi_b(-\mathbf{k},\,0) + i\int_0^{\eta_f} d\eta\, J_a\tilde{\varphi}_a\right\}, \tag{2.24}$$

where $\tilde{\varphi}_a$ is the solution of the equation of motion with source K_a,

$$(\delta_{ab}\partial_\eta + \Omega_{ab})\,\tilde{\varphi}_b(\eta) = -K_a(\eta)\,, \tag{2.25}$$

[1] We integrate the functional delta (2.16) following the procedure of [38]

which is given by

$$\tilde{\varphi}_a(\eta_a) = g_{ab}(\eta_a, 0)\varphi_b(0) - \int d\eta_b \, g_{ab}(\eta_a, \eta_b) K_b(\eta_b) \, . \tag{2.26}$$

Substituting (2.26) into (2.24) we get

$$\begin{aligned} &Z_0[J_a,\, K_b;\, P^0] = \\ &\int \mathcal{D}\varphi_a(0) \, \exp\left\{ -\frac{1}{2}\varphi_a(\mathbf{k},\, 0)\, (\mathbf{P^{0-1}})_{ab}(k)\, \varphi_b(-\mathbf{k},\, 0) + i \int_0^{\eta_f} d\eta \, J_a(\mathbf{k}, \eta) g_{ab}(\eta, 0) \varphi_b(-\mathbf{k}, 0) \right\} \\ &\exp\left\{ +i \int_0^{\eta_f} d\eta_a \, d\eta_b \, J_a(\mathbf{k}, \eta_a) g_{ab}(\eta_a, \eta_b) K_b(-\mathbf{k},\, \eta_b) \right\} \, . \end{aligned} \tag{2.27}$$

Keeping in mind the rules of the Gaussian integration, we integrate over the initial conditions $\varphi_a(0)$, leading to the result

$$\begin{aligned} Z_0[J_a,\, K_b;\, P^0] = \exp\Big\{ -\int d\eta_a d\eta_b \Big[&\frac{1}{2} J_a(\mathbf{k}, \eta_a) g_{ac}(\eta_a, 0) P^0_{cd}(k\,; \eta_a,\, \eta_b) g_{bd}(\eta_b, 0) J_b(-\mathbf{k}, \eta_b) \\ &+ i J_a(\mathbf{k}, \eta_a) g_{ab}(\eta_a, \eta_b) K_b(-\mathbf{k},\, \eta_b) \Big] \Big\} \, , \end{aligned} \tag{2.28}$$

The power spectrum evolved at linear order is

$$P^L_{ab}(k\,; \eta_a,\, \eta_b) = g_{ac}(\eta_a, 0) g_{bd}(\eta_b, 0) P^0_{cd}(k) \, , \tag{2.29}$$

thus we have

$$\begin{aligned} Z_0[J_a,\, K_b;\, P^0] = \exp\Big\{ -\int d\eta_a d\eta_b \Big[&\frac{1}{2} J_a(\mathbf{k}, \eta_a) P^L_{ab}(k\,; \eta_a,\, \eta_b) J_b(-\mathbf{k}, \eta_b) \\ &+ i J_a(\mathbf{k}, \eta_a) g_{ab}(\eta_a, \eta_b) K_b(-\mathbf{k},\, \eta_b) \Big] \Big\} \, . \end{aligned} \tag{2.30}$$

Starting from this explicit expression we can recover the results of linear theory. For instance, the power-spectrum,

$$\langle \varphi_a(\mathbf{k}, \eta_a) \varphi_b(\mathbf{k}', \eta_b) \rangle \equiv \delta(\mathbf{k} + \mathbf{k}') P_{ab}(k\,; \eta_a,\, \eta_b) \, , \tag{2.31}$$

is given (at linear order) by the double derivative of Z_0 with respect to the source

J_a,

$$\frac{(-i)^2}{Z_0}\,\frac{\delta^2 Z_0[J_a,\,K_b;\,P^0]}{\delta J_a(\mathbf{k},\eta_a)\,\delta J_b(\mathbf{k}',\eta_b)}\bigg|_{J_a,\,K_b=0} = \delta(\mathbf{k}+\mathbf{k}')P^L_{ab}(k\,;\eta_a,\,\eta_b)\,. \tag{2.32}$$

Using eq. (2.5) in (2.31) we recover the linear behavior of the power-spectrum, eq. (2.29).

The cross-derivative gives the retarded propagator

$$\delta(\mathbf{k}+\mathbf{k}')g_{ab}(\eta_a,\,\eta_b) = \frac{i}{Z_0}\,\frac{\delta^2 Z_0[J_a,\,K_b;\,P^0]}{\delta J_a(\mathbf{k},\eta_a)\delta K_b(\mathbf{k}',\eta_b)}\bigg|_{J_a,\,K_b=0}\,. \tag{2.33}$$

Thus, from a single object, Z_0, we are able to obtain all the quantities of interest, that is, the propagator, the power-spectrum, and all higher order correlation functions, by taking appropriate derivatives of it with respect to the sources. The generalizations of equations (2.32) and (2.33) to the power-spectrum and propagator of the full non-linear theory will be given in eq. (2.41) below.

Before going ahead we explicit the solutions of classical equation of motion for χ_b with source J_a [2]

$$\chi_b(\eta)(-\overleftarrow{\partial_\eta}\,\delta_{bc}+\Omega_{bc}) = -J_a(\eta)\,, \tag{2.34}$$

because we will use it in the following. It can be solved by using the equation

$$g_{ab}(\eta_a,\eta)(-\overleftarrow{\partial_\eta}\,\delta_{bc}+\Omega_{bc}) = \delta_{ac}\delta(\eta_a-\eta) \tag{2.35}$$

as

$$\chi_b(\mathbf{k},\eta) = -\int \mathrm{d}\eta_a J_a(\mathbf{k},\eta_a)g_{ab}(\eta_a,\eta)\,. \tag{2.36}$$

Turning the interaction γ_{abc} on, the generating functional (2.20) can be rewritten as

$$\begin{aligned} &Z[J_a,\,K_b;\,P^0] = \\ &\exp\left\{-i\int d\eta\, e^\eta\,\gamma_{abc}\left(\frac{-i\delta}{\delta K_a}\frac{-i\delta}{\delta J_b}\frac{-i\delta}{\delta J_c}\right)\right\}\,Z_0[J_a,\,K_b;\,P^0]\,, \end{aligned} \tag{2.37}$$

with Z_0 given by Eq. (2.30). Higher orders correlators can be obtained by expanding

[2] It comes out performing integration over φ_a field of the integral expression of Z_0.

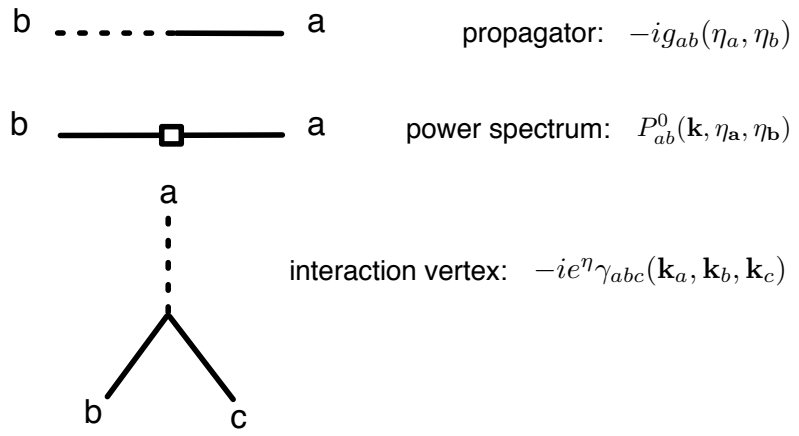

Figure 2.1: The Feynman Rules for cosmological perturbation theory

the exponential in powers of γ_{abc}. From this expression for Z one can read out the Feynman rules. The three fundamental building blocks, *i.e.* the propagator g_{ab}, the linearly evolved power-spectrum P^L_{ab}, and the trilinear vertex $e^\eta\,\gamma_{abc}$, can be represented by the Feynman diagrams in Fig. 2.1. Continuous and dashed lines indicate φ_a and χ_a legs, respectively.

The expression (2.37) is equivalent, at any order in PT, to

$$\begin{aligned} Z[J_a,\, K_b;\, P^0] &= \int \mathcal{D}\varphi_a \mathcal{D}\chi_b \exp\Big\{-\frac{1}{2}\int d\eta_a d\eta_b \chi_a P^0_{ab}\delta(\eta_a)\delta(\eta_b)\chi_b \\ &+ i\int d\eta \left[\chi_a g^{-1}_{ab}\varphi_b - e^\eta\,\gamma_{abc}\chi_a\varphi_b\varphi_c + J_a\varphi_a + K_b\chi_b\right]\Big\}, \end{aligned} \tag{2.38}$$

where we have taken into account equation (2.36) evaluated for $\eta = 0$. Notice that the primordial power-spectrum, P^0_{ab}, is directly coupled to χ fields only, showing the role of these fields in encoding the information on the statistics of the initial conditions. This will be more clear when we will explain the physical meaning of the *full propagator*. In general Eq. (2.38) holds for non linear initial conditions and in the following we will work in this context.

As usual, it is more convenient to discuss connected correlators, which can be

derived from the generating functional,

$$W = -i \log Z \,, \tag{2.39}$$

through which we can define expectation values of the fields φ_a and χ_b in the presence of sources,

$$\bar{\varphi}_a[J_c, K_d] = \frac{\delta W[J_c, K_d]}{\delta J_a} \,, \qquad \bar{\chi}_b[J_c, K_d] = \frac{\delta W[J_c, K_d]}{\delta K_b} \,. \tag{2.40}$$

Full, connected Green functions are given by the second derivatives of W, according to the relations,

$$\begin{aligned}
\left.\frac{\delta^2 W}{\delta J_a \, \delta J_b}\right|_{J_a,\, K_b=0} &\equiv i \, \delta_D(\mathbf{k}+\mathbf{k}') P_{ab} \,, \\
\left.\frac{\delta^2 W}{\delta J_a \, \delta K_b}\right|_{J_a,\, K_b=0} &\equiv -\delta_D(\mathbf{k}+\mathbf{k}') G_{ab}, \\
\left.\frac{\delta^2 W}{\delta K_a \, \delta J_b}\right|_{J_a,\, K_b=0} &\equiv -\delta_D(\mathbf{k}+\mathbf{k}') G_{ba} \,, \\
\left.\frac{\delta^2 W}{\delta K_a \, \delta K_b}\right|_{J_a,\, K_b=0} &\equiv \langle \chi_a(\mathbf{k}, \eta_a) \chi_b(\mathbf{k}', \eta_b) \rangle \,.
\end{aligned} \tag{2.41}$$

Following the standard procedure we define the generator of one-particle irreducible Green functions (1PI), namely the effective action. This will allow us to express the full connected Green functions in terms of full propagators and full 1PI. It is defined as the Legendre transform of W

$$\Gamma[\bar{\varphi}_a, \, \bar{\chi}_b] = W[J_a, K_b] - \int d\eta \, d^3\mathbf{k} \, (J_a \chi \varphi_a + K_b \bar{\chi}_b) \,. \tag{2.42}$$

Derivatives of Γ with respect to $\bar{\varphi}_a$ and $\bar{\chi}_a$ give rise to 1PI n-point functions. There is a particular class of 1PI functions that vanishes at every loop order: the functions with all the external legs of type φ_a. Indeed the contributions to a 1PI n-point function at l-loop order contain the product of $m = n + 2(l-1)$ basic vertices,

$$\chi\varphi\varphi(\eta_1) \; \chi\varphi\varphi(\eta_2) \cdots \chi\varphi\varphi(\eta_m) \,. \tag{2.43}$$

In order to have a 1PI function, at most one of the fields in each vertex can be an 'external' field, that is, it is not joined to fields in the other vertices via a propagator ($\chi - \varphi$ connection) or a power-spectrum ($\varphi - \varphi$ connection). Moreover, in order to have a n-point function like Eq. (2.44), with no χ-field as an external field, every χ has to be contracted with a φ field belonging to a different vertex, via a retarded propagator. One can then realize that any diagram with all the external legs of type φ_a contains at least one closed loop of propagators, which vanish due to the presence of the causal θ-functions in η. Therefore one can write the subsequent identity

$$\left.\frac{\delta^n \Gamma[\bar{\varphi}_a, \bar{\chi}_b]}{\delta\bar{\varphi}_{a_1}(\eta_1)\cdots\delta\bar{\varphi}_{a_n}(\eta_n)}\right|_{\bar{\varphi}_a=\bar{\chi}_b=0} = 0 \qquad \text{for any } n\,. \tag{2.44}$$

The two-point 1PI are given by second derivatives of the effective action, in doing this we define

$$\begin{aligned}
\left.\frac{\delta^2\Gamma[\bar{\varphi}_a, \bar{\chi}_b]}{\delta\bar{\varphi}_a\delta\bar{\varphi}_b}\right|_{\bar{\varphi}_a,\bar{\chi}_b=0} &= 0\,,\\
\left.\frac{\delta^2\Gamma[\bar{\varphi}_a, \bar{\chi}_b]}{\delta\bar{\chi}_a\delta\bar{\varphi}_b}\right|_{\bar{\varphi}_a,\bar{\chi}_b=0} &\equiv \left(g^{-1}_{ab} - \Sigma_{ab}\right)\delta_D(\mathbf{k}_a+\mathbf{k}_b)\,,\\
\left.\frac{\delta^2\Gamma[\bar{\varphi}_a, \bar{\chi}_b]}{\delta\bar{\varphi}_a\delta\bar{\chi}_b}\right|_{\bar{\varphi}_a,\bar{\chi}_b=0} &\equiv \left(g^{-1}_{ba} - \Sigma_{ba}\right)\delta_D(\mathbf{k}_a+\mathbf{k}_b)\,,\\
\left.\frac{\delta^2\Gamma[\bar{\varphi}_a, \bar{\chi}_b]}{\delta\bar{\chi}_a\delta\bar{\chi}_b}\right|_{\bar{\varphi}_a,\bar{\chi}_b=0} &\equiv \left(iP^0_{ab}(k)\delta(\eta)\delta(\eta_b) + i\Phi_{ab}\right)\delta_D(\mathbf{k}_a+\mathbf{k}_b)\,,
\end{aligned} \tag{2.45}$$

where we have isolated the 'free' (*i.e.* linear) parts (which can be read off from Eq. (2.38)) and the 'interacting' ones, i.e. Σ_{ab} and Φ_{ab}.

With the help of the definitions (2.40) and (2.42) it is easy to verify that the four quantities in equations (2.41) form a matrix that is minus the inverse of that formed by the four quantities in (2.45), which implies that

$$\left.\frac{\delta^2 W}{\delta K_a\,\delta K_b}\right|_{J_a,\,K_b=0} \equiv \langle\chi_a(\mathbf{k},\eta_a)\chi_b(\mathbf{k}',\eta_b)\rangle = 0\,. \tag{2.46}$$

Therefore the full propagator and power-spectrum can be written in terms of the

free ones, the Σ_{ab} and Φ_{ab} functions. The equations that relate these quantities are

$$P_{ab} = P^I_{ab} + P^{II}_{ab}\,, \tag{2.47}$$

where

$$\begin{aligned} P^I_{ab}(k;\eta_a,\eta_b) &= G_{ac}(k;\eta_a,0)G_{bd}(k;\eta_b,0)P^0_{cd}(k)\,, \\ P^{II}_{ab}(k;\eta_a,\eta_b) &= \int_0^{\eta_a} ds_1 \int_0^{\eta_b} ds_2\, G_{ac}(k;\eta_a,s_1)G_{bd}(k;\eta_b,s_2)\Phi_{cd}(k;s_1,s_2) \end{aligned} \tag{2.48}$$

and

$$G_{ab}(k;\eta_a,\eta_b) = \left[g^{-1}_{ba} - \Sigma_{\varphi_a\chi_b}\right]^{-1}(k;\eta_a,\eta_b)\,, \tag{2.49}$$

where the last expression has to be interpreted in a formal sense, that is,

$$G_{ab}(k;\eta_a,\eta_b) = g_{ab}(\eta_a,\eta_b) + \int ds_1 ds_2 g_{ac}(\eta_a,s_1)\Sigma_{\varphi_c\chi_d}(k;s_1,s_2)g_{db}(s_2,\eta_b) + \cdots\,. \tag{2.50}$$

The physical meaning of the propagator can be read out from Eq. (2.47), by setting one of the two times, e.g. η_b, equal to the initial time, *i.e.* $\eta_b = 0$. One gets the exact relation between non-linear power spectra and propagators,

$$P_{ab}(k;\eta_a,0) = G_{ac}(k;\eta_a,0)P^0_{cb}(k)\,, \tag{2.51}$$

where we have used the property of the full propagator $G_{bd}(k;\eta,0) \to \delta_{bd}$ for $\eta \to 0^+$, descending from equations (2.7) and (2.50). Therefore, the propagator connects the equal-time initial PS $P^0_{ab}(k) \equiv P_{ab}(k;\eta_a = \eta_b = 0)$ to the cross-correlator between the initial fields and the 'final' ones evaluated at $\eta_a > 0$. This further clarifies the role of the χ fields in encoding the informations on the statistics of the initial conditions.

If the initial time is taken to correspond to a very high redshift, so that the non-linearities can be neglected in all the range of scales under consideration, one can approximate the initial PS with the linear one,

$$P^0_{ab}(k) \simeq P^0(k)u_a u_b, \tag{2.52}$$

where the u_a vector has been defined in eq. (2.9) and takes into account the fact that the perturbations are in the linear growing mode at $\eta = 0$. In this case, we see that the late-time cross correlators are entirely given in terms of $P^0(k)$ and the two combinations,

$$G_a(k;\,\eta,0) \equiv G_{ac}(k;\,\eta,0)u_c, \quad (a=1,2)\,. \tag{2.53}$$

Equations (2.47) and (2.49) by themselves, however, do not rely on PT, and therefore offer the opportunity of computing the two-point correlators non-perturbatively. A convenient way to deal with the propagator in a non-perturbative way is to cast eq. (2.50) in a closed form

$$\begin{aligned} G_{ab}(k;\,\eta_a,\eta_b) &= g_{ab}(\eta_a,\eta_b) \\ &\quad + \int_{\eta_b}^{\eta_a} ds_1 \int_{\eta_b}^{s_1} ds_2\, g_{ac}(\eta_a,s_1)\Sigma_{cd}(k;\;s_1,\,s_2)\, G_{db}(k;\,s_2,\eta_b)\,, \end{aligned} \tag{2.54}$$

which is equivalent to (2.50), as can be shown by expanding the full propagator G at the RHS iteratively in the 'self-energy' Σ. Then, by deriving eq. (2.54) with respect to η_a we get

$$\begin{aligned} \partial_{\eta_a} G_{ab}(k;\,\eta_a,\eta_b) &= -\Omega_{ac}G_{cb}(k;\,\eta_a,\eta_b) \\ &\quad + \int_{\eta_b}^{\eta_a} ds\,\Sigma_{ac}(k;\,\eta_a\,,s)\,G_{cb}(k;\,s,\eta_b)\,, \end{aligned} \tag{2.55}$$

which gives the exact (*i.e.* non-perturbative) evolution equation for the full propagator. Equation (2.55) is easier to handle rather than Eq. (2.54) and thus it will be the starting point for our evaluation of G_{ab}.

2.3 Diagrammatic formulation

Historically, the first proposal to revisit the PT has been given by Crocce and Scoccimarro in [20] and they called it "Renormalized Perturbation Theory". Following

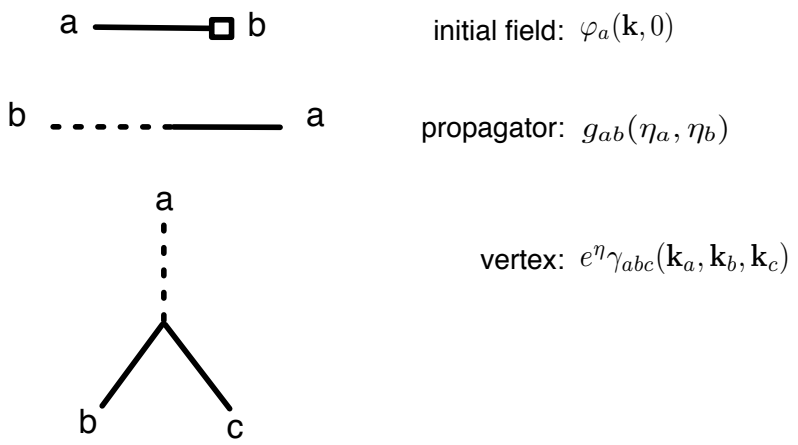

Figure 2.2: Diagramatics Rules for cosmological perturbation theory

a more intuitive approach they identified the basic building blocks directly from the analysis of the fields evolution equations (2.4, 2.10). They are given by the initial field $\varphi_a(0)$, the linear propagator g_{ab} and the vertex γ_{abc}. Their graphical representations are shown in Fig. 2.2 where, for clarity, we have drawn the building blocks with the same graphical notation used in the previous section. With this tools, as we will review in the following, the inclusion of the statistical properties of the fields results straightforward. Feynman diagrams constructed by these rules are in one to one correspondence with those considered in the previous section.

To achieve the set of diagrams corresponding to the nth order term in Eq. (2.11) one has to draw all topologically different trees with $n-1$ vertices (branchings) and n initial conditions. Each tree is obtained as follows: from the final time variable η we draw a line backwards (a linear propagator) until it reaches a vertex, where the line bifurcates into two branches, with each of them continuing until they reach another vertex (through the use of a propagator) or an initial field (through the use of the initial field representation) at $\eta = 0$. If the branching is asymmetric it carries a factor of 2 overall. This process is repeated at each vertex until all the branches end up in initial fields.

Each diagram with $n-1$ vertices represents an integral contributing to $\varphi^{(n)}$. The rules to obtain these integrals are as follows. Each of the n initial fields $\varphi(0)$ is char-

Figure 2.3: Diagrammatics notation for the initial power spectrum.

acterized by a momentum $\mathbf{k}_i$. Each branching corresponds to a vertex $\gamma(\mathbf{k}, \mathbf{k}_1, \mathbf{k}_2)$. Each interaction happens at a given time s_j ($0 \leq s_j \leq \eta$) and conserves momentum ($\mathbf{k} = \mathbf{k}_1 + \mathbf{k}_2$). Finally, all the intermediate wave vectors are integrated over as well as all the time variables s_j, each between $[0, \eta]$.

Including the statistics, assuming Gaussian growing mode initial conditions we have that pairs of initial fields $\varphi(0)$ are replaced by the initial power spectrum as one of the basic building blocks (Fig. 2.3).

In this framework the power spectrum

$$\langle \varphi_a(\mathbf{k}, \eta) \varphi_b(\mathbf{k}', \eta) \rangle = \delta_D(\mathbf{k} + \mathbf{k}') P_{ab}(\mathbf{k}, \eta) \,, \tag{2.56}$$

can be straightforward computed (by the expansion (2.11))

$$\delta_D(\mathbf{k}+\mathbf{k}') P_{ab}(\mathbf{k}, \eta) = \sum_{\ell=0}^{\infty} \delta_D(\mathbf{k}+\mathbf{k}') P_{ab}^{(\ell)}(\mathbf{k}, \eta) = \sum_{\ell=0}^{\infty} \sum_{m=1}^{2\ell+1} \langle \varphi_a^{(m)}(\mathbf{k}, \eta) \varphi_b^{(2\ell+2-m)}(\mathbf{k}', \eta) \rangle . \tag{2.57}$$

where $P_{ab}^{(\ell)}(\mathbf{k}, \eta)$ is the ℓ-loop contribution to the PS. With the Feynaman rules given above one can draw the graphical representations for the PS at each loop order.

We can also define the full non-linear propagator that is given by

$$G_{ab}(k, \eta) \delta_D(\mathbf{k} - \mathbf{k}') \equiv \left\langle \frac{\delta \varphi_a(\mathbf{k}, \eta)}{\delta \varphi_b(\mathbf{k}', 0)} \right\rangle . \tag{2.58}$$

With the help of the Eq. (2.11) it is possible to rewrite the non linear propagator separating the linear part from the non linear contributions

$$G_{ab}(k, \eta) = g_{ab}(\eta) + \sum_{n=2}^{\infty} \left\langle \frac{\delta \varphi_a^{(n)}(\mathbf{k}, \eta)}{\delta \varphi_b(\mathbf{k}, 0)} \right\rangle . \tag{2.59}$$

Implementing this diagrammatic method and analyzing the Feynman graphs,

Crocce and Scoccimarro [20] found out the full power spectrum and full propagator equations, namely Eq. (2.47) and Eq. (2.54).

2.4 Multi-point propagators approach

Another method to implement a re-summation scheme has been proposed in [30]. Extending the definition of propagator, they give a different theoretical formulation of the cosmological perturbation theory based on the idea of "multi-point propagators". Physically these new objects tell us how the field $\varphi_a(\mathbf{k},\eta)$ is correlated to p initial conditions, *i.e.* p initial fields $\phi_b(\mathbf{k},0)$. Here we assume Gaussian initial conditions, however recently this idea has been extended considering non-Gaussian initial conditions [34].

Generalizing the full propagator definition (2.58) it results that a really natural way to introduce these "multi-point propagators" consists in deriving the φ_a field at time s with respect to p initial conditions

$$\frac{1}{p!}\,\langle \frac{\delta^p \varphi_a(\mathbf{k},s)}{\delta\varphi_{b_1}(\mathbf{k}_1,0)\dots\delta\varphi_{b_p}(\mathbf{k}_p,0)}\rangle = \delta_D(\mathbf{k}-\mathbf{k}_{1\dots p})\tilde{\Gamma}^{(p)}_{ab_1\dots b_p}(\mathbf{k}_1,\dots,\mathbf{k}_p,s)\ , \qquad (2.60)$$

where $\mathbf{k}_{1\dots p}=\mathbf{k}_1+\dots+\mathbf{k}_p$, for an arbitrary number of points. $\tilde{\Gamma}^{(p)}$ denotes the $(p+1)$-*point propagator*, that depends by translation invariance only on p wavenumbers in Fourier space. $\tilde{\Gamma}^{(1)}$ denotes the two-point propagator G.

These objects represent the average values of the emerging nonlinear mode $\mathbf{k}$ given n initial modes in the linear regime.

In this section we will briefly review the main results founded in the first part of [30].

These new functions $\tilde{\Gamma}$ can be represented diagrammatically as in Fig. 2.4. They can be also computed order by order in perturbation theory: it is an obvious consequence of Eqs. (2.11) and (2.12).

Considering again Eq. (2.12) one can also get a formal expression for the con-

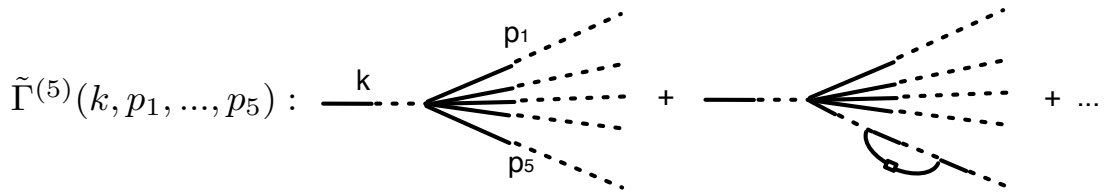

Figure 2.4: Representation of the multi-point propagator $\tilde{\Gamma}^{(5)}$. Here are drawn two perturbative contributions: tree-level and one-loop.

nected cross-correlation functions and find this worthwhile result:

$$\begin{aligned}\langle\varphi_a(\mathbf{k})\varphi_{c_1}(-\mathbf{k}_1,0)\dots\varphi_{c_p}(-\mathbf{k}_p,0)\rangle_c &= p!\,\delta_D(\mathbf{k}-\mathbf{k}_{1\dots p})\\ &\times\tilde{\Gamma}^{(p)}_{ab_1\dots b_p}\,P_{b_1c_1}(k_1)\dots P_{b_pc_p}(k_p)\,,\end{aligned}\tag{2.61}$$

Assuming Gaussian and growing mode initial conditions we have that $P_{ab}(k)$ can be written using the expansion in Eq. (2.11)

$$\begin{aligned}\delta_D(\mathbf{k}_1+\mathbf{k}_2)P_{ab}(k_1,s) &\equiv \langle\varphi_a(\mathbf{k}_1,s)\varphi_b(\mathbf{k}_2,s)\rangle\\ &= \sum_{n_1,n_2}\langle\varphi_a^{(n_1)}(\mathbf{k}_1,s)\varphi_b^{(n_2)}(\mathbf{k}_2,s)\rangle\,.\end{aligned}\tag{2.62}$$

Starting from Eq. (2.62) one can write down the power spectrum as a sum of product of $\tilde{\Gamma}^{(n)}$ functions

$$\begin{aligned}P_{ab}(\mathbf{k},\eta) = \sum_n n!\int \mathrm{d}^3\mathbf{q}_1\dots\mathrm{d}^3\mathbf{q}_n\,\delta_D(\mathbf{k}-\mathbf{q}_1\dots n)\,\tilde{\Gamma}^{(n)}_a\left(\mathbf{q}_1,\dots,\mathbf{q}_n,\eta\right)\\ \times\tilde{\Gamma}^{(n)}_b\left(\mathbf{q}_1,\dots,\mathbf{q}_n,\eta\right)P_0(q_1)\dots P_0(q_n)\,,\end{aligned}\tag{2.63}$$

where we have introduced the shorthand notation,

$$\tilde{\Gamma}^{(n)}_a(\mathbf{q}_1,\dots,\mathbf{q}_n) = \Gamma^{(n)}_{ac_1\dots c_n}(\mathbf{q}_1,\dots,\mathbf{q}_n)\,u_{c_1}\dots u_{c_n},\tag{2.64}$$

and used the following property,

$$\tilde{\Gamma}^{(n)}_{ab_1\dots b_n}\left(\mathbf{k}_1,\dots,\mathbf{k}_n\right) = \tilde{\Gamma}^{(n)}_{ab_1\dots b_n}\left(-\mathbf{k}_1,\dots,-\mathbf{k}_n\right)\,.\tag{2.65}$$

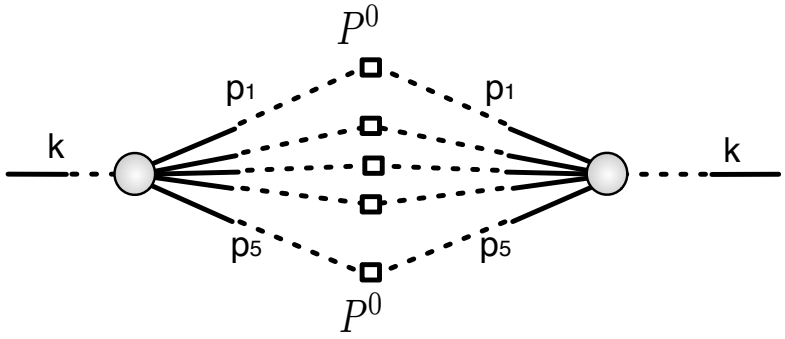

Figure 2.5: Contracted multi-point propagator. The square represents the initial power spectrum and the large circle represents the fully nonlinear multi-point propagator.

Hence, contracting the multi-point propagator in such way, one is able to write down the full power spectrum. We underline that the $\tilde{\Gamma}^{(n)}$'s appearing in Eq. (2.63) are the full ones, thus, in principle it is worthwhile to compute those first. In the next chapter we will explain a way to do that. The sum (2.63) corresponds to a contraction of $\tilde{\Gamma}^{(n)}$ diagrams when the initial conditions lines are glued together to form initial power spectrum as shown in Fig. 2.5. The permutation factor represents the number of ways of contracting the $(n+1)-$point propagator.

In this section we have presented a different re-summation scheme and further studies on it may be interesting. An useful point, for instance, is that in Eq. (2.63) for $a = b$ the result is a sum of positive terms, while the standard perturbation theory does not exhibit a similar behavior. Hence the approach here explained seems more useful in order to compute the correlation functions. We can also give an expression similar to Eq. (2.63) for the bispectrum and so on but this is beyond the scope of this thesis. Recently this re-summation approach has also been implemented for non-Gaussian initial conditions [34].

2.5 Closure theory

Here we summarized the theoretical approach achieved by Taruya and Hiramatsu [26]. They consider an alternative statistical method widely accepted in the subject of statistical theory of turbulence. It simply describe the non linearities of mat-

ter power spectrum doing a systematic expansion and the truncation of the naive perturbation and, after that, one applies the so-called reversed expansion. This drives to a reorganization of the perturbative expansion, in other words a class of higher-order corrections is systematically re-summed.

Considering Eq. (2.4) and also the statistical nature of the system we get the exact evolution equation for the power spectrum [3]:

$$\begin{aligned}\widehat{\mathbf{\Sigma}}_{abcd}(\eta)\left\langle\varphi_c(\mathbf{k},\eta)\,\varphi_d(\mathbf{k}',\eta)\right\rangle \\ = e^{\eta}\Big[\,\gamma_{bpq}(\mathbf{k},-\mathbf{q},-\mathbf{p})\Big\langle\varphi_a(\mathbf{k},\eta)\,\varphi_p(\mathbf{q},\eta)\,\varphi_q(\mathbf{p},\eta)\Big\rangle \\ +\gamma_{apq}(\mathbf{k},-\mathbf{q},-\mathbf{p})\Big\langle\varphi_b(\mathbf{k}',\eta)\,\varphi_p(\mathbf{q},\eta)\,\varphi_q(\mathbf{p},\eta)\Big\rangle\Big]\,. \quad (2.66)\end{aligned}$$

In the same way we get for different time power spectrum

$$\begin{aligned}\widehat{\mathbf{\Lambda}}_{ab}(\eta)\left\langle\varphi_b(\mathbf{k},\eta)\,\varphi_c(\mathbf{k}',\eta')\right\rangle \\ = e^{\eta}\gamma_{apq}(\mathbf{k},-\mathbf{q},-\mathbf{p})\Big\langle\varphi_c(\mathbf{k}',\eta')\,\varphi_p(\mathbf{q};\eta)\,\varphi_q(\mathbf{p},\eta)\Big\rangle. \quad (2.67)\end{aligned}$$

Here, we have introduced the two kinds of operators, $\widehat{\mathbf{\Sigma}}_{abcd}$ and $\widehat{\mathbf{\Lambda}}_{ac}$:

$$\widehat{\mathbf{\Sigma}}_{abcd}(\eta)\equiv\delta_{ac}\delta_{bd}\,\frac{\partial}{\partial\eta}+\delta_{ac}\,\Omega_{bd}+\delta_{bd}\,\Omega_{ac},\qquad\widehat{\mathbf{\Lambda}}_{ab}(\eta)\equiv\delta_{ab}\,\frac{\partial}{\partial\eta}+\Omega_{ab}. \quad (2.68)$$

The closure theory also allows to define the propagator as

$$G_{ab}(\mathbf{k},\eta|\mathbf{k}',\eta')\equiv\frac{\delta\varphi_a(\mathbf{k};\eta)}{\delta\varphi_b(\mathbf{k}';\eta')}\,. \quad (2.69)$$

This definition matches with (2.41) and (2.58) when also the statistical properties of the system are taken into account. Making a functional derivative of equation (2.4), we obtain the governing equation for the propagator

$$\widehat{\mathbf{\Lambda}}_{ab}(\eta)\,G_{bc}(\mathbf{k},\eta|\mathbf{k}',\eta')=2e^{\eta}\,\gamma_{apq}(\mathbf{k},-\mathbf{q},-\mathbf{p})\,\varphi_p(\mathbf{q};\eta)\,G_{qc}(\mathbf{p},\eta|\mathbf{k}',\eta') \quad (2.70)$$

[3] Repeated indices/momenta are summed/integrated over.

with the boundary condition:

$$G_{ab}(\mathbf{k},\eta'|\mathbf{k}',\eta') = \delta_{ab}\ \delta_D(\mathbf{k}-\mathbf{k}'). \tag{2.71}$$

Equations (2.66) and (2.67) are not yet closed because they contain the higher-order correlation functions (or bi-spectra). In order to obtain the closed set of evolution equations, it is necessary to derive the evolution equations for higher-order correlation functions. However, the repetition of this treatment produces an infinite number of evolution equations and one cannot obtain a closed set of equations. This is the so-called *closure problem* for dynamics of statistical quantities. Note that the closure problem considered here is very close to the concept of BBGKY hierarchy. On the other hand, the origin of the closure problem essentially comes from the non-linearity of equation (2.4). Hence, to derive a closed set of moment equations, one must introduce some truncation procedures by approximately treating the non-linear interaction in a self-consistent manner. The self-consistent truncation procedure is referred to as the closure theory (or closure approximation) in the statistical theory of turbulence and various closure theories have been so far exploited. In what follows, we especially consider the so-called *reversed expansion procedure*.

2.5.1 Reversed expansion in two steps

We need to introduce the fictitious parameter λ, which represents the strength of the non-linearity, and consider the weakly non-linear regime. We rewrite the field φ_a and the propagator G_{ab} with

$$\varphi_a(\mathbf{k};\eta) = \lambda\,\tilde{\varphi}_a(\mathbf{k};\eta), \qquad G_{ab}(\mathbf{k},\eta|\mathbf{k}',\eta') = \lambda\,\tilde{G}_{ab}(\mathbf{k},\eta|\mathbf{k}',\eta'). \tag{2.72}$$

In terms of these, the basic equations (2.4) and (2.70) respectively become

$$\widehat{\mathbf{\Lambda}}_{ab}(\eta)\ \tilde{\varphi}_b(\mathbf{k};\eta) = \lambda\, e^{\eta}\gamma_{abc}(\mathbf{k},\,-\mathbf{p},\,-\mathbf{q})\tilde{\varphi}_b(\mathbf{p},\eta)\,\tilde{\varphi}_c(\mathbf{q},\eta), \tag{2.73}$$

$$\widehat{\mathbf{\Lambda}}_{ab}(\eta)\,\tilde{G}_{bc}(\mathbf{k},\eta|\mathbf{k}',\eta') = 2\lambda e^{\eta}\,\gamma_{apq}(\mathbf{k},-\mathbf{q},-\mathbf{p})\,\tilde{\varphi}_p(\mathbf{q};\eta)\,\tilde{G}_{qc}(\mathbf{p},\eta|\mathbf{k}',\eta') \tag{2.74}$$

We can regard λ as a small expansion parameter and consider the sequent assumptions: the fluctuation is tiny and the non linearity is weakly, the statistics of initial conditions is Gaussian and at the leading order, the field $\tilde{\varphi}_a$ and the propagator $\tilde{G}_{bc}$ are statistically independent at the leading order.

The first step consists in the computation of the correlators using the perturbative calculation. Then, inverting the expansion and setting the fictitious parameter λ to 1 at the final step, one achieves a closed set of evolution equations. This technique can be regarded as the result of renormalization and/or resummation of the perturbative expansion.

First step: naive perturbation

Expanding, with respect to λ, the quantities $\tilde{\varphi}_a$ and $\tilde{G}_{ab}$ can be written in this way:

$$\begin{aligned} \tilde{\varphi}_a(\mathbf{k},\eta) &= \tilde{\varphi}_a^{(0)}(\mathbf{k},\eta) + \lambda\, \tilde{\varphi}_a^{(1)}(\mathbf{k},\eta) + \cdots , \\ \tilde{G}_{ab}(\mathbf{k},\eta|\mathbf{k}',\eta') &= \tilde{G}_{ab}^{(0)}(\mathbf{k},\eta|\mathbf{k}',\eta') + \lambda\, \tilde{G}_{ab}^{(1)}(\mathbf{k},\eta|\mathbf{k}',\eta) + \cdots . \end{aligned} \tag{2.75}$$

The equations for zeroth-order quantities are source-free (without coupling). The boundary condition for propagator gives

$$\tilde{G}_{ab}^{(0)}(\mathbf{k},\eta'|\mathbf{k}',\eta') = \delta_{ab}\,\delta_D(\mathbf{k}-\mathbf{k}'), \qquad \tilde{G}_{ab}^{(1)}(\mathbf{k},\eta'|\mathbf{k}',\eta') = 0. \tag{2.76}$$

Also, the boundary condition for the first-order quantity $\tilde{\varphi}_a^{(1)}$ at the initial time is

$$\tilde{\varphi}_a^{(1)}(\mathbf{k},0) = 0. \tag{2.77}$$

Thus, the zeroth-order propagator $\tilde{G}_{ab}^{(0)}$ satisfying the boundary condition (2.76) can be expressed in the following form:

$$\tilde{G}_{ab}^{(0)}(\mathbf{k},\eta|\mathbf{k}',\eta') = \tilde{G}_{ab}(\mathbf{k}|\eta,\eta')\ \delta_D(\mathbf{k}-\mathbf{k}'). \tag{2.78}$$

The perturbative expression for the power spectra are

$$P_{ab}(k,\eta) = \lambda^2\ \tilde{P}_{ab}(k,\eta) \simeq \lambda^2\ \left\{\tilde{P}^{(0)}_{ab}(k,\eta) + \mathcal{O}(\lambda^2)\right\},$$
$$P_{ab}(k,\eta,\eta') = \lambda^2\ \tilde{P}_{ab}(k,\eta,\eta') \simeq \lambda^2\ \left\{\tilde{P}^{(0)}_{ab}(k,\eta,\eta') + \mathcal{O}(\lambda^2)\right\}. \quad (2.79)$$

where the definitions of the zeroth-order terms are given by

$$\left\langle \tilde{\varphi}^{(0)}_a(\mathbf{k},\eta)\, \tilde{\varphi}^{(0)}_b(\mathbf{k}',\eta)\right\rangle = \delta_D(\mathbf{k}+\mathbf{k}')\, \tilde{P}^{(0)}_{ab}(k,\eta),$$
$$\left\langle \tilde{\varphi}^{(0)}_a(\mathbf{k},\eta)\, \tilde{\varphi}^{(0)}_b(\mathbf{k}';\eta')\right\rangle = \delta_D(\mathbf{k}+\mathbf{k}')\, \tilde{P}^{(0)}_{ab}(k,\eta,\eta'). \quad (2.80)$$

Then, after few algebraic manipulations, the perturbative expansions of the evolution equations for the relevant quantities become

$$\widehat{\mathbf{\Sigma}}_{abcd}(\eta)\, \tilde{P}_{cd}(k,\eta) \simeq \lambda^2 e^{\eta} \int d^3\mathbf{q} \Big[\gamma_{bpq}(\mathbf{k},\mathbf{q},-\mathbf{k}-\mathbf{q})\, F^{(2)}_{apq}(\mathbf{k},\mathbf{q},-\mathbf{k}-\mathbf{q},\,\eta)$$
$$+ \gamma_{apq}(-\mathbf{k},\mathbf{q},\mathbf{k}-\mathbf{q})\, F^{(2)}_{bpq}(-\mathbf{k},\mathbf{q},\mathbf{k}-\mathbf{q},\,\eta)\Big] \,+\, \mathcal{O}(\lambda^4), \quad (2.81)$$

$$\widehat{\mathbf{\Lambda}}_{ab}(\eta)\, \tilde{P}_{bc}(k,\eta,\eta') \simeq$$
$$\lambda^2 e^{\eta} \int d^3\mathbf{q}\ \gamma_{apq}(-\mathbf{k},\mathbf{q},\mathbf{k}-\mathbf{q})\, K^{(2)}_{cpq}(-\mathbf{k},\mathbf{q},\mathbf{k}-\mathbf{q},\,\eta,\eta') \,+\, \mathcal{O}(\lambda^4)\,, \quad (2.82)$$

$$\widehat{\mathbf{\Lambda}}_{ab}(\eta) \left\langle \tilde{G}_{bc}(\mathbf{k},\eta|\mathbf{k}',\eta')\right\rangle \simeq\ 4\,\lambda^2\, e^{\eta}\, \delta_D(\mathbf{k}-\mathbf{k}') \int_{\eta'}^{\eta} \mathrm{d}\eta'' e^{\eta''} \int \mathrm{d}^3\mathbf{q}\ \gamma_{apq}(-\mathbf{k},\mathbf{q},\mathbf{k}-\mathbf{q})$$
$$\times\ \gamma_{lrs}(\mathbf{q}-\mathbf{k}',-\mathbf{q},\mathbf{k}')\tilde{G}_{ql}(|\mathbf{k}-\mathbf{q}||\eta,\eta'')\, \tilde{P}^{(0)}_{pr}(q,\eta,\eta'')\, \tilde{G}_{sc}(\mathbf{k}'|\eta'',\eta') \,+\, \mathcal{O}(\lambda^4)\,, \quad (2.83)$$

where

$$F^{(2)}_{apq}(\mathbf{k},\mathbf{k}_1,\mathbf{k}_2,\eta) = 2 \int_0^{\eta} \mathrm{d}\eta'\, e^{\eta'} \Big[\tilde{G}_{ql}(\mathbf{k}_2|\eta,\eta')\, \gamma_{lrs}(-\mathbf{k}-\mathbf{k}_1,\mathbf{k},\mathbf{k}_1)$$
$$\times \tilde{P}^{(0)}_{ar}(k,\eta,\eta')\tilde{P}^{(0)}_{ps}(k_1,\eta,\eta')$$
$$+\ \tilde{G}_{pl}(\mathbf{k}_1|\eta,\eta')\, \gamma_{lrs}(-\mathbf{k}-\mathbf{k}_2,\mathbf{k},\mathbf{k}_2)\, \tilde{P}^{(0)}_{ar}(k,\eta,\eta')\, \tilde{P}^{(0)}_{qs}(k_2,\eta,\eta')$$
$$+\ \tilde{G}_{al}(\mathbf{k}|\eta,\eta')\, \gamma_{lrs}(-\mathbf{k}_1-\mathbf{k}_2,\mathbf{k}_1,\mathbf{k}_2)\, \tilde{P}^{(0)}_{pr}(k_1,\eta,\eta')\, \tilde{P}^{(0)}_{qs}(k_2,\eta,\eta')\Big]\,, \quad (2.84)$$

$K^{(2)}_{cpq}(\mathbf{k}',\mathbf{k}_1,\mathbf{k}_2,\eta,\eta')$

$$
\begin{aligned}
= \; & 2 \int_0^{\eta} d\eta''\, e^{\eta''} \left\{ \tilde{P}^{(0)}_{cr}(k',\eta',\eta'')\theta(\eta'-\eta'') + \tilde{P}^{(0)}_{rc}(k',\eta'',\eta')\theta(\eta''-\eta') \right\} \\
& \times \Big[\tilde{G}_{ql}(\mathbf{k}_2|\eta,\eta'')\, \gamma_{lrs}(-\mathbf{k}'-\mathbf{k}_1,\mathbf{k}',\mathbf{k}_1)\, \tilde{P}^{(0)}_{ps}(k_1,\eta,\eta'') \\
& + \tilde{G}_{pl}(\mathbf{k}_1|\eta,\eta'')\, \gamma_{lrs}(-\mathbf{k}'-\mathbf{k}_2,\mathbf{k}',\mathbf{k}_2)\, \tilde{P}^{(0)}_{qs}(k_2,\eta,\eta'') \Big] \\
& + 2 \int_0^{\eta'} d\eta''\, \tilde{G}_{cl}(\mathbf{k}'|\eta',\eta'')\, \gamma_{lrs}(-\mathbf{k}_1-\mathbf{k}_2,\mathbf{k}_1,\mathbf{k}_2)\, \tilde{P}^{(0)}_{pr}(k_1,\eta,\eta'')\, \tilde{P}^{(0)}_{qs}(k_2,\eta,\eta'')\,.
\end{aligned}
\tag{2.85}
$$

In principle it is possible to express the $\mathcal{O}(\lambda^4)$ and higher-orders of the correlation functions in terms of $P^{(0)}_{ab}$ since it can be shown that formal solution of $\tilde{\varphi}^{(n)}_a$ can be always written in terms of $\tilde{\varphi}^{(0)}_a$ and $\tilde{G}^{(0)}_{ab}$.

Second step: reversed expansion procedure

We are now ready to apply the procedure of reversed expansion. It consists of inverting Eqs. (2.79) and doing the same for the propagator:

$$
\begin{aligned}
& \tilde{P}^{(0)}_{ab}(k,\eta) = \tilde{P}_{ab}(k,\eta) + \mathcal{O}(\lambda^2)\,, \qquad \tilde{P}^{(0)}_{ab}(k,\eta,\eta') = \tilde{P}_{ab}(k,\eta,\eta') + \mathcal{O}(\lambda^2)\,, \\
& \delta_D(\mathbf{k}-\mathbf{k}')\; \tilde{G}_{ab}(\mathbf{k}|\eta,\eta') \; = \left\langle \tilde{G}_{ab}(\mathbf{k},\eta|\mathbf{k}',\eta') \right\rangle + \; \mathcal{O}(\lambda^2).
\end{aligned}
\tag{2.86}
$$

This procedure corresponds to the resummation of the perturbation series. Thus, at the leading order, equations (2.81), (2.81) and (2.83) are written in terms of the true field variables $\tilde{P}_{ab}$, $\tilde{P}_{ab}$ and $\tilde{G}_{ab}$.

We do not more treat λ as small parameter. This is just a book-keeping parameter and we finally set it to unity. Dropping the tilde over the quantities $\tilde{P}_{ab}$ and $\tilde{G}_{ab}$, we at last reach the closure equations:

$$
\begin{aligned}
\widehat{\mathbf{\Sigma}}_{abcd}(\eta)\, P_{cd}(k,\eta) = \; & e^{\eta} \int \mathrm{d}^3\mathbf{q} \Big[\gamma_{bpq}(\mathbf{k},\mathbf{q},-\mathbf{k}-\mathbf{q})\, F_{apq}(\mathbf{k},\mathbf{q},-\mathbf{k}-\mathbf{q},\,\eta) \\
& + \gamma_{apq}(-\mathbf{k},\mathbf{q},\mathbf{k}-\mathbf{q})\, F_{bpq}(-\mathbf{k},\mathbf{q},\mathbf{k}-\mathbf{q},\,\eta) \Big],
\end{aligned}
\tag{2.87}
$$

$$
\widehat{\mathbf{\Lambda}}_{ab}(\eta)\, P_{bc}(k,\eta,\eta') = \; e^{\eta} \int \mathrm{d}^3\mathbf{q}\; \gamma_{apq}(-\mathbf{k},\mathbf{q},\mathbf{k}-\mathbf{q})\, K_{cpq}(-\mathbf{k},\mathbf{q},\mathbf{k}-\mathbf{q},\,\eta,\eta'),
\tag{2.88}
$$

$$
\widehat{\mathbf{\Lambda}}_{ab}(\eta)\, G_{bc}(\mathbf{k}|\eta,\eta') = \; 4\, e^{\eta} \int_{\eta'}^{\eta} d\eta''\, e^{\eta''} \int d^3\mathbf{q}\; \gamma_{apq}(-\mathbf{k},\mathbf{q},\mathbf{k}-\mathbf{q})\, \gamma_{lrs}(\mathbf{q}-\mathbf{k},-\mathbf{q},\mathbf{k})
$$

$$\times G_{ql}(|\mathbf{k}-\mathbf{q}||\eta,\eta'')\,P_{pr}(q,\eta,\eta'')\,G_{sc}(\mathbf{k}|\eta'',\eta'). \tag{2.89}$$

The explicit expressions for the kernels F_{bpq} and K_{cpq} can be simplified using the fact that they always appear as the product of $\gamma_{bpq}F_{apq}$ and $\gamma_{apq}K_{cpq}$. Thus we have

$$\begin{aligned}
&F_{apq}(\mathbf{k},\mathbf{k}_1,\mathbf{k}_2,\eta) = \\
&\quad 2\int_0^\eta d\eta''\, e^{\eta''}\Big[\,2\;G_{ql}(k_2|\eta,\eta'')\,\gamma_{lrs}(-\mathbf{k}-\mathbf{k}_1,\mathbf{k},\mathbf{k}_1)\,P_{ar}(k,\eta,\eta'')P_{ps}(k_1,\eta,\eta'') \\
&\quad +\;G_{al}(k|\eta,\eta'')\,\gamma_{lrs}(-\mathbf{k}_1-\mathbf{k}_2,\mathbf{k}_1,\mathbf{k}_2)\,P_{pr}(k_1,\eta,\eta'')\,P_{qs}(k_2,\eta,\eta'')\Big], \qquad (2.90)\\
&K_{cpq}(\mathbf{k}',\mathbf{k}_1,\mathbf{k}_2,\eta,\eta') \\
&\quad =\;4\int_0^\eta \mathrm{d}\eta''\, e^{\eta''}\;G_{ql}(k_2|\eta,\eta'')\,\gamma_{lrs}(\mathbf{k}',-\mathbf{k}_1,\mathbf{k}',\mathbf{k}_1)\,P_{ps}(k_1,\eta,\eta'') \\
&\quad \times\Big\{P_{cr}(k',\eta',\eta'')\theta(\eta'-\eta'')+P_{rc}(k';\eta'',\eta')\theta(\eta''-\eta')\Big\} \\
&\quad +\;2\int_0^{\eta'} d\eta''\,G_{cl}(k'|\eta',\eta'')\,\gamma_{lrs}(-\mathbf{k}_1-\mathbf{k}_2,\mathbf{k}_1,\mathbf{k}_2)\,P_{pr}(k_1,\eta,\eta'')\,P_{qs}(k_2,\eta,\eta''),
\end{aligned} \tag{2.91}$$

These are the starting equations of the *closure theory*. This approach does not use Feynman diagrams and the other QFT tools. Hence the comparison with the previous approach is non straightforward. Until now we can just note that here we are dealing with approximate computable equations. Contrariwise Eqs. (2.47,2.54) are so far exact but we must to specify Φ_{ab} and Σ_{ab} functions. Thus in the previous approaches the approximations will arise when we will compute the 1PI functions.

2.6 Time-Renormalization Group equations for the non linear PS

In this section we briefly review the Time-Remornalization Group approach (TRG) introduced in [28] to compute the non linear PS. Applying the equation of motion in Eq. (2.4) to the (equal-time) PS, the bispectrum,

$$\langle\varphi_a(\mathbf{k},\eta)\varphi_b(\mathbf{p},\eta)\varphi_c(\mathbf{q},\eta)\rangle = \delta_D(\mathbf{k}+\mathbf{p}+\mathbf{q})\,B_{abc}(\mathbf{k},\mathbf{p},\mathbf{q};\eta)\,, \tag{2.92}$$

and to the higher order correlators, one gets an infinite system of coupled differential equations. Truncating the hierarchy by setting the trispectum (*i.e.* the connected four-point function) to zero, one is left with the closed system

$$\begin{aligned}\partial_\eta P_{ab}(\mathbf{k}\,;\eta) = &-\Omega_{ac}P_{cb}(\mathbf{k}\,;\eta) - \Omega_{bc}P_{ac}(\mathbf{k}\,;\eta)\\ &+e^\eta \int d^3q\, [\gamma_{acd}(\mathbf{k},\,-\mathbf{q},\,\mathbf{q}-\mathbf{k})\, B_{bcd}(\mathbf{k},\,-\mathbf{q},\,\mathbf{q}-\mathbf{k};\,\eta)\\ &\qquad +B_{acd}(\mathbf{k},\,-\mathbf{q},\,\mathbf{q}-\mathbf{k};\,\eta)\,\gamma_{bcd}(\mathbf{k},\,-\mathbf{q},\,\mathbf{q}-\mathbf{k})]\ ,\end{aligned}$$

$$\begin{aligned}\partial_\eta B_{abc}(\mathbf{k},\,-\mathbf{q},\,\mathbf{q}-\mathbf{k};\,\eta) = &-\Omega_{ad}B_{dbc}(\mathbf{k},\,-\mathbf{q},\,\mathbf{q}-\mathbf{k};\,\eta)\\ &-\Omega_{bd}B_{adc}(\mathbf{k},\,-\mathbf{q},\,\mathbf{q}-\mathbf{k};\,\eta)\\ &-\Omega_{cd}B_{abd}(\mathbf{k},\,-\mathbf{q},\,\mathbf{q}-\mathbf{k};\,\eta)\\ &+2e^\eta\,[\gamma_{ade}(\mathbf{k},\,-\mathbf{q},\,\mathbf{q}-\mathbf{k})P_{db}(\mathbf{q}\,;\eta)P_{ec}(\mathbf{k}-\mathbf{q}\,;\eta)\\ &+\gamma_{bde}(-\mathbf{q},\,\mathbf{q}-\mathbf{k},\,\mathbf{k})P_{dc}(\mathbf{k}-\mathbf{q}\,;\eta)P_{ea}(\mathbf{k}\,;\eta)\\ &+\gamma_{cde}(\mathbf{q}-\mathbf{k},\,\mathbf{k},\,-\mathbf{q})P_{da}(\mathbf{k}\,;\eta)P_{eb}(\mathbf{q}\,;\eta)]\ .\end{aligned} \tag{2.93}$$

The formal solution of the system (2.93) is given by

$$\begin{aligned}P_{ab}(\mathbf{k}\,;\eta) = &\, g_{ac}(\eta,0)\, g_{bd}(\eta,0)P_{cd}(\mathbf{k}\,;\eta=0)\\ &+\int_0^\eta d\eta' e^{\eta'} \int d^3q\, g_{ae}(\eta,\eta')g_{bf}(\eta,\eta')\\ &\quad\times[\gamma_{ecd}(\mathbf{k},\,-\mathbf{q},\,\mathbf{q}-\mathbf{k})\, B_{fcd}(\mathbf{k},\,-\mathbf{q},\,\mathbf{q}-\mathbf{k};\,\eta')\\ &\qquad+\gamma_{fcd}(\mathbf{k},\,-\mathbf{q},\,\mathbf{q}-\mathbf{k})\, B_{ecd}(\mathbf{k},\,-\mathbf{q},\,\mathbf{q}-\mathbf{k};\,\eta')]\ ,\end{aligned}$$

$$\begin{aligned}&B_{abc}(\mathbf{k},\,-\mathbf{q},\,\mathbf{q}-\mathbf{k};\,\eta) =\\ &\quad g_{ad}(\eta,0)g_{be}(\eta,0)g_{cf}(\eta,0)B_{def}(\mathbf{k},\,-\mathbf{q},\,\mathbf{q}-\mathbf{k};\,\eta=0)\\ &\qquad+2\int_0^\eta d\eta' e^{\eta'}\, g_{ad}(\eta,\eta')g_{be}(\eta,\eta')g_{cf}(\eta,\eta')\\ &\qquad\quad\times[\gamma_{dgh}(\mathbf{k},\,-\mathbf{q},\,\mathbf{q}-\mathbf{k})P_{eg}(\mathbf{q}\,;\eta')P_{fh}(\mathbf{q}-\mathbf{k}\,;\eta')\\ &\qquad\qquad+\gamma_{egh}(-\mathbf{q},\,\mathbf{q}-\mathbf{k},\,\mathbf{k})P_{fg}(\mathbf{q}-\mathbf{k}\,;\eta')P_{dh}(\mathbf{k}\,;\eta')\\ &\qquad\qquad+\gamma_{fgh}(\mathbf{q}-\mathbf{k},\,\mathbf{k},\,-\mathbf{q})P_{dg}(\mathbf{k}\,;\eta')P_{eh}(\mathbf{q}\,;\eta')]\ ,\end{aligned} \tag{2.94}$$

which shows that the non-linear PS in this approach is given by a formally 1-loop expression in which non-linear PS' replace the linear ones. In this respect, the TRG approach is fully consistent with the computation of the propagator presented in the next chapter, which is based, as well, on improving over the Crocce and Scoccimarro [39] approximation by replacing linear PS' with non-linear ones.

In the field theoretical language, with this approximation procedure, we are not including the vertex renormalization, while including the renormalization of the PS. This approach is quite similar to the one presented in the previous section: the main difference concerns the renormalization/re-summation of the propagator. In fact, with this approach we do not take care of the calculation of the full propagator. Another really interesting point about this method is that it is really easy and not require a field theory background. Finally it can be extended to a wide range of different cosmological models.

2.7 Extension to ΛCDM cosmologies

It is possible to extend the validity of these approaches to ΛCDM cosmologies to a very good approximation [39]. We redefine

$$\varphi_a(\mathbf{k},\eta) \equiv e^{-\eta}\Big(\delta(\mathbf{k},\eta),\ -\theta(\mathbf{k},\eta)/\mathcal{H}f\Big), \tag{2.95}$$

where the f function is defined in this way: $f \equiv \mathrm{d}\ln D_+/\mathrm{d}\ln a$. D_+ is the linear growth factor of the growing mode. The time variable is reinterpreted as

$$\eta \equiv \ln(D_+(\tau)/D_+(0)). \tag{2.96}$$

The evolution equations have the same form as in Eq. (2.4) with the only change [6]

$$\Omega_{ab} \equiv \begin{bmatrix} 1 & -1 \\ -3\Omega_m/2f^2 & 3\Omega_m/2f^2 \end{bmatrix}, \tag{2.97}$$

This result is exact but it carries a problem about the Laplace transform solution in Eq. (2.10). This happens because in Eq. (2.97) both Ω_m and f are now

functions of time. Thus growing mode will be correct but the decaying mode is not correct anymore, since in general it is given by the Hubble constant H which does not scale as $D_+^{-3/2}$ in the general case. Anyway, as we explained in Section 1.3.1, during most of the time evolution $\Omega_m/f^2 \approx 1$. Hence in the standard perturbation theory the dependence of the perturbative solutions in the values of Ω_m and Ω_Λ is extremely weak [2, 40, 41]. In other words, almost all of the information about the cosmological parameters is encoded in the linear growth factor $D_+(\tau)$. Therefore, when we will be concerning with the ΛCDM cosmologies we will simply replace $a(\tau)$ by the corresponding linear growth factor $D_+(\tau, \Omega_m, \Omega_\Lambda)$.

leveraging the full propagator definition

Chapter 3

Nonlinear propagators in different frameworks

In this chapter we study the propagator of density and velocity fields, the main ingredient that enters into a well-controlled extension of perturbation theory. Actually it becomes more and more relevant when one approaches the non linear regime. It gives the cross-correlation between the perturbation at a given time and length scale and the initial condition at the same scale as summarized in Eq. (2.51). It is not an observable quantity but it is a fundamental ingredient for the computation of the power spectrum because (check Eq. (2.47)) it is deeply dependent on the propagator. Hence one of the main task of these new approaches to cosmological perturbations theory is reduced to the computation of the propagator.

The first full propagator calculation is due to Crocce and Scoccimarro [39] (hereafter, CS). Leveraging a re-summation procedure, they computed the propagator analytically in the high momentum limit. Then they found a nice technique to match this result with the small momentum limit of the propagator.

In the first section we clarify the relation between the evolution equation of the propagator (2.55) and the re-summation of "chain diagrams" performed in CS. In the next section we will explain the different propagator re-summation derived form the closure theory [26]. Then we will briefly review the "multi point propagators" results [30]. Finally we discuss how to go beyond the CS result by taking into

account the renormalized PS in the "chain-diagrams".

3.1 Factorization and the Crocce-Scoccimarro propagator

In order to get insight on the content of the propagator exact evolution equation, Eq. (2.55), we will consider a perturbative expansion for the propagator and the 'self-energy',

$$\begin{aligned} G_{ab}(k;\,\eta_a,\eta_b) &= \sum_{n=0}^{\infty} G_{ab}^{(n)}(k;\,\eta_a,\eta_b)\,, \\ \Sigma_{ab}(k;\,\eta_a,\eta_b) &= \sum_{n=1}^{\infty} \Sigma_{ab}^{(n)}(k;\,\eta_a,\eta_b)\,, \end{aligned} \tag{3.1}$$

where, as usual, the index n counts the number of power spectra contained in the n-th order contributions to G_{ab} and Σ_{ab}. Notice that at zeroth order Σ_{ab} receives no contribution, while

$$G_{ab}^{(0)}(k;\,\eta_a,\eta_b) = g_{ab}(\eta_a-\eta_b)\,. \tag{3.2}$$

Inserting (3.1) in (2.55), and equating terms of the same order, we get the evolution equation for the n-th order contribution to the full propagator,

$$\begin{aligned} \partial_{\eta_a} G_{ab}^{(n)}(k;\,\eta_a,\eta_b) = &- \Omega_{ac}\, G_{cb}^{(n)}(k;\,\eta_a,\eta_b) \\ &+ \Theta_{n,0} \sum_{j=0}^{n-1} \int_{\eta_b}^{\eta_a} ds\, \Sigma_{ac}^{(n-j)}(k;\,\eta_a\,,s)\, G_{cb}^{(j)}(k;\,s,\eta_b)\,, \end{aligned} \tag{3.3}$$

where $\Theta_{n,0}$ is zero for $n=0$ and one otherwise.

3.1.1 Factorization at large momentum

In the large external momentum limit the leading diagrams contributing to the last line of Eq. (3.3) are the so-called chain-diagrams (see Fig. 3.2) already discussed by CS in [39], all the other contributions being suppressed by inverse powers of k. We

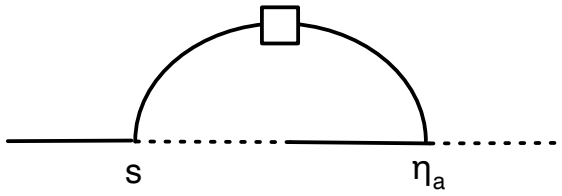

Figure 3.1: $\Sigma^{(1)}_{ac}$, the1-loop contribution to the self-energy.

Figure 3.2: Chain-diagrams.

are going to prove that in this limit the sum can be computed analytically, giving the remarkable factorized result

$$\sum_{j=0}^{n-1} \int_{\eta_b}^{\eta_a} ds\, \Sigma^{(n-j)}_{ac}(k;\, \eta_a\,, s)\, G^{(j)}_{cb}(k;\, s, \eta_b) \\ \stackrel{\text{large } k}{\longrightarrow}\; G^{(n-1)}_{\mathbf{a}b}(k;\, \eta_a, \eta_b) \int_{\eta_b}^{\eta_a} ds\, \Sigma^{(1)}_{\mathbf{a}c}(k;\, \eta_a\,, s)\, u_c\,, \tag{3.4}$$

where we used the boldface for the index a in the last line to indicate that it is *not* summed over. The 1-loop contribution to the self-energy is given by the expression

$$\Sigma^{(1)}_{ac}(k;\, \eta_a\,, s) = \\ 4e^{\eta_a + s} \int d^3q\, \gamma_{ade}(\mathbf{k}, -\mathbf{q}, \mathbf{q}-\mathbf{k}) P^0(q) u_d u_f g_{eh}(\eta_a - s) \gamma_{hfc}(\mathbf{k}-\mathbf{q}, \mathbf{q}, -\mathbf{k})\,, \tag{3.5}$$

corresponding to the diagram in Fig. 3.1. Notice that the PS appearing in Eq. (3.5) is the linear one.

Now we will show, at large momentum, Eq. (3.4) holds. The first point to notice is that, as shown by CS in [39], the leading contributions at large k and at a fixed

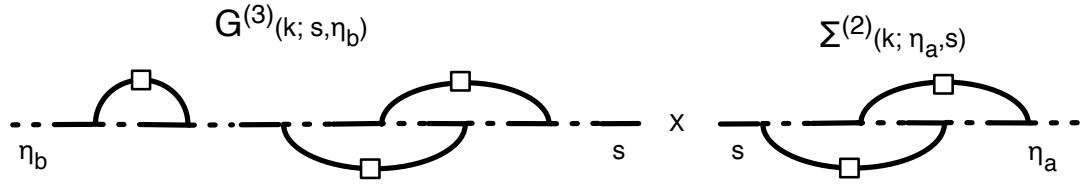

Figure 3.3: A 5-loop contribution to the sum of Eq. (3.4).

loop order n goes as k^{2n}, and is given by the chain-diagrams of Fig. 3.2. These diagrams are such that the $2n$ propagators are lined up in a single chain carrying the momentum k, and any of the n power spectra, carrying a lower momentum q_i, is connected to the propagator chain by both its legs. Each of the $2n$ vertices now contributes a factor

$$u_c \gamma_{acb}(\mathbf{k}\,, -\mathbf{q}\,, \mathbf{q}-\mathbf{k}) \stackrel{\text{large}\,k}{\longrightarrow} \frac{1}{2}\frac{\mathbf{k}\cdot\mathbf{q}}{q^2}\,\delta_{ab}\,, \tag{3.6}$$

where the u_c comes from the PS (see Eq. (3.7) below), giving the above mentioned $O(k^{2n})$ behavior. Since the linear propagators are momentum-independent, the integrals over the loop momenta decouple one another, each one giving a contribution proportional to the 1-loop 'self-energy',

$$\begin{aligned}
&\Sigma^{(1)}_{a_i b_i}(k;\, s_{a_i}, s_{b_i}) = \, 4\, e^{s_{a_i}+s_{b_i}} \int d^3q_i P(q_i) u_{c_i} u_{e_i} \,\times \\
&\gamma_{a_i c_i d_i}(\mathbf{k}, \mathbf{q}_i, -\mathbf{k}-\mathbf{q}_i) g_{d_i h_i}(s_{a_i} - s_{b_i}) \gamma_{h_i e_i b_i}(\mathbf{k}+\mathbf{q}_i, -\mathbf{q}_i, -\mathbf{k}) \\
&\stackrel{\text{large}\,k}{\longrightarrow} -k^2\sigma^2\, e^{s_{a_i}+s_{b_i}}\, g_{a_i b_i}(s_{a_i} - s_{b_i})\,,
\end{aligned} \tag{3.7}$$

where

$$\sigma^2 \equiv \frac{1}{3}\int d^3q \frac{P(q)}{q^2}\,, \tag{3.8}$$

and we have used Eq. (3.6).

Thanks to the composition property of the linear propagators

$$g_{ac}(\eta_a - \eta_c) g_{cb}(\eta_c - \eta_b) = g_{ab}(\eta_a - \eta_b)\,, \tag{3.9}$$

the chain of linear propagators emerging in the large k limit of (3.7) combine into a single one, $g_{ab}(\eta_a - \eta_b)$, independent of the intermediate times.

In order to discuss the time integrals, we consider a generic n-loop contribution to the sum (3.4) (see Fig. 3.3 for a 5-loop example). The 'self-energy' is a $n-j$ loop quantity and the propagator a j-loop one. Fixing the intermediate time s, the 'self-energy' diagram has thus $2(n-j)-2$ intermediate times, while the propagator has $2j$. The 'self-energy' time integrals give

$$\begin{aligned}&\int_s^{\eta_a} dt_1 \int_s^{t_1} dt_2 \cdots \int_s^{t_{2(n-j)-3)}} dt_{2(n-j)-2}\; e^{\eta_a + \sum_{i=1}^{2(n-j)-2} t_i} \\ &= \frac{e^{\eta_a}(e^{\eta_a} - e^s)^{2(n-j)-2}}{(2n-2j-2)!}\,.\end{aligned} \tag{3.10}$$

On the other hand, the propagator time integrals are

$$\int_{\eta_b}^{s} d\tau_1 \int_{\eta_b}^{\tau_1} d\tau_2 \cdots \int_{\eta_b}^{\tau_{2j-1}} d\tau_{2j}\; e^{\sum_{k=1}^{2j} \tau_k} = \frac{(e^s - e^{\eta_b})^{2j}}{(2j)!}\,. \tag{3.11}$$

Multiplying (3.10) by (3.11) and by the remainig e^s time factor, and then integrating over s from η_b to η_a, as in the LHS of (3.4) one gets the time coefficient

$$\frac{e^{\eta_a}(e^{\eta_a} - e^{\eta_b})^{2n-1}}{(2n-1)!}\,, \tag{3.12}$$

which is independent of j, *i.e.* is the same for any term in the sum in Eq. (3.4), and depends only on the total loop order, n. The sum over j ensures that the n power spectra are attached to the propagator chain in all possible ways, *i.e.* that all the pairings between the $2n$ vertices are taken into account. There are $(2n-1)!!$ such pairings, so, using Eqs. (3.7) and (3.12), we obtain the LHS of (3.4) in the large momentum limit,

$$\begin{aligned}&\frac{e^{\eta_a}(e^{\eta_a} - e^{\eta_b})^{2n-1}}{(2n-1)!}(2n-1)!!(-k^2\sigma^2)^n \\ &= \frac{1}{(n-1)!}\left[-k^2\sigma^2\frac{(e^{\eta_a} - e^{\eta_b})^2}{2}\right]^{n-1} (-k^2\sigma^2)e^{\eta_a}(e^{\eta_a} - e^{\eta_b})\end{aligned}$$

$$= \frac{1}{(n-1)!}\left[-k^2\sigma^2\frac{(e^{\eta_a}-e^{\eta_b})^2}{2}\right]^{n-1}\int_{\eta_b}^{\eta_a} ds\,\Sigma^{(1)}_{ac}(k;\,\eta_a,s)u_c\,. \qquad (3.13)$$

The contribution to the propagator from chain-diagrams at $(n-1)$-loop order can be computed straightforwardly, by using the same properties considered above [39]. The integration over the $2(n-1)$ intermediate times gives

$$\int_{\eta_b}^{\eta_a} dt_1\int_{\eta_b}^{t_1} dt_2\cdots\int_{\eta_b}^{t_{2n-3}} dt_{2n-2}e^{\sum_{i=1}^{2n-2}t_i} = \frac{(e^{\eta_a}-e^{\eta_b})^{2n-2}}{(2n-2)!}\,. \qquad (3.14)$$

Since there are $(2n-3)!!$ chain-diagrams at $n-1$ order, the propagator in the large k limit reads

$$G^{(n-1)}_{\mathbf{a}b}(k;\,\eta_a,\eta_b) \overset{\text{large } k}{\longrightarrow} \frac{1}{(n-1)!}\left[-k^2\sigma^2\frac{(e^{\eta_a}-e^{\eta_b})^2}{2}\right]^{n-1} g_{\mathbf{a}b}(\eta_a-\eta_b), \qquad (3.15)$$

which, comparing with the last line of (3.13), proves Eq. (3.4).

Hence we can sum Eq. (3.3) over n and we get the evolution equation for the full propagator in the large momentum limit

$$\begin{aligned}\partial_{\eta_a} G_{ab}(k;\,\eta_a,\eta_b) = &- \Omega_{ac}\,G_{cb}(k;\,\eta_a,\eta_b)\\ &+ G_{\mathbf{a}b}(k;\,\eta_a,\eta_b)\int_{\eta_b}^{\eta_a} ds\,\Sigma^{(1)}_{\mathbf{a}c}(k;\,\eta_a\,,s)\,u_c\,. \qquad (3.16)\end{aligned}$$

3.1.2 Factorization at small momentum

In the opposite limit, $k\to 0$, higher order contributions to the propagator are suppressed, and linear perturbation theory is recovered. In order to take into account the first non-linear corrections in this limit, one can truncate the series in (3.1) at $n=1$, *i.e.* at 1-loop order. Moreover, we will consider the evolution of the two combinations G_a, introduced in Eq. (2.53). Therefore, the relevant term in the sum of Eq. (3.3) in the small k limit is the one for $n=1$, namely,

$$\int_{\eta_b}^{\eta_a} ds\,\Sigma^{(1)}_{ac}(k;\,\eta_a\,,s)\,g_{cb}(s-\eta_b)u_b = \int_{\eta_b}^{\eta_a} ds\,\Sigma^{(1)}_{ac}(k;\,\eta_a\,,s)\,u_c\,, \qquad (3.17)$$

where we have used the property of the linear propagator,

$$g_{ab}(\eta)u_b = u_a\,. \tag{3.18}$$

Modulo terms at least of 2-loop order, the above expression can be rewritten as

$$G_{\mathbf{a}b}(k;\,\eta_a,\eta_b)\,u_b \int_{\eta_b}^{\eta_a} ds\,\Sigma^{(1)}_{\mathbf{a}c}(k;\,\eta_a\,,s)\,u_c\,, \tag{3.19}$$

which gives the same equation as the one for large k, Eq. (3.16), contracted by u_b [1].

3.1.3 Some considerations

It is remarkable that the same factorization holds in the two limits of large and small k. This result drive us to extend the factorization result for each momentum values. In the large momentum limit, one gets

$$\int_{\eta_b}^{\eta_a} ds\,\Sigma^{(1)}_{ac}(k;\,\eta_a\,,s)\,u_c \stackrel{\text{large k}}{\longrightarrow} -k^2\sigma^2\,e^{\eta_a}(e^{\eta_a}-e^{\eta_b})\,,\quad (\text{for } a=1,2)\,, \tag{3.20}$$

with the velocity dispersion

$$\sigma^2 \equiv \frac{1}{3}\int d^3q \frac{P^0(q)}{q^2}\,. \tag{3.21}$$

Inserting this in Eq. (3.16) and integrating in η_a reproduces the Gaussian decay of the large momentum propagator found by CS in Ref. [39],

$$G_{ab}(k;\,\eta_a,\eta_b)u_b = \exp\left(-k^2\sigma^2\frac{(e^{\eta_a}-e^{\eta_b})^2}{2}\right)\quad (\text{for } a=1,2)\,. \tag{3.22}$$

The solution of Eq. (3.16) at low k gives, by virtue of Eq. (3.17), the 1-loop propagator.

The above discussion clarifies the comparison between the present approach and

[1] If we do not contract by u_b, the factorization still holds exactly for the individual components of the propagator at small k if one takes the $\eta_b \to -\infty$ limit. For finite η_b, the factorization is not exact anymore, but it is anyway a very good approximation.

the one in [39]. Their result corresponds to the double approximation needed to pass from the exact equation (2.55) to the approximated one, Eq. (3.16), namely the factorization of the integral in Eq. (2.55),

$$\int_{\eta_b}^{\eta_a} ds\, \Sigma_{ac}(k;\, \eta_a\,, s)\, G_{cb}(k;\, s, \eta_b) \simeq G_{\mathbf{a}b}(k;\, \eta_a, \eta_b) \int_{\eta_b}^{\eta_a} ds\, \tilde{\Sigma}_{\mathbf{a}c}(k;\, \eta_a\,, s)\, u_c\,, \tag{3.23}$$

and the use of the purely 1-loop 'self-energy' in the factorized expression at the RHS above,

$$\tilde{\Sigma}_{\mathbf{a}c}(k;\, \eta_a\,, s) \simeq \Sigma^{(1)}_{\mathbf{a}c}(k;\, \eta_a\,, s)\,. \tag{3.24}$$

In the rest of this thesis, we will refer to the approximations considered in this section as the CS result and we will go beyond this approximation in a consistent way. We will keep the factorized form of the equation for any k, but will consider new contributions to the 'self-energy'. As we will show, this corresponds to resumming a larger class of diagrams than just the infinite chains considered by CS.

3.2 Closure theory propagator

In the closure theory we are concerned with approximated propagator evolution equation (2.89). The technique developed in the previous section is similar to that used by Taruya and Himaratsu [26]. They study this equation first in the large momentum limit and then in the small momentum limit and finally they analytically match the two solutions.

3.2.1 High momentum limit

We consider Eq. (2.89) in the large momentum limit where the vertex function behavior is described by Eq. (3.6). Moreover we further approximate the different-time power spectrum $P_{pr}(q;\eta,\eta'')$ with the linear order quantity obtaining a PS constant in time.

Taking advantage of these assumptions the governing equation for non-linear

propagator (2.89) is greatly simplified and we obtain

$$\widehat{\mathbf{\Lambda}}_{ab}(\eta)\; G_{bc}(k;\eta,\,\eta') = -(k\sigma)^2 \int_{\eta'}^{\eta} d\eta''\, G_{ab}(k;\eta,\,\eta'')\, G_{bc}(k;\eta'',\,\eta')\, e^{\eta+\eta''}, \qquad (3.25)$$

where the quantity σ is the velocity dispersion given by equation (3.21). The differential equations (3.25) can be solved analytically given the following ansatz

$$G_{ab}(k;\eta,\,\eta') = g_{ab}(\eta,\,\eta')\, f(k;\eta-\eta')$$

with the initial condition, $f(k;0) = 1$. Using the composition rules of the linear propagator Eq. (3.9) we have to solve

$$\frac{\partial}{\partial\tau} f(k;\tau) = -(k\sigma)^2 \int_0^{\tau} d\tau'\, f(k;\tau-\tau')\, f(k;\tau'). \qquad (3.26)$$

Here, for convenience, we introduced the new time variable $\tau = e^{\eta} - e^{\eta'}$. By involving the Laplace transform technique one gets

$$f(k;\tau) = \frac{J_1(2x)}{x}\,; \qquad x = k\,\sigma\,\tau \qquad (3.27)$$

where $J_1(x)$ is a Bessel function of the first kind.

Finally we have the analytical expression for the propagator in the high-k limit:

$$G_{ab}(k;\eta,\,\eta') = g_{ab}(\eta,\,\eta')\, \frac{J_1(2k\sigma(e^{\eta}-e^{\eta'}))}{k\sigma(e^{\eta}-e^{\eta'})}\,. \qquad (3.28)$$

As expected the functional form of the propagator is different from the CS propagator. Indeed Eq. (2.89) does not take into account all the chain diagrams considered by CS since here we are not renormalizing the vertex.

3.2.2 The small-k limit: the one-loop solution

The closure theory reproduce, in a consistent way, the one-loop result for the propagator. To achieve this result in the RHS of Eq. (2.89) we take the linear propagator and the linear power spectrum instead of the full functions. After these substitutions

the one-loop correction to the propagator is

$$G^{(1)}_{ab}(k,\eta,\eta') = 4\int_{\eta'}^{\eta} d\eta_1\, e^{\eta_1}\; g_{ac}(\eta,\eta_1) \int_{\eta'}^{\eta_1} d\eta_2\, e^{\eta_2} \int d^3\mathbf{q}\; \gamma_{cpq}(-\mathbf{k},\mathbf{q},\mathbf{k}-\mathbf{q}) \times\gamma_{lrs}(\mathbf{q}-\mathbf{k},-\mathbf{q},\mathbf{k})\, g_{ql}(\eta_1,\eta_2)\, P^0_{pr}(q;\eta_1,\eta_2)\, g_{sb}(\eta_2,\eta')\,. \tag{3.29}$$

In the large scale limit, where the linear theory still works, this is a good approximation for the propagator computation (as explained in the previous section).

Following CS, the one-loop results on the propagator can be written down in the following way:

$$G^{(1)}_{ab}(k;\eta,\eta') = \frac{1}{5}\begin{pmatrix} 3\,X_{11} & 2\,X_{12} \\ 3\,X_{21} & 2\,X_{22} \end{pmatrix} + \frac{e^{-(5/2)(\eta-\eta')}}{5}\begin{pmatrix} 2\,Y_{11} & -2\,Y_{12} \\ -3\,Y_{21} & 3\,Y_{22} \end{pmatrix}, \tag{3.30}$$

where the matrices X_{ab} and Y_{ab} are given by

$$\begin{aligned} X_{ab} &= e^{2\eta'}\begin{pmatrix} \alpha(\eta-\eta')f(k) - \beta_g(\eta-\eta')i(k) & \alpha(\eta-\eta')f(k) - \beta_g(\eta-\eta')h(k) \\ \alpha(\eta-\eta')g(k) + \gamma_g(\eta-\eta')h(k) & \alpha(\eta-\eta')g(k) - \dfrac{3}{2}\,\gamma_g(\eta-\eta')i(k) \end{pmatrix}, \\ Y_{ab} &= e^{2\eta'}\begin{pmatrix} \delta(\eta-\eta')g(k) - \gamma_d(\eta-\eta')h(k) & \delta(\eta-\eta')f(k) - \gamma_d(\eta-\eta')h(k) \\ \delta(\eta-\eta')g(k) + \beta_d(\eta-\eta')i(k) & \delta(\eta-\eta')f(k) - \dfrac{2}{3}\,\beta_d(\eta-\eta')h(k) \end{pmatrix}. \end{aligned} \tag{3.31}$$

The explicit expressions of the functions used above are here reported. First of all we give the time dependent ones:

$$\begin{aligned} \alpha(\eta) &= e^{2\eta} - \frac{7}{5}\,e^{\eta} + \frac{2}{5}\,e^{-3\eta/2}, \\ e^{\eta}\beta_g(\eta) &= e^{-3\eta/2}\beta_d(\eta) = \frac{3}{5}\,e^{2\eta} - e^{\eta} + \frac{2}{5}\,e^{-\eta/2}, \\ e^{\eta}\gamma_g(\eta) &= e^{-3\eta/2}\gamma_d(\eta) = \frac{2}{5}\,e^{2\eta} - e^{\eta/2} + \frac{3}{5}\,e^{-\eta/2}, \\ \delta(\eta) &= \frac{2}{5}\,e^{7\eta/2} - \frac{7}{5}\,e^{\eta} + 1. \end{aligned}$$

Further, we list the explicit expressions for the scale-dependent functions f, g, h

and i:

$$
\begin{aligned}
f(k) &= \frac{1}{504}\int\frac{\mathrm{d}^3\mathbf{q}}{k^3q^5}\Big\{6k^7q-79k^5q^3+50k^3q^5-21kq^7 \\
&\qquad +\frac{3}{4}\left(k^2-q^2\right)^3\left(2k^2+7q^2\right)\ln\left|\frac{k-q}{k+q}\right|^2\Big\}P^0(q), \\
g(k) &= \frac{1}{168}\int\frac{\mathrm{d}^3\mathbf{q}}{k^3q^5}\Big\{6k^7q-41k^5q^3+2k^3q^5-3kq^7 \\
&\qquad +\frac{3}{4}(k^2-q^2)^3\left(2k^2+q^2\right)\ln\left|\frac{k-q}{k+q}\right|^2\Big\}P^0(q), \\
h(k) &= \frac{1}{24}\int\frac{\mathrm{d}^3\mathbf{q}}{k^3q^5}\Big\{6k^7q+k^5q^3+9kq^7 \\
&\qquad +\frac{3}{4}(k^2-q^2)^2\left(2k^4+5k^2q^2+3q^4\right)\ln\left|\frac{k-q}{k+q}\right|^2\Big\}P^0(q), \\
i(k) &= -\frac{1}{72}\int\frac{d^3\mathbf{q}}{k^3q^5}\Big\{6k^7q+29k^5q^3-18k^3q^5+27kq^7 \\
&\qquad +\frac{3}{4}(k^2-q^2)^2\left(2k^4+9k^2q^2+9q^4\right)\ln\left|\frac{k-q}{k+q}\right|^2\Big\}P^0(q).
\end{aligned}
$$

3.2.3 Matching analytically the two limit solutions

We are looking for an analytical expression that reproduces the results of the sections 3.2.1 and 3.2.2 respectively in the large and small momentum limit. This procedure should give us a good approximation for the full propagator. The propagator computed up to one-loop order shows the following behavior in the high-k limit

$$
g_{ab}(\eta,\eta')+G^{(1)}_{ab}(k;\eta,\eta') \;\stackrel{k\to\infty}{\longrightarrow}\; g_{ab}(\eta,\eta')\left\{1-\frac{1}{2}\left(k\,\sigma\right)^2 e^{2(\eta+\eta')}\right\},
$$

where we have only considered the dominant terms at $\eta\to\infty$. On the other hand we can further expand Eq. (3.28) in the large momentum limit and we obtain

$$
G_{ab}(k;\eta,\eta') \;\simeq\; g_{ab}(\eta,\eta')\left\{1-\frac{x^2}{2}+\cdots\right\}\;;\quad x=k\,\sigma_{\rm v}\,(e^{\eta}-\eta^{\eta'}).
$$

Comparing these two expressions, the approximate solution smoothly matching these asymptotic behaviors at $\eta \to \infty$ may be

$$G_{ab}^{\rm approx}(k;\eta,\eta') = \frac{e^{\eta-\eta'}}{5}\begin{pmatrix} 3\,P_{11} & 2\,P_{12} \\ 3\,P_{21} & 2\,P_{22} \end{pmatrix} + \frac{e^{-(3/2)(\eta-\eta')}}{5}\begin{pmatrix} 2\,Q_{11} & -2\,Q_{12} \\ -3\,Q_{21} & 3\,Q_{22} \end{pmatrix} \quad (3.32)$$

Here, the matrices P_{ab} and Q_{ab} are defined as

$$P_{ab} = \frac{J_1(2\widetilde{X}_{ab})}{\widetilde{X}_{ab}}, \qquad Q_{ab} = \frac{J_1(2\widetilde{Y}_{ab})}{\widetilde{Y}_{ab}} \quad (3.33)$$

with $\widetilde{X}_{ab} \equiv |2X_{ab}|^{1/2}$ and $\widetilde{Y}_{ab} \equiv |2Y_{ab}|^{1/2}$. In the weakly non-linear regime, the propagator $G_{ab}^{\rm approx}$ correctly reproduces the one-loop results. In the large-k limit, the function (3.32) asymptotically approaches the solution (3.28).

The procedure followed to find out an analytical approximated expression for the propagator is closed to that implemented by CS in [39]. The main difference is that here we have a damping oscillation while in CS propagator we have a exponential behavior. This is due basically to the lack of the vertex renormalization of this approach.

3.3 Multi-point propagators: re-summation at large momentum

As it was presented in the Section 2.4, the multi-point propagators approach seems not really attractive, but an interesting result about a re-summation scheme was found in [30]. This allows to implement a kind of re-rummation scheme also in the power spectrum computation. In this section we will summarize the main results achieved in [30]. They have been computed assuming Gaussian initial conditions.

So far there is no way to analytically interpolate between the large and small momentum limit solutions. Hence we will do that giving a prescription.

In order to explain the large momentum computation we have to identify which are the dominant diagrams in this limit. The idea is really similar to that used

with the two-point propagator in Section 3.1, where we have considered the "chain diagrams". Here, instead of a "propagator chain", we have a "propagator chains tree" (see Fig. 3.4): each branch of the diagrams is a propagator chain and each power spectrum is connected to the "propagator chains tree" by both its legs. When the whole propagator chains tree is in the high-k limit we have that these diagrams are dominant for the same reasons explained for the two-point propagator in Section 3.1. Note that at a given order different diagrams may have different propagator chains tree (Fig. 3.5). We will call "tree chain diagrams" these diagrams.

In the large-k limit the three-point propagator $\tilde{\Gamma}^{(2)}$ defined in Eq. (2.60) is given by the sum over the whole set of dominant loop diagrams,

$$\tilde{\Gamma}^{(2)}_{abc} = \sum_{n\geq 0} \tilde{\Gamma}^{(2)}_{abc,\ \mathrm{n-loops}}\,. \tag{3.34}$$

Computing the one-loop three-point propagator one gets [2]

$$\tilde{\Gamma}^{(2)}_{abc,\ \mathrm{1loop}} = -\frac{k_3^2\,\sigma_v^2}{2}\ \tilde{\Gamma}^{(2)}_{abc,\ \mathrm{tree}}\ \left(e^{\eta_a}-1\right)^2. \tag{3.35}$$

where $\tilde{\Gamma}^{(2)}_{abc,\ \mathrm{tree}}$ is $\tilde{\Gamma}^{(2)}$ computed at tree level, k_3 is the momentum and η_a is the time of the external field φ_a. With a lengthy calculation it is possible to compute the three-point propagator at n-loop order and then sum over n. We are left with this result

$$\tilde{\Gamma}^{(2)}_{abc} = \exp\left(-\frac{\sigma^2 k_3^2}{2}\left(e^{\eta_a}-1\right)^2\right)\ \tilde{\Gamma}^{(2)}_{abc,\mathrm{tree}}\,. \tag{3.36}$$

Following the same lines used for the three-point propagator it is possible to show that the results can be extended to $\tilde{\Gamma}^{(p)}$. So we have

$$\tilde{\Gamma}^{(p)} = \exp\left(-\frac{k_p^2\sigma^2}{2}(e^{\eta_a}-1)^2\right)\ \tilde{\Gamma}^{(p)}_{\mathrm{tree}}\,. \tag{3.37}$$

This result shows that the multipoint propagators decay with the same rate as the two point propagator in the large-k limit and are proportional to their tree-level

[2] Taking advantage of the property (3.6).

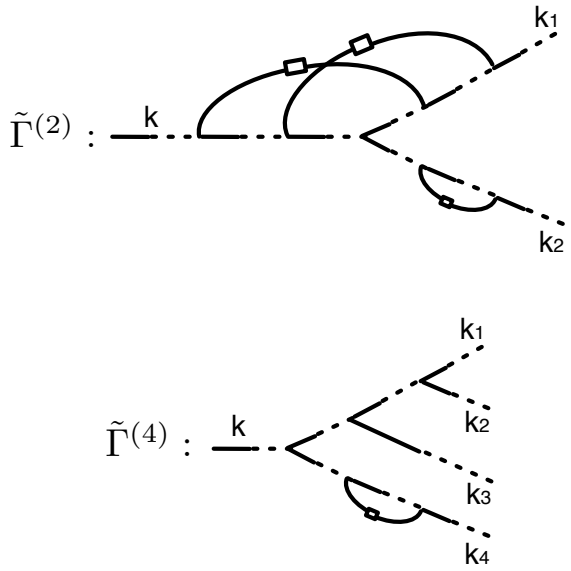

Figure 3.4: "Propagator chains tree": examples of dominant loop corrections for tree-point (on top) and five-point (on bottom) propagator.

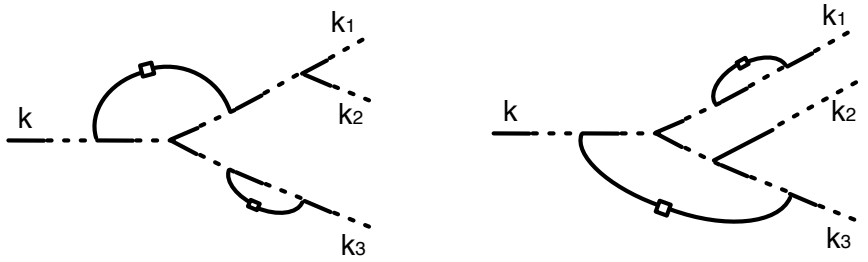

Figure 3.5: Multi-point propagators exhibits different propagator chains trees. This is an example for the four-point propagator.

values. Furthermore, to compute $\tilde{\Gamma}$ for each k value we will use this prescription

$$\tilde{\Gamma}^{(p)} = \frac{\tilde{\Gamma}^{(1)}(k_p)}{\tilde{\Gamma}^{(1)}_{\rm tree}(k_p)}\ \tilde{\Gamma}^{(p)}_{\rm tree}, \tag{3.38}$$

which reduces to Eq. (3.37) in the high-k limit, and approximately incorporates (through the full scale-dependence of the two-point propagator $\Gamma^{(1)}$ explained in Section (3.1)) the fact that at low-k propagators decay slower than their high-k limit.

3.4 Extended factorization: the renormalized chain-diagrams

In this section we will explain a new remarkable result: we show that, taking advantage of the suitable properties of the propagator evolution equation (2.55), the large-k factorization property, Eq. (3.4), holds for a more general class of diagrams than the 'chain'-ones discussed by CS. More specifically, here we show that by replacing all the linear power spectra, $P^0_{ab}(q) = P^0(q)u_a u_b$, appearing in the chain-diagrams by a – for now – generic *non-linear* PS, of the form $P^{\rm nl}_{ab}(q; s_a, s_b)$, one still gets the property (3.23) in the large-k limit, where now,

$$\tilde{\Sigma}_{\mathbf{a}c}(k;\, \eta_a\,, s) \simeq \Sigma^{\rm PSnl}_{\mathbf{a}c}(k;\, \eta_a\,, s)\,. \tag{3.39}$$

$\Sigma^{\rm PSnl}_{\mathbf{a}c}$ is obtained from the 1-loop self-energy by replacing P^0_{ab} by $P^{\rm nl}_{ab}$, as indicated in the diagram in Fig. 3.6.

3.4.1 High momentum limit: exact factorization

The factorization property [3],

$$\sum_{j=0}^{n-1} \int_{\eta_b}^{\eta_a} ds\, \Sigma^{(n-j)}_{ac}(k;\, \eta_a\,, s)\, G^{(j)}_{cb}(k;\, s, \eta_b)$$

[3] Now the upper indices count the number of non-linear PS in a given contribution to Σ and G.

$$\stackrel{\text{large } k}{\longrightarrow} G^{(n-1)}_{\mathbf{a}b}(k;\,\eta_a,\eta_b)\int_{\eta_b}^{\eta_a} ds\,\Sigma^{\rm PSnl}_{\mathbf{a}c}(k;\,\eta_a\,,s)u_c\,, \tag{3.40}$$

can be proved also if one considers a generic form for the non linear PS, *i.e.*

$$P^{\rm nl}_{ab}(q;s_a,s_b) = P^{\rm nl}_{ba}(q;s_b,s_a)\,, \tag{3.41}$$

and therefore it holds if one renormalizes the linear PS by including non-linearities in different consistent approximations, such as, perturbation theory, TRG, and so on.

The starting point is to realize that the LHS of Eq. (3.40) is obtained by pairing in all possible ways the $2n$ vertices – including the extremal one at time η_a – connected by the chain of $2n$ propagators. Moreover, the large momentum property of the vertex, Eq. (3.6), still holds if it is contracted by a generic vector A_a, giving

$$A_c\gamma_{acb}(\mathbf{k}\,,-\mathbf{q}\,,\mathbf{q}-\mathbf{k}) \stackrel{\text{large } k}{\longrightarrow} A_2\,\frac{1}{2}\frac{\mathbf{k}\cdot\mathbf{q}}{q^2}\,\delta_{ab}\,. \tag{3.42}$$

Therefore, in the large k limit, we have

$$\begin{aligned}
&\sum_{j=0}^{n-1}\int_{\eta_b}^{\eta_a} ds\,\Sigma^{(n-j)}_{ac}(k;\,\eta_a\,,s)\,G^{(j)}_{cb}(k;\,s,\eta_b)\\
&\stackrel{\text{large } k}{\longrightarrow}\left(\frac{-k^2}{3}\right)^n\int_{\eta_b}^{\eta_a} ds_1\int_{\eta_b}^{s_1} ds_2\cdots\int_{\eta_b}^{s_{2n-2}} ds_{2n-1}\left(\int\Pi_{i=1}^n d^3q_i\right)\times\\
&e^{\eta_a+\sum_{i=1}^{2n-1}s_i}\sum_{2n\,\text{pairings}}\frac{P^{\rm nl}_{22}(q_1;\eta_a,s_{a_1})}{q_1^2}\cdots\frac{P^{\rm nl}_{22}(q_n;s_{a_{2n-2}},s_{a_{2n-1}})}{q_n^2}\,.
\end{aligned} \tag{3.43}$$

Notice that the time-integrand is, by construction, invariant under the exchange of any of the $2n-1$ variables, $s_i \leftrightarrow s_j$, therefore we will use the property

$$\begin{aligned}
&\int_{\eta_b}^{\eta_a} ds_1\int_{\eta_b}^{s_1} ds_2\cdots\int_{\eta_b}^{s_{N-1}} ds_N\,\mathcal{F}[s_1,\cdots,s_N] =\\
&\qquad\qquad\frac{1}{N!}\int_{\eta_b}^{\eta_a} ds_1\int_{\eta_b}^{\eta_a} ds_2\cdots\int_{\eta_b}^{\eta_a} ds_N\,\mathcal{F}[s_1,\cdots,s_N]\,,
\end{aligned} \tag{3.44}$$

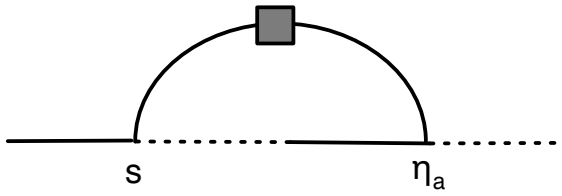

Figure 3.6: $\Sigma^{\rm PSnl}_{ac}(k;\,\eta_a\,,s)$: 1-loop self-energy with the insertion of the non linear PS.

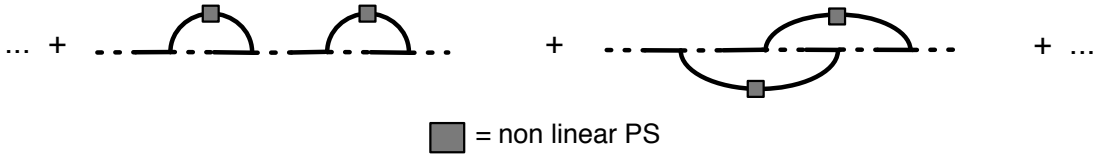

Figure 3.7: Renormalized chain-diagrams.

where the function $\mathcal{F}[s_1,\cdots,s_N]$ is totally symmetric. Eq. (3.43) can then be rewritten as

$$\left(\frac{-k^2}{3}\right)^n \frac{1}{(2n-1)!}\int_{\eta_b}^{\eta_a} ds_1 \int_{\eta_b}^{\eta_a} ds_2 \cdots \int_{\eta_b}^{\eta_a} ds_{2n-1} \left(\int \Pi_{i=1}^{n} d^3q_i\right) \times$$
$$e^{\eta_a+\sum_{i=1}^{2n-1} s_i} \sum_{2n\,\text{pairings}} \frac{P_{22}^{\rm nl}(q_1;\eta_a,s_{a_1})}{q_1^2}\cdots\frac{P_{22}^{\rm nl}(q_n;s_{a_{2n-2}},s_{a_{2n-1}})}{q_n^2} =$$
$$\left(\frac{-k^2}{3}\right)\int_{\eta_b}^{\eta_a} ds\, e^{\eta_a+s}\int d^3q \frac{P_{22}^{\rm nl}(q;\eta_a,s)}{q^2}\times$$
$$\left[\left(\frac{-k^2}{3}\right)^{n-1}\frac{1}{(2n-2)!}\int_{\eta_b}^{\eta_a} ds_1 \int_{\eta_b}^{\eta_a} ds_2 \cdots \int_{\eta_b}^{\eta_a} ds_{2n-2} \left(\int \Pi_{i=1}^{n-1} d^3q_i\right)\times\right.$$
$$\left. e^{\sum_{i=1}^{2n-2} s_i} \sum_{2n-2\,\text{pairings}} \frac{P_{22}^{\rm nl}(q_1;s_{a_1},s_{a_2})}{q_1^2}\cdots\frac{P_{22}^{\rm nl}(q_{n-1};s_{a_{2n-3}},s_{a_{2n-2}})}{q_{n-1}^2}\right], \tag{3.45}$$

which, multiplied by $g_{ab}(\eta_a-\eta_b)$, gives the RHS of (3.40) (see also (3.7) and (3.15)).

So, in the large momentum limit, we are left with

$$\begin{aligned}\partial_{\eta_a} G_{ab}(k;\,\eta_a,\eta_b) = &- \Omega_{ac}\, G_{cb}(k;\,\eta_a,\eta_b) \\ &+ G_{\mathbf{a}b}(k;\,\eta_a,\eta_b)\int_{\eta_b}^{\eta_a} ds\,\tilde{\Sigma}_{\mathbf{a}c}(k;\,\eta_a\,,s)\,u_c\,,\end{aligned} \tag{3.46}$$

where the limit of $\Sigma^{\rm PSnl}_{\mathbf{a}c}$ is given by

$$\int_{\eta_b}^{\eta_a} ds\,\Sigma^{\rm PSnl}_{\mathbf{a}c}(k;\,\eta_a\,,s)u_c \overset{\text{large } k}{\longrightarrow} \left(\frac{-k^2}{3}\right)\int_{\eta_b}^{\eta_a} ds\,e^{\eta_a+s}\int d^3q\frac{P^{\rm nl}_{22}(q;\eta_a,s)}{q^2}\,. \tag{3.47}$$

The differential equation (3.46) can be easily addressed and it results in

$$G_{ab}(k;\,\eta_a,\eta_b)u_b = \exp\left(-k^2\sigma^2_{\rm nl}(\eta_a,\eta_b)\frac{(e^{\eta_a}-e^{\eta_b})^2}{2}\right)\quad(\text{for } a=1,2)\,, \tag{3.48}$$

where

$$\sigma^2_{\rm nl}(\eta_a,\eta_b)\frac{(e^{\eta_a}-e^{\eta_b})^2}{2} \equiv \frac{1}{3}\int_{\eta_b}^{\eta_a} ds_1\int_{\eta_b}^{s_1} ds_2\,e^{s_1+s_2}\int d^3q\frac{P^{\rm nl}_{22}(q;s_1,s_2)}{q^2}\,. \tag{3.49}$$

The effect of the inclusion of these subleading corrections is clear: at large momenta the propagator still decays exponentially, but with the decay law of Eq. (3.22) replaced by Eq. (3.48). Notice that only the "22" (*i.e.* velocity-velocity) component of the PS appears in the exponential above. Since it is known that this component receives negative corrections at the non-linear level, (see, for instance, [28, 32]), we expect that the improved propagator will be enhanced w.r.t the CS one at large k.

3.4.2 The small momentum limit: how to recover the linear theory

In the opposite limit, $k \to 0$, we are no longer guaranteed that Eq. (3.39) is still a good approximation, and that the contributions to the $\tilde{\Sigma}_{ac}$ obtained by replacing the linear PS with the non-linear one are the only leading ones. A powerful guiding criterium in this regard is the requirement that linear theory is recovered for small momenta. Indeed, from the exact equations (2.50) and (2.54), one concludes that,

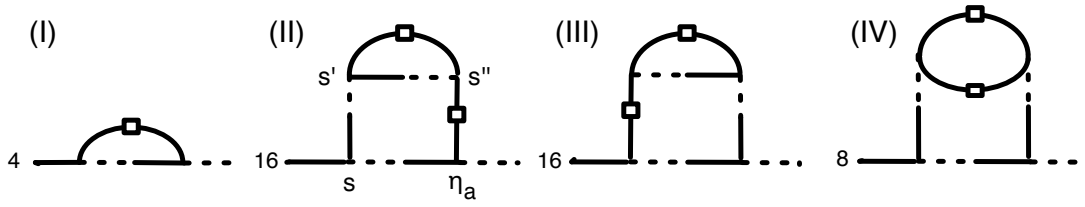

Figure 3.8: $\Sigma^{\rm PS1l}_{ac}(k;\,\eta_a\,,s)$: the self-energy with the insertion of the PS up to 1-loop order.

in order to have $G_{ab}(k;\eta_a,\eta_b)\to g_{ab}(\eta_a-\eta_b)$ as $k\to 0$ the 'self-energy' has to vanish in this limit

$$\Sigma_{ab}(k;\,\eta_a,\,s)\stackrel{k\to 0}{\longrightarrow}0\,, \tag{3.50}$$

therefore, by virtue of Eq. (3.23), we should also have $\tilde{\Sigma}_{ac}(k;\,\eta_a\,,s)$ vanishing for $k\to 0$. In the approximation (3.39) this is not automatically realized. Indeed, one finds

$$\begin{aligned}&\int_{\eta_b}^{\eta_a} ds\,\Sigma^{\rm PSnl}_{ac}(k;\,\eta_a\,,s)\,u_c\stackrel{k\to 0}{\longrightarrow}\\ &\frac{1}{3}\delta_{a1}\int_{\eta_b}^{\eta_a} ds\,e^{\eta_a+s}\int d^3q\left[g_{2d}(\eta_a-s)P^{\rm nl}_{1d}(q;\eta_a,s)-g_{1d}(\eta_a-s)P^{\rm nl}_{2d}(q;\eta_a,s)\right].\end{aligned} \tag{3.51}$$

Of course, if one puts back the linear PS, $P^0_{ab}=P^0u_au_b$, in place of $P^{\rm nl}_{ab}$ in the expression above, one recovers the 1-loop self-energy, which vanishes in the $k\to 0$ limit as can be directly checked from Eq. (3.51), using Eq. (3.18) (the first non-vanishing contribution goes as k^2).

On the other hand, moving a step further and using the 1-loop result for $P^{\rm nl}_{ab}$, namely, including the diagrams of Fig. 3.8 in the computation of the self-energy, one finds a non-vanishing limit for $k\to 0$. Indeed, one can check that the contributions from the remaining 2-loop diagrams listed in Fig. 3.9 exactly cancel those of Fig. 3.8, recovering in this way the physical requirement of Eq. (3.50).

At large k the contributions V and VI in Fig. 3.9 would give rise to chain-diagrams for the propagator with the insertion of a linear PS. These contributions are already taken into account by diagram I in Fig. 3.8, so, in order to avoid double

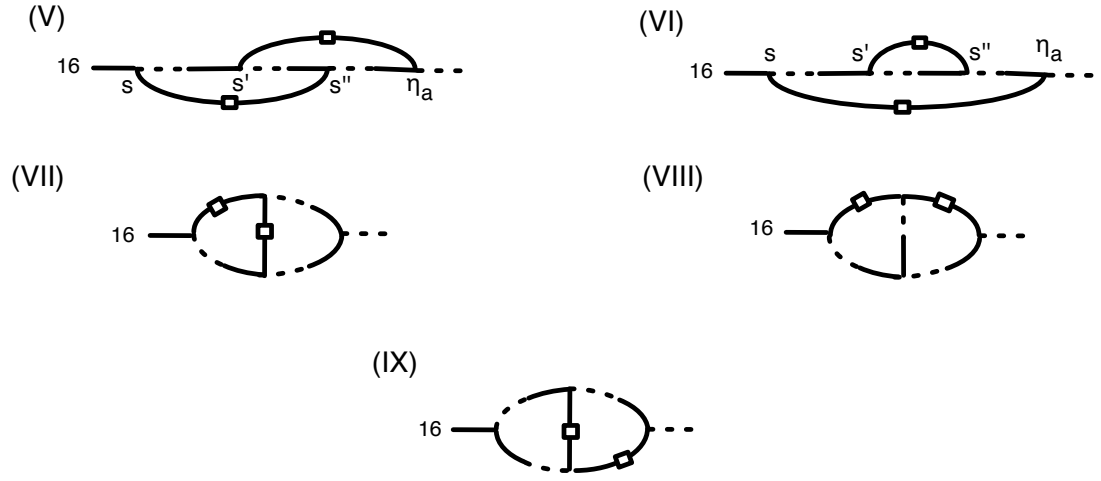

Figure 3.9: $\Sigma_{ac}^{2\mathrm{l}_{\mathrm{rest}}}$: the 2-loop contributions to the self-energy not included in $\Sigma_{ac}^{\mathrm{PS1l}}$.

counting, we do not have to include them. The remaining diagrams, VII-IX, are subdominant at large k w.r.t. the chain-diagrams. On the other hand, at small k, all the diagrams in Fig. 3.9 are essential in order to recover linear theory. Therefore, an approximation to $\tilde{\Sigma}_{ac}$ giving the '1-loop renormalized' chain-diagrams (*i.e.* the chain-diagrams with the 1-loop PS replacing the linear one) in the large k limit, and recovering linear theory for $k \to 0$, is given by

$$\begin{aligned} \tilde{\Sigma}_{ac}(k;\,\eta_a\,,s) &\simeq \Sigma_{ac}^{\mathrm{PS1l}}(k;\,\eta_a\,,s) + \lim_{k\to 0}\Sigma_{ac}^{2\mathrm{l}_{\mathrm{rest}}}(k;\,\eta_a\,,s) \\ &= \Sigma_{ac}^{\mathrm{PS1l}}(k;\,\eta_a\,,s) - \lim_{k\to 0}\Sigma_{ac}^{\mathrm{PS1l}}(k;\,\eta_a\,,s)\,, \end{aligned} \tag{3.52}$$

where $\Sigma_{ac}^{\mathrm{PS1l}}$ and $\Sigma_{ac}^{2\mathrm{l}_{\mathrm{rest}}}$ are the contributions to the self-energy computed from the diagrams of Figs. 3.8 and 3.9, respectively.

A further extension of the resummation program is to use as non-linear PS in the computation of $\Sigma_{ac}^{\mathrm{PSnl}}$ the one computed with the Time Renormalization Group (TRG) approach introduced in [28] and briefly reviewed in Section 2.6. As discussed in [28], the TRG equations, truncated at the bispectrum level, incorporate perturbative corrections in which the PS lines are iteratively replaced by their 1-loop corrections. This procedure resums perturbative contributions at all orders, of which some 3 and 4-loop examples are listed in Fig. 3.10. The TRG approach is

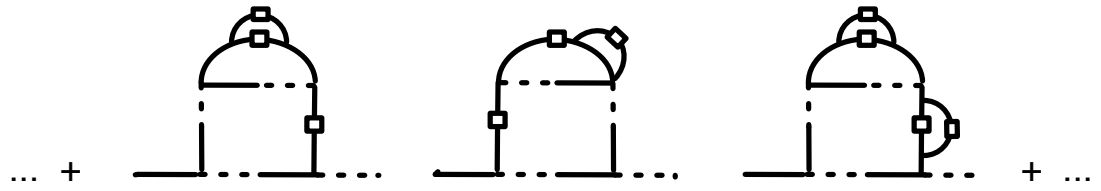

Figure 3.10: Some of the contributions included in $\tilde{\Sigma}_{ab}$ when the non-linear PS is given by the one computed via the TRG.

able to reproduce the non-linear PS at $z = 0$ up to $k \lesssim 0.2$ h/Mpc (that is, in the BAO region) at the few percent level [28, 42].

The TRG, as it is, gives the non-linear PS computed at equal times, that is $P_{ab}^{\rm TRG}(q;\eta,\eta)$. On the other hand, in the computation of the self-energy, we need the PS computed at different times, see Eqs. (3.47, 3.51). The relation between the equal-times PS and the one computed at different times can be read from Eq. (2.51), where we can now take the initial time to be any generic time, s. When dealing with $P_{ab}^{\rm TRG}(q;\eta_a,s)$ we will therefore replace it by

$$P_{ab}^{\rm TRG}(q;\eta_a,s) \simeq G_{ac}^{CS}(q;\eta_a,s) P_{cb}^{\rm TRG}(q;s,s)\,, \tag{3.53}$$

where, for practical reasons, we have replaced the full propagator with, G_{ac}^{CS}, the propagator computed à la Crocce-Scoccimarro according to the approximation discussed in Section 3.1.

As in the computation of the $\Sigma_{ac}^{\rm PS1l}$, we find a non-vanishing $k \to 0$ limit for the self-energy computed with $P^{\rm TRG}$. We follow the same arguments discussed above and, also in this case, we incorporate the relevant corrections in this limit by using the prescription

$$\tilde{\Sigma}_{ac}(k;\,\eta_a\,,s) \simeq \Sigma_{ac}^{P^{\rm TRG}}(k;\,\eta_a\,,s) - \lim_{k\to 0} \Sigma_{ac}^{P^{\rm TRG}}(k;\,\eta_a\,,s)\,. \tag{3.54}$$

3.4.3 Final evolution equation

To summarize the results of this section, the evolution equation for the propagator including next-to-leading corrections (the renormalized chain-diagrams plus the

contributions needed to recover the proper $k \to 0$ limit) is given by

$$\begin{aligned} \partial_{\eta_a} G_{ab}(k;\, \eta_a, \eta_b) = & - \Omega_{ac}\, G_{cb}(k;\, \eta_a, \eta_b) \\ & + G_{\mathbf{a}b}(k;\, \eta_a, \eta_b) \int_{\eta_b}^{\eta_a} ds\, \tilde{\Sigma}_{\mathbf{a}c}(k;\, \eta_a\,, s)\, u_c\,, \end{aligned} \tag{3.55}$$

which we will solve for any scale k using the two approximations, Eqs. (3.52) and (3.54), for the self-energy $\tilde{\Sigma}_{ac}$.

Chapter 4

From nonlinear propagator to nonlinear power spectrum

In the current accepted cosmological model, the structures grow through a process of gravitational instabilities driven by fluctuations in the dark matter distribution. Following the physical laws governing this evolution, we achieve a model where the structures form in a hierarchical way. This means that the small scale perturbations collapse first and the large scale perturbations collapse later. One of the main observable object that encodes informations on these nonlinear gravitational processes is the mass power spectrum, $P(k)$, the Fourier transform of the two-point correlations function. As we approach to smaller scale, the power spectrum exhibits a higher growth with respect to its linear value showing the nonlinear behavior of the gravitational instabilities.

Achieving an exhaustive comprehension of this nonlinear features is one of the crucial task of the structures formation study. The analytical or semi-analytical description of these effects may be our best opportunity to establish stronger constraints in the value of the cosmological parameters and to deeper investigate the nature of the gravitational collapse.

More specifically, it has become increasingly important to combine the results coming from the cosmic microwave background with constraints taken from other observable quantities. In particular, an excellent probe of cosmological fluctuations

consists in measuring the power spectrum of large-scale structures (LSS), as demonstrated successfully by *Sloan Digital Sky Surveys* (SDSS) that has measured the Baryonic Acoustic Oscillations [43, 44]. Furthermore the CMB data analysis shows a degeneracy among some cosmological parameters [45] that can be broken by LSS constraints. With the help of these inputs most of the cosmological parameters can be constrained to better that a few percent accuracy.

From the theory point of view, hence, the goal is the prediction of the power spectrum. In the large-scale structures case, the nonlinearities make this subject a very difficult task. However, in the last years, new promising semi-analytical approaches to the PS computation have been developed and compared to N-Body simulations in the Baryon Acoustic Oscillations range of scales [21, 22, 23, 24, 25, 27, 28, 29, 46, 31, 32, 33, 35]. These methods have been applied also to less standard – although interesting – cosmological scenarios [47, 48, 49, 50] and models with various types of primordial non-Gaussianity [37, 51, 34]. We select the main scenarios and briefly review the analytical techniques developed to reach increasing accuracy.

4.1 Renormalized perturbation theory: the power spectrum

In the contest of renormalized perturbation theory Crocce and Scoccimarro [20, 25], leveraging again on results of turbulence theory, propose a method to compute the nonlinear power spectrum. Here we summarize the analytical result that they got on this computation.

As starting point we consider the equation for the full power spectrum achieved in Chapter (2), namely Eq. (2.47) that we report here

$$\begin{aligned} P_{ab}(k;\eta,\eta) &= G_{ac}(k;\eta,0)G_{bd}(k;\eta,0)P^0_{cd}(k) \\ &\quad + \int_0^\eta ds_1 \int_0^\eta ds_2\, G_{ac}(k;\eta,s_1)G_{bd}(k;\eta,s_2)\Phi_{cd}(k;s_1,s_2)\,. \end{aligned} \tag{4.1}$$

In order to obtain a computable equation from (4.1) we need to find out an approx-

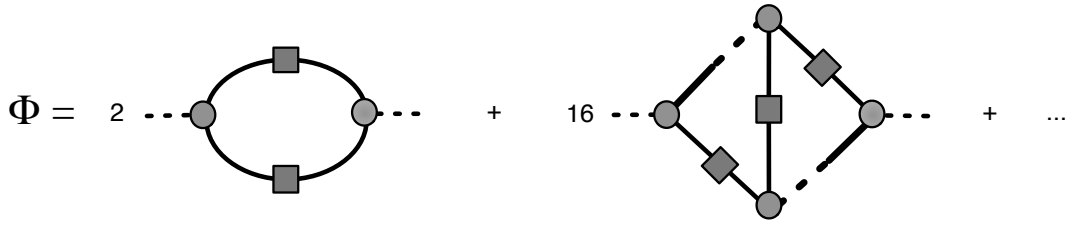

Figure 4.1: Renormalized diagrams for Φ.

imated expression for the full propagator and for the Φ_{ab} function.

To deal with the 1PI function we note that, at least up to two loop order, the series of diagrams of this 1PI function can be reorganized substituting the full power spectrum, the full propagator and the full vertex in place of the linear ones. We call these new objects "renormalized digrams". Following this procedure, to avoid double counting, the number of diagrams inevitably decrease and the graphical representation of Φ_{ab} results simplified. Therefore we are left with the two renormalized diagrams drawn in Fig. 4.1. It can been shown that, if we consider just these two contributions, we recover the one-loop and two-loop corrections to Φ_{ab} and an infinite series of contributions computed at all orders in perturbation theory. Nevertheless, we are not taking into account all the infinite series of corrections.

The previous approximations are not yet enough to address the power spectrum computation, since in the RHS of Eq. (4.1) there are the full PS and the full vertex. Hence we further approximate replacing the full vertex with the linear one and using the following formula for the different time power spectrum

$$P_{ab}(k;\eta_a,\eta_b) \simeq G_{ac}(k;\eta_a,0)G_{bd}(k;\eta_b,0)P^0(k)u_c u_d\,, \tag{4.2}$$

where we have considered Gaussian growing mode initial conditions taken from the linear theory.

Next, using the notation adopted by Crocce and Scoccimarro in (1.22), we will call (with abuse of notation) $P_{1Loop}(\mathbf{k};\eta)$ the contribution coming from the first renormalized diagram of Fig. 4.1 and $P_{2Loop}(\mathbf{k};\eta)$ the contribution coming from the

second diagram. Thus one gets

$$\begin{aligned} P_{1Loop}(k;\eta) &= 2\int_0^\eta \mathrm{d}s_1\, e^{s_1}\int_0^\eta \mathrm{d}s_2\, e^{s_2}\int \mathrm{d}^3q\,\big[G(k;\eta,s_1)\gamma(-\mathbf{k},\mathbf{q},\mathbf{k}-\mathbf{q})\bar{G}(q;s_1,0) \\ &\quad\times\bar{G}(|\mathbf{k}-\mathbf{q}|;s_1,0)\big]_a\, P^0(q)P^0(|\mathbf{k}-\mathbf{q}|)\,[G(k;\eta,s_2)\gamma(\mathbf{k},-\mathbf{q},-\mathbf{k}+\mathbf{q}) \\ &\quad\times\bar{G}(q;s_2,0)\bar{G}(|\mathbf{k}-\mathbf{q}|,s_2,0)\big]_b \end{aligned} \tag{4.3}$$

where,

$$\bar{G}_a(k,s) = G_{ab}(k,s)u_b \qquad \text{and} \qquad [G\,\gamma\,\bar{G}\,\bar{G}]_a = G_{ab}\gamma_{bcd}\bar{G}_c\bar{G}_d\,. \tag{4.4}$$

Similarly for density-density component of the power spectrum, namely $P_{11}(k;\eta)$, the second renormalized diagram of Fig. 4.1 gives

$$\begin{aligned} P_{2Loop}(k;\eta) &= 16\int \mathrm{d}^3q\int \mathrm{d}^3p\Lambda_{2Loop}(\mathbf{k},\mathbf{q},\mathbf{p};\eta)\Lambda_{2Loop}(-\mathbf{k},-\mathbf{p},-\mathbf{q};\eta)P^0(q) \\ &\quad\times P^0(p)P^0(|\mathbf{k}-\mathbf{p}-\mathbf{q}|)\,, \end{aligned} \tag{4.5}$$

with

$$\begin{aligned} \Lambda_{2Loop}(\mathbf{k},\mathbf{q},\mathbf{p};\eta) &= \int_0^\eta \mathrm{d}s_1\, e^{s_1}\int_0^{s_1} \mathrm{d}s_2 e^{s_2}G_{1b}(k;\eta,s_1)\gamma(-\mathbf{k},\mathbf{k}-\mathbf{q},\mathbf{q}) \\ &\quad\times G_{cf}(|\mathbf{k}-\mathbf{q}|;s_1,s_2)\bar{G}_d(\mathbf{q};s_1,0)\gamma_{fgh}(\mathbf{q}-\mathbf{k},\mathbf{p},\mathbf{k}-\mathbf{p}-\mathbf{q}) \\ &\quad\times\bar{G}_g(p;s_2,0)\bar{G}_h(|\mathbf{k}-\mathbf{p}-\mathbf{q}|;s_2,0)\,. \end{aligned} \tag{4.6}$$

Finally to compute the equal time power spectrum we consider

$$P_{11}(k;\eta,\eta) \simeq \bar{G}_1(k;\eta,0)\bar{G}_1(k;\eta,0)P^0(k) + P_{1Loop}(k;\eta) + P_{2Loop}(k;\eta)\,. \tag{4.7}$$

Eq. (4.2) gives us the cruder approximation of this calculation, indeed with this choice we are neglecting the mode-mode coupling given by Eq. (2.47), so the $P_{1Loop}(k;\eta)$ and $P_{2Loop}(k;\eta)$ contributions are damped with respect to the non approximated ones.

On the other hand to deal with the propagator we consider the analytical interpolation explained in Section 3.1 of the previous chapter, or rather the analogous

result founded in CS. Actually, in Ref. [25], it has been stated that the propagator needs to be slightly correct considering also further corrections, but the problem has not been addressed satisfactorily.

4.2 Power spectrum from closure theory

In Chapter 2 we introduced the *closure theory* for cosmological perturbation. It gives evolution equations for the power spectrum (2.87,2.88) and for the propagator (2.89). Now we briefly explain the technique elaborated in Ref. [26] in order to deal with the power spectrum evolution equation.

It can been shown that the formal solutions to the closure differential Eqs. (2.87,2.88) for the power spectra are the following

$$\begin{aligned} P_{ab}(k;\eta) &= G_{ac}(k;\eta,0)\, G_{bd}(k;\eta,0)\, P_{cd}(k;0) \\ &\quad + \int_0^\eta d\eta_1 \int_0^\eta d\eta_2\, G_{ac}(k;\eta,\eta_1) G_{bd}(k;\eta,\eta_2) \Phi_{cd}(k;\eta_2,\eta_1)\,, \quad (4.8) \\ P_{ab}(k;\eta,\eta') &= G_{ac}(k;\eta,0)\, G_{bd}(k;\eta',0)\, P_{cd}(k;0) \\ &\quad + \int_0^\eta d\eta_1 \int_0^{\eta'} d\eta_2\, G_{ac}(k;\eta,\eta_1) G_{bd}(k;\eta',\eta_2) \Phi_{cd}(k;\eta_2,\eta_1)\,, \quad (4.9) \end{aligned}$$

where the $\Phi(k;\eta_1,\eta_2)$ function represents the mode-mode coupling between different Fourier modes and it is given by

$$\begin{aligned} \Phi_{ab}(k;\eta_1,\eta_2) = 2 \int d^3\mathbf{q}\, \gamma_{ars}(-\mathbf{k},\mathbf{q},\mathbf{k}-\mathbf{q})\, \gamma_{bpq}(-\mathbf{k},\mathbf{q},\mathbf{k}-\mathbf{q}) \\ \times e^{\eta_1+\eta_2} \Big\{ P_{pr}(q;\eta_1,\eta_2) P_{qs}(|\mathbf{k}-\mathbf{q}|;\eta_1,\eta_2)\, \theta(\eta_1-\eta_2) \\ + P_{rp}(q;\eta_2,\eta_1) P_{sq}(|\mathbf{k}-\mathbf{q}|;\eta_2,\eta_1)\, \theta(\eta_2-\eta_1) \Big\}. \quad (4.10) \end{aligned}$$

The formal expressions (4.8,4.9) is equivalent to that obtained in Chapter 2, namely Eq. (2.47). The differences arises when we consider the functional form of Φ_{ab}, in other words here we gave the explicit expression for this functional. In RPT theory that corresponds to consider the contribution of Φ_{ab} given by the first renormalized diagram of Fig. 4.1 taking the linear vertex instead of the full one. In

this respect, the closure theory gives a recipe to compute the correlation functions with a re-summation scheme but it does not use the quantum field theory language and tools.

At this point, when we consider Eqs. (4.8,4.10,4.9), we are dealing again with formal equations, hence we have to find out a method to address this problem. In this regard, we introduce the Born approximation technique. It consist in applying the iterative approximation scheme to compute Eqs. (4.8,4.9). Therefore the power spectra $P_{ab}(k;\eta)$ and $P_{ab}(k;\eta,\eta')$ are first evaluated (first order Born-approximation) by substituting the linear-order quantities into the RHS of the formal equations. As second step, called second order Born approximation, one repeats the iterative substitution of the leading-order solutions into the RHS on the integral solutions. In principle, this treatment work out a good result insofar the contribution from the mode-mode coupling is small, compared to the first term in the right hand side of integral equations.

To implement the approximation method explained above we consider first the linear initial power spectrum

$$P_{ab}(k;0) = P^0(k)u_a u_b \tag{4.11}$$

where we have assumed Gaussian growing mode initial conditions. So, the different time power spectrum results in

$$P_{ab}(k;\eta,\eta') = P^{(\mathrm{I})}_{ab}(k;\eta,\eta') + P^{(\mathrm{II})}_{ab}(k;\eta,\eta') + \cdots \ ,$$

where

$$\begin{aligned} P^{(\mathrm{I})}_{ab}(k;\eta,\eta') &= \bar{G}_a(k;\eta,0)\bar{G}_b(k;\eta',0)\,P^0(k), \\ P^{(\mathrm{II})}_{ab}(k;\eta,\eta') &= 2\int \mathrm{d}^3\mathbf{q}\, I_a(\mathbf{k},\,\mathbf{q};\eta,\,0)\, I_b(\mathbf{k},\,\mathbf{q};\eta',\,0)\, P^0(q)\, P_0(|\mathbf{k}-\mathbf{q}|). \end{aligned}$$

with, as usual, $\bar{G}_a \equiv G_{a1} + G_{a2}$. Substituting the iterative solutions of different time

P_{ab} into the integral expression (4.8), one obtains

$$P_{ab}(k;\eta) = P_{ab}^{(\mathrm{i})}(k;\eta) + P_{ab}^{(\mathrm{ii})}(k;\eta) + P_{ab}^{(\mathrm{iii})}(k;\eta) + \cdots; \tag{4.12}$$

$$\begin{aligned}
P_{ab}^{(\mathrm{i})}(k;\eta) &= \bar{G}_a(k|\eta,\eta_0)\bar{G}_b(k;\eta,0)e^{2\eta_0}P^0(k), \\
P_{ab}^{(\mathrm{ii})}(k;\eta) &= 2\int \mathrm{d}^3\mathbf{q}\, I_a(\mathbf{k},\,\mathbf{q};\eta,\,0)\, I_b(\mathbf{k},\,\mathbf{q};\eta,\,0)\, P^0(q)\, P_0(|\mathbf{k}-\mathbf{q}|), \\
P_{ab}^{(\mathrm{iii})}(k;\eta) &= 8\int \mathrm{d}^3\mathbf{p}\int \mathrm{d}^3\mathbf{q}\, J_a(\mathbf{k},\mathbf{p},\mathbf{q};\eta,\,0)J_b(\mathbf{k},\,\mathbf{p},\,\mathbf{q};\eta,\,0) \\
&\qquad \times\, P^0(|\mathbf{k}-\mathbf{p}|)P^0(q)P^0(|\mathbf{p}-\mathbf{q}|).
\end{aligned} \tag{4.13}$$

Here, the functions I_a and J_a are respectively given by

$$\begin{aligned}
I_a(\mathbf{k},\,\mathbf{q};\eta,\,0) &= \int_0^\eta d\eta'\, e^{\eta'}\, G_{al}(k;\eta,\eta')\,\gamma_{lrs}(-\mathbf{k},\mathbf{q},\mathbf{k}-\mathbf{q})\,\bar{G}_r(q|\eta',\eta_0)\,\bar{G}_s(|\mathbf{k}-\mathbf{q}|;\eta',0), \\
J_a(\mathbf{k},\,\mathbf{p},\,\mathbf{q};\eta,\,0) &= \int_0^\eta \mathrm{d}\eta_1\, e^{\eta_1} \int_0^\eta \mathrm{d}\eta_2\, e^{\eta_2}\, G_{al}(k;\eta,\eta_1)\,\gamma_{lrs}(-\mathbf{k},\mathbf{p},\mathbf{k}-\mathbf{p})\, G_{rc}(p;\eta_1,\eta_2) \\
&\quad \times\, \gamma_{cpq}(-\mathbf{p},\mathbf{q},\mathbf{p}-\mathbf{q})\,\bar{G}_p(q|;\eta_2,0)\bar{G}_q(|\mathbf{p}-\mathbf{q}|;\eta_2,0)\bar{G}_s(|\mathbf{k}-\mathbf{p}|;\eta_1,0).
\end{aligned} \tag{4.14}$$

Now, the comparison with the Crocce and Scoccimarro computation presented in the previous section becomes straightforward. The $P_{ab}^{(\mathrm{i})}$ and $P_{ab}^{(\mathrm{ii})}$ terms are respectively in one to one correspondence with the $\bar{G}_1(k;\eta,0)\bar{G}_1(k;\eta,0)P^0(k)$ and $P_{1Loop}(k;\eta)$ terms of Eq. (4.7). The differences arise when one considers the $P_{ab}^{(\mathrm{iii})}(k;\eta)$ contribution, it differs from $P_{2Loop}(k;\eta)$ by a factor 2. This is due to the different approach to the problem, indeed here we are dealing with a crude "perturbative" expansion of the formal Eqs. (4.8,4.9), while in the previous section we analyze in a more rigorous way the exact expansion series of the Φ_{ab} function.

Finally, in order to obtain a self consistent approach to the problem, we use for the propagator the analytical result developed in the previous chapter, see Eq. (3.32). However, as in the RPT approach, this propagator should be slightly modified in light of N-body simulations, as argued in Ref. [31].

4.3 Alternative power spectrum computations

The aim of this section is to give some hints about implementations of the multi-point propagators and the re-summed propagator computed in Section (3.4) in order to calculate the nonlinear power spectrum. So far, these results have not been enough developed for this purpose.

4.3.1 Multi-point propagators to address the power spectrum

As we explained in Chapter 2, an alternative way to recast the series of cosmological perturbations is given by the "multi-point propagators" approach. The results on the re-summation of this object, briefly reviewed in Section 3.3, make this approach more attractive, and further analysis on it may be promising. For examples, as mentioned in [30], by means of Eq. (2.63) one can expresses the power spectrum up to one-loop order, getting

$$P(k;\eta) = \left[\Gamma^{(1)}(k;\eta)\right]^2 P^0(k) + 2\int \mathrm{d}^3q \left[\Gamma^2(\mathbf{k}-\mathbf{q},\mathbf{q};\eta)\right]^2 P^0(|\mathbf{k}-\mathbf{q}|)P^0(q)\,. \quad (4.15)$$

Note that RHS terms of Eq. (4.15) are both positive, hence this is an enhance with respect to PT, where we are dealing also with negative terms. Moreover this expression and Eq. (2.47) are equivalent when Φ_{ab} function is computed at the one-loop level and the two-point and three-point propagator are computed taking into account their large-k damping. To find out a method to compare Eq. (2.47) with the perturbative expansion expressed in (2.63) is an important task. Computing higher order contributions to the power spectrum calculation using multi-point propagator approach results worthwhile in order to check the validity of this new formulation.

4.3.2 The re-summing propagator into the re-summed power spectrum and vice versa

Considering the exact formal equations for the power spectrum and the propagator, respectively Eqs. (2.47) and (2.54), it results clearly that the two expressions are mutually dependent. Indeed, when we go beyond the CS propagator taking into account the nonlinear power spectrum, we face this problem (section Section 3.4). Therefore we need to implement a kind of approximation scheme, in order to find out an approximate solution of the integral equations.

What we want to do now is to use the propagator computed in Section 3.4 with the $P_{ab}^{\rm TRG}$ power spectrum and to couple it with an approximated version of Eq. (2.47). As first step, leveraging the RPT results, we consider the contribution of Φ_{ab} given by the first diagram of Fig. 4.1 replacing the full vertex with the linear one. Doing this we are left with the following Φ_{ab} functional form

$$\begin{aligned}\Phi_{ab}(k;s_1,s_2) = 2\int d^3\mathbf{q}\,\gamma_{ars}(-\mathbf{k},\mathbf{q},\mathbf{k}-\mathbf{q})\,\gamma_{bpq}(-\mathbf{k},\mathbf{q},\mathbf{k}-\mathbf{q}) \\ \times e^{s_1+s_2}\Big\{P_{pr}(q;s_1,s_2)P_{qs}(|\mathbf{k}-\mathbf{q}|;\ s_1,s_2)\,\theta(s_1-s_2) \\ +P_{rp}(q;s_2,s_1)P_{sq}(|\mathbf{k}-\mathbf{q}|;s_2,s_1)\,\theta(s_2-s_1)\Big\}. \quad (4.16)\end{aligned}$$

that, as previously mentioned, correspond to the formal results of the closure theory, namely Eq. (4.10). As second step, to be consistent with the nonlinear propagator computation, we replace the different time power spectra of Eq. (4.16) with

$$P_{ab}(q;s_a,s_b) \simeq G^E_{ac}(q;s_a,s_b)P^{\rm TRG}_{cb}(q;s_b,s_b)\theta(s_a-s_b) \quad (4.17)$$

where G^E is the extended nonlinear propagator computed following the guidelines described in Section 3.4.

Here we have extended the previous power spectrum computations taking into account next to leading re-rummations in the propagator computation and considering the approximation (4.17) for the non linear power spectra of Eq. (4.16). An accurate analytical and numerical studies of these insights is needed.

Chapter 5

Propagator evolution equations: numerical implementation

This chapter is dedicated to the numerical solutions of the propagator evolution equations. We shall focus in particular on the detailed study of the features related to the next to leading re-summation scheme presented in Section (3.4). This is done by comparing the behaviors of three different propagators approximations: the CS propagator, the new one computed using the one-loop approximation for the non-linear PS and finally using the TRG PS. Furthermore, to better address this issue we will define the "effective velocity dispersion" related to each propagator.

We investigate a ΛCDM cosmology close to the best-fit model ($\Omega_m = 0.25$, $\Omega_b h^2 = 0.0224$, $h = 0.72$, $n = 0.97$ and $\sigma_8 = 0.8$). The initial time, $\eta = 0$, is taken to correspond to the physical redshift $z_{in} = 100$. At $\eta = 0$ we set the initial conditions for the evolution equation (3.55) and for the TRG equations needed to compute the PS (see 2.6). We set the initial conditions for the PS by matching it with the linear PS obtained by the CAMB code [52]. For the propagator, we use the explicit expression given in Eq. (2.7). The integration of the TRG equations requires also initial values for the bispectra. We set them to zero, *i.e.*, we neglect all non-Gaussianities generated at redshifts higher than $z = 100$.

In Fig. 5.1 we plot our results for the propagators $G_a(k;\, \eta_a, 0)$ defined in Eq. (2.53) (G_1 in the left panel, G_2 in the right panel), computed at final times $\eta(z)$ corre-

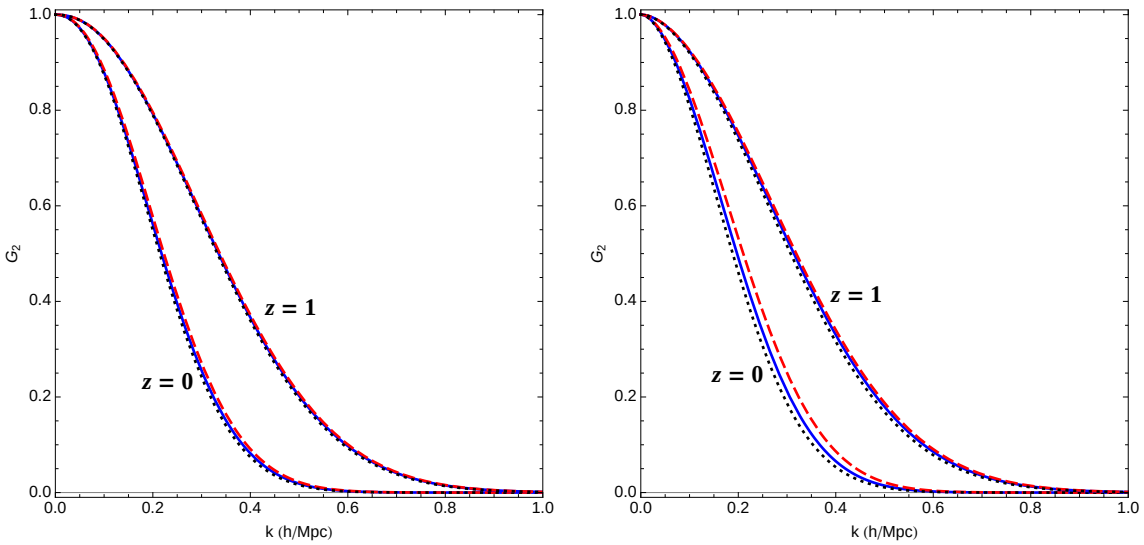

Figure 5.1: The density (left panel) and velocity (right panel) propagators at redshifts $z = 0$ and $z = 1$. The black-dotted lines are the propagator computed in the CS approximation. The purple-dashed lines are obtained using the 1-loop PS in $\tilde{\Sigma}$, while the blue-continuous lines are obtained by using the PS from the TRG.

sponding to redshift $z = 0$ and $z = 1$. The dotted black lines correspond to the Crocce-Scoccimarro result, *i.e.* to the integration of Eq. (3.16), where the linear PS has been used to compute $\Sigma^{(1)}_{ac}$. The dashed red lines are obtained by using the 1-loop approximation for the non-linear PS in $\tilde{\Sigma}_{ac}$, while the continuous blue lines are obtained by using the TRG PS.

In Fig. 5.2 we plot the relative difference between the propagators computed with the two different approximations for the non-linear PS and the one computed in the Crocce-Scoccimarro approximation.

As a general trend, the effect of the inclusion of the new class of diagrams considered in this thesis leads to a weaker damping of the propagators at intermediate and large k's, compared to the one obtained considering only the chain-diagrams of CS. The effect is stronger for the velocity propagator than for the density one.

The computation with the 1-loop PS suffers from an intrinsic uncertainty, due to the dependence on the (UV) momentum cutoff employed in the loop integrals. This is an unavoidabe limitation of the 1-loop approximation, due to the fact that the 1-loop PS takes unphysical negative values at large k's, especially when the two time

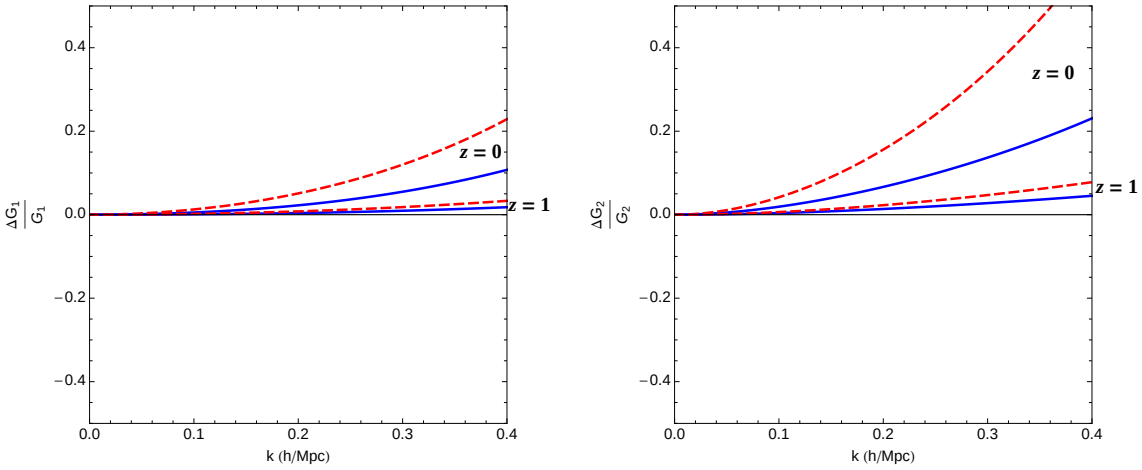

Figure 5.2: Relative differences between the improved propagators and the one obtained in the CS approximation. Line-codes as in Fig. 5.1

arguments are very different. In Fig. 5.3, we show the cutoff dependence by plotting the same quantities as in Fig. 5.2, computed using the 1-loop approximation for the PS and UV cutoffs $q_{\rm max} = 1$ and $2\,$h/Mpc. The cutoff dependence is quite strong for the G_2 propagator, showing that its computation using the 1-loop PS is clearly unreliable at low redshift. On the other hand, the results for $G_{1,2}$ obtained using the PS computed with the TRG, which is always positive, do not exhibit UV problems.

An alternative way to show the effects of our improved approximation is to define an effective velocity dispersion,

$$\sigma^2_{eff,a}(k;\eta,0) = \frac{-2}{k^2(e^\eta-1)^2}\ln(G_a(k;\eta,0))\,, \tag{5.1}$$

which, in the high-k limit, reduces to $\sigma^2_{\rm nl}(\eta,0)$ defined in Eq. (3.48). In figs. 5.4, 5.5, we plot $\sigma^2_{eff,1}$ (on the left) and $\sigma^2_{eff,2}$ (on the right) as a function of k: the line code is the same as in figs. 5.1 and 5.2.

Finally, in figs. 5.6 and 5.7 we plot $\sigma^2_{eff,a}$ as a function of redshift for three fixed values of the momentum: $k = 0.5,\ 0.15,\ 0.001\,$h/Mpc.

Our results show that, for $z \lesssim 2$, the subleading effects neglected in the Crocce-Scoccimarro approximation start to play a relevant role. For the density propagator

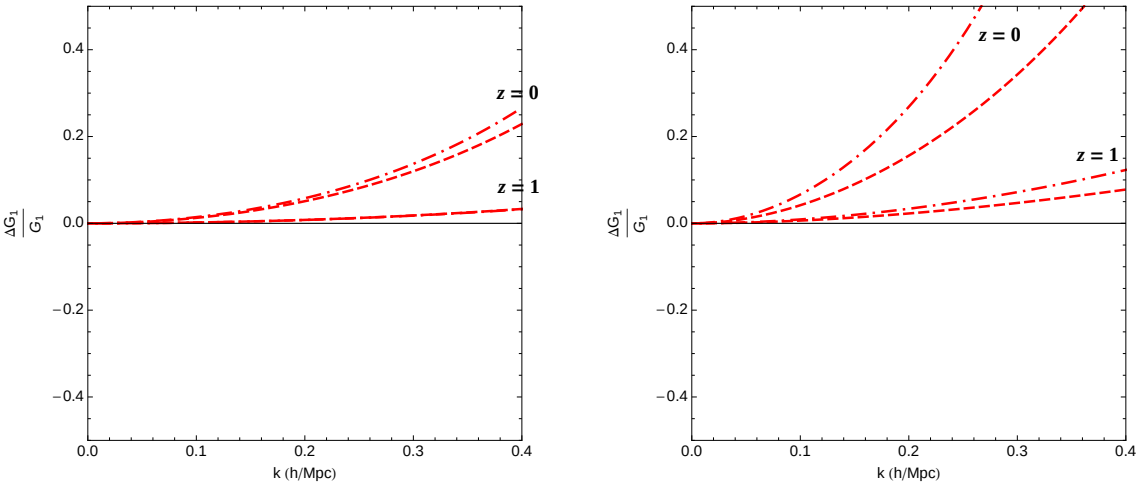

Figure 5.3: The dependence on the UV-cutoff of the improved propagator obtained by using the 1-loop approximation for the non-linear PS. Dashed lines are obtained using $q_{uv} = 1$ h/Mpc^{-1}, while dash-dotted lines are obtained with $q_{uv} = 2$ h/Mpc^{-1}.

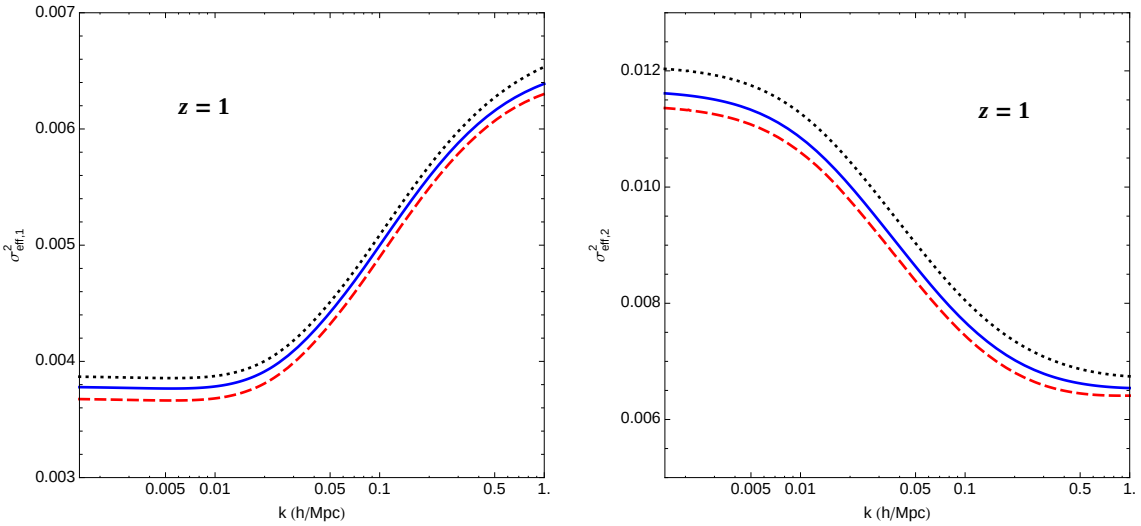

Figure 5.4: $\sigma^2_{eff,a}$ at $z = 1$ computed from G_a (see Eq. 5.1). Line-codes as in Fig. (5.1).

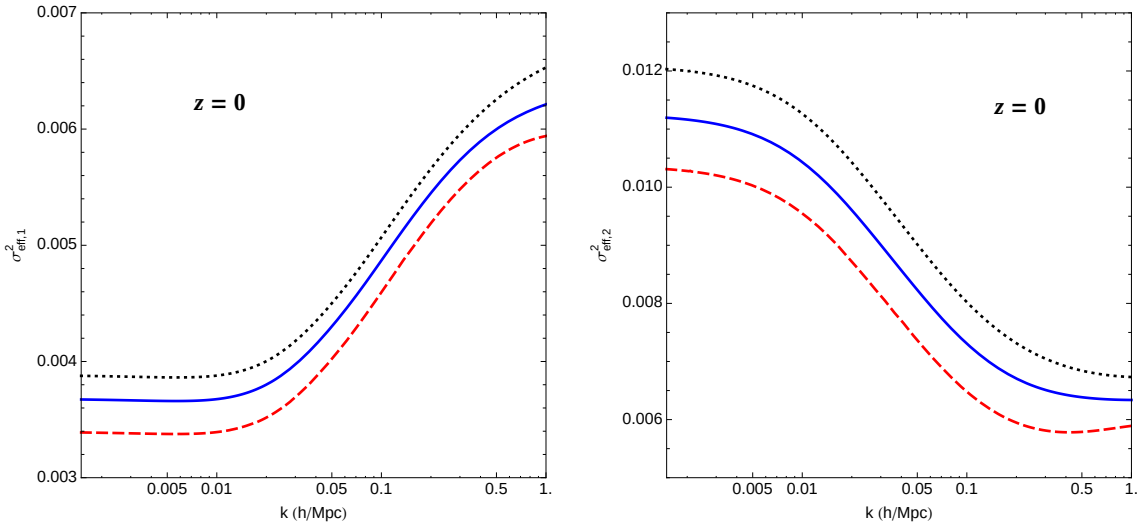

Figure 5.5: The same as Fig. 5.4 but at $z = 0$.

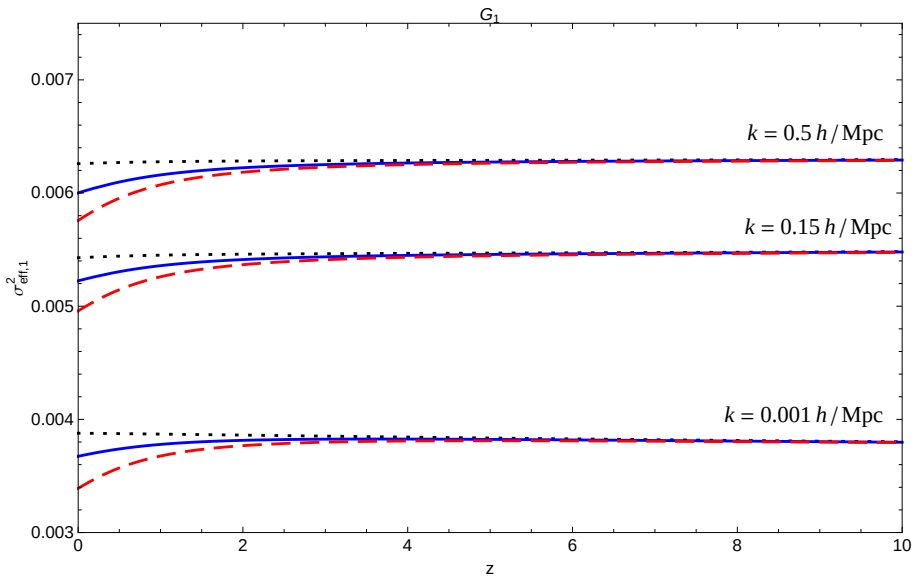

Figure 5.6: $\sigma^2_{eff,1}(z)$ as a function of redshift for three different momentum scales. Line-codes as in Fig. 5.1.

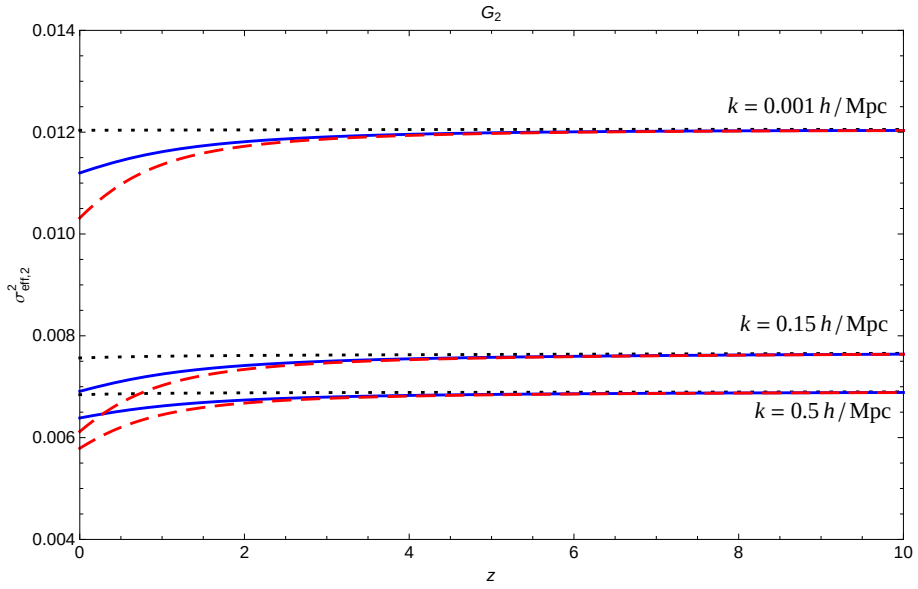

Figure 5.7: Same as Fig. 5.6 for $\sigma^2_{eff,2}(z)$

G_1 they are larger that 1% for $k \geq 0.14\,\mathrm{h/Mpc}$ at $z = 0$ and for $k \geq 0.31\,\mathrm{h/Mpc}$ at $z = 1$. For the velocity propagator G_2 the effect is stronger. It is larger than 1% for $k \geq 0.07\,\mathrm{h/Mpc}$ at $z = 0$ and for $k \geq 0.17\,\mathrm{h/Mpc}$ at $z = 1$. These effects should clearly be taken into account in a computation aiming to reproduce the BAO power spectrum at the percent level. At $k = 0.2\,\mathrm{h/Mpc}$, that is, well inside the BAO range of scales, and at $z = 0$, the deviation from the Crocce-Scoccimarro resummation is 2.2 % for G_1 and 6.7 % for G_2.

The sign of the correction is the same in both approximations considered for the non-linear PS (*i.e.* 1-loop and TRG): the propagators are less damped than the Crocce-Scoccimarro one. This can be easily understood analytically by looking at the difference between Eq. (3.22) and Eq. (3.48). In the former, the large-k damping is modulated, via σ^2, by the linear PS, P^0, while, in the latter, it is modulated by the velocity-velocity component of the non-linear PS, *i.e.* by $P^{\rm nl}_{22}$, see Eq. (3.49). Now, unlike the non-linear density-density PS, $P^{\rm nl}_{11}$, which is enhanced w.r.t. the linear one, $P^{\rm nl}_{22}$ receives negative corrections, and is therefore smaller than P^0 at intermediate and large k's (see, for instance, [28, 32]). As a consequence, we get $\sigma^2_{\rm nl} < \sigma^2$ and therefore a smaller damping at large k. The same trend persists at

smaller k's, as is shown in figs. 5.4 and 5.5.

Chapter 6

Conclusions

In this thesis we present new semi-analytical approaches to cosmological perturbation theory. The aim of this new theoretical implementation is to achieve a well-controlled description of gravitational clustering at nonlinear scale. Most of these methods make use of the *nonlinear propagator*, which is the suitable object that gives us the cross-correlation between the final density, or velocity, perturbations and the initial ones. Being a key ingredient in the computation of observable correlation functions, the prediction of the nonlinear propagator is an important task of these new methods. In the last years, several studies have shown that the nonlinear propagator strongly depends on the scale considered, namely it decays nearly exponentially on nonlinear scales. In this context, the achievement of more accurate prediction becomes more and more important. Such is the main goal of this thesis.

We have extended the computation of the non-linear propagator pioneered in CS, which was based on the resummation of the chain-diagrams at all orders in PT. We have taken into account new contributions, obtained by replacing the linear PS appearing in the chain-diagrams by the non-linear PS. We have proved the remarkable property (see Section3.4), that this wider class of renormalized chain-diagrams can be exactly resummed in the large k limit. In the same spirit of CS, we required that PT is recovered in the $k \to 0$ limit, which implies taking into account diagrams not belonging to the renormalized-chain diagrams class.

The resummation of this extended class of diagrams is greatly simplified by the

use of the time evolution equation for the full propagator, Eq. (3.55). Instead of dealing with a complex diagrammatic analysis, the task is reduced to the solution of a differential equation for the full propagator. The crucial element in this equation is the self-energy $\tilde{\Sigma}_{ab}$. Approximating it with the 1-loop self-energy gives the CS result. On the other hand, the renormalized chain-diagrams resummation is achieved by considering a $\tilde{\Sigma}_{ab}$ which is still formally 1-loop, but with the linear PS replaced by the non-linear one, see Fig. 3.6. We have tested two different approximations for the non-linear PS: the 1-loop approximation, and the result of the TRG evolution [28]. The former gives results that depend sensibly on the UV cutoff in the loop integral. This is to be expected since, at low redshift, the 1-loop PS becomes unreliable, and even negative, al large momenta. On the other hand, the PS from the TRG evolution does not suffer from UV problems. Moreover, as discussed in detail in [28], the solution of the TRG equations for the PS is formally a 1-loop expression, in which the linear PS' are replaced by non-linear ones, and is therefore fully consistent with the spirit of our treatment for the propagator in this thesis.

The numerical results show that the new effects are quite relevant in the BAO scales, where they are in the few percent range at z=0. They should therefore be taken into account in computations of the PS in the BAO range based on the use of renormalized propagators, such as RPT. Indeed, in [25], the effect of next-to leading order corrections to the propagator was advocated in order to reconcile the RPT results on the PS with N-Body simulations. The authors correctly identified the effect of these corrections with a renormalization of the linear PS which, through the quantity σ^2, modulates the Gaussian decay of the propagator at large momentum. However, instead of performing an explicit computation as the one presented in this work, they implemented an ad hoc procedure, by replacing the linear PS with the non-linear one as obtained in the halo model [53, 54]. This is inconsistent, since, by doing so, one is using the density PS, whereas the large-k limit resummation involves the velocity PS, see Eq. (3.47). As a result, the procedure illustrated in [25] leads to a wrong prediction on the sign of the corrections to the CS propagator induced by the subleading corrections.

We stress that our conclusion that the effect of these corrections is to enhance the

propagator w.r.t. the CS result is by no means based on a particular approximation of the non-linear PS. Different choices for the latter may give different results on the *size* of these corrections, but the sign is only determined by the assumption that the non-linear velocity PS is smaller than the linear one, which is verified in all consistent approximations (see, for instance, [28, 32])

A careful reconsideration of the comparison with N-body simulation is therefore needed, both for the density and for the velocity propagators. Should the discrepancy mentioned in [28, 25] persist, it would imply that other effects should be taken into account. One possibility would be to include diagrams not belonging to the renormalized chain class. At 2-loop order, it would mean to include diagrams VII, VIII, and IX in Fig. 3.9 also at large k. Notice that these contributions do not exponentiate in the large-k limit or, equivalently, they break the factorization property of Eq. (3.4) and, consequently, they give a propagator which deviates from the gaussian decay form found by CS at large k. Another possible reason for the discrepancy could be the effect of small scale non-linearities, which translates in a non-vanishing velocity dispersion at intermediate scales see, for instance, [55]. The inclusion of this effect in the computation of the (resummed) propagator will be analyzed elsewhere.

Finally we propose a method to implement the power spectrum computation taking into account this new results on the propagator. To this end further analysis and comparison with numerical simulations are necessary and will be subject of future work.

Bibliography

[1] E. Komatsu et al. Seven-Year Wilkinson Microwave Anisotropy Probe (WMAP) Observations: Cosmological Interpretation. *Astrophys. J. Supp.*, 192:18, 2011, 1001.4538.

[2] F. Bernardeau, S. Colombi, E. Gaztanaga, and R. Scoccimarro. Large-scale structure of the universe and cosmological perturbation theory. *Phys. Rept.*, 367:1–248, 2002, astro-ph/0112551.

[3] A. J. S. Hamilton. Formulae for Growth Factors In Expanding Universes Containing Matter and a Cosmological Constant. *Mon. Not. Roy. Astron. Soc.*, 322:419, 2001, astro-ph/0006089.

[4] M. H. Goroff, Benjamin Grinstein, S. J. Rey, and Mark B. Wise. Coupling of Modes of Cosmological Mass Density Fluctuations. *Astrophys. J.*, 311:6–14, 1986.

[5] Bhuvnesh Jain and Edmund Bertschinger. Second order power spectrum and nonlinear evolution at high redshift. *Astrophys. J.*, 431:495, 1994, astro-ph/9311070.

[6] Roman Scoccimarro et al. Nonlinear evolution of the bispectrum of cosmological perturbations. *Astrophys. J.*, 496:586, 1998, astro-ph/9704075.

[7] Sean M. Carroll, William H. Press, and Edwin L. Turner. The Cosmological constant. *Ann. Rev. Astron. Astrophys.*, 30:499–542, 1992.

[8] James N. Fry. The Galaxy correlation hierarchy in perturbation theory. *Astrophys. J.*, 279:499–510, 1984.

[9] Roman Scoccimarro and Joshua Frieman. Loop Corrections in Non-Linear Cosmological Perturbation Theory. *Astrophys. J. Suppl.*, 105:37, 1996, astro-ph/9509047.

[10] R. Juszkiewicz. On the evolution of cosmological adiabatic perturbations in the weakly non-linear regime. *Mon. Not. Roy. Astron. Soc.*, 197:931–940, December 1981.

[11] E. T. Vishniac. Why weakly non-linear effects are small in a zero-pressure cosmology. *Mon. Not. Roy. Astron. Soc.*, 203:345–349, April 1983.

[12] R. Juszkiewicz, D. H. Sonoda, and J. D. Barrow. Non-linear gravitational clustering. *Mon. Not. Roy. Astron. Soc.*, 209:139–144, July 1984.

[13] P. Coles. Second-order evolution of cold dark matter perturbations. *Mon.Not.Roy.Astron.Soc.*, 243:171–176, 1990.

[14] Yasushi Suto and Misao Sasaki. Quasi nonlinear theory of cosmological self-gravitating systems. *Phys.Rev.Lett.*, 66:264–267, 1991.

[15] Nobuyoshi Makino, Misao Sasaki, and Yasushi Suto. Analytic approach to the perturbative expansion of nonlinear gravitational fluctuations in cosmological density and velocity fields. *Phys.Rev.*, D46:585–602, 1992.

[16] C. M. Baugh and G. Efstathiou. A Comparison of the Evolution of Density Fields in Perturbation Theory and Numerical Simulations - Part One - Nonlinear Evolution of the Power Spectrum. *Mon. Not. Roy. Astron. Soc.*, 270:183–+, September 1994.

[17] E. L. Lokas, R. Juszkiewicz, F. R. Bouchet, and E. Hivon. Previrialization: Perturbative and N-Body Results. *Astrophys. J.*, 467:1–+, August 1996, arXiv:astro-ph/9508032.

[18] Roman Scoccimarro and Josh Frieman. Loop corrections in nonlinear cosmological perturbation theory 2. Two point statistics and selfsimilarity. *Astrophys.J.*, 473:620, 1996, astro-ph/9602070.

[19] James N. Fry. The Minimal power spectrum: Higher order contributions. *Astrophys. J.*, 421:21–26, 1994.

[20] Martin Crocce and Roman Scoccimarro. Renormalized Cosmological Perturbation Theory. *Phys. Rev.*, D73:063519, 2006, astro-ph/0509418.

[21] P. Valageas. Large-N expansions applied to gravitational clustering. *Astronomy and Astrophysics*, 465:725–747, April 2007, arXiv:astro-ph/0611849.

[22] Patrick McDonald. Dark matter clustering: a simple renormalization group approach. *Phys. Rev.*, D75:043514, 2007, astro-ph/0606028.

[23] Sabino Matarrese and Massimo Pietroni. Baryonic acoustic oscillations via the renormalization group. *Mod. Phys. Lett.*, A23:25–32, 2008, astro-ph/0702653.

[24] Sabino Matarrese and Massimo Pietroni. Resumming Cosmic Perturbations. *JCAP*, 0706:026, 2007, astro-ph/0703563.

[25] Martin Crocce and Roman Scoccimarro. Nonlinear Evolution of Baryon Acoustic Oscillations. *Phys. Rev.*, D77:023533, 2008, 0704.2783.

[26] Atsushi Taruya and Takashi Hiramatsu. A Closure Theory for Non-linear Evolution of Cosmological Power Spectra. *ApJ*, 674:617–635, 2008, 0708.1367.

[27] Takahiko Matsubara. Resumming Cosmological Perturbations via the Lagrangian Picture: One-loop Results in Real Space and in Redshift Space. *Phys. Rev.*, D77:063530, 2008, 0711.2521.

[28] Massimo Pietroni. Flowing with Time: a New Approach to Nonlinear Cosmological Perturbations. *JCAP*, 0810:036, 2008, 0806.0971.

[29] Takahiko Matsubara. Nonlinear perturbation theory with halo bias and redshift- space distortions via the Lagrangian picture. *Phys. Rev.*, D78:083519, 2008, 0807.1733.

[30] Francis Bernardeau, Martin Crocce, and Roman Scoccimarro. Multi-Point Propagators in Cosmological Gravitational Instability. *Phys. Rev.*, D78:103521, 2008, 0806.2334.

[31] Atsushi Taruya, Takahiro Nishimichi, Shun Saito, and Takashi Hiramatsu. Nonlinear Evolution of Baryon Acoustic Oscillations from Improved Perturbation Theory in Real and Redshift Spaces. *Phys. Rev.*, D80:123503, 2009, 0906.0507.

[32] Takashi Hiramatsu and Atsushi Taruya. Chasing the non-linear evolution of matter power spectrum with numerical resummation method: solution of closure equations. *Phys. Rev.*, D79:103526, 2009, 0902.3772.

[33] Atsushi Taruya, Takahiro Nishimichi, and Shun Saito. Baryon Acoustic Oscillations in 2D: Modeling Redshift- space Power Spectrum from Perturbation Theory. *Phys. Rev.*, D82:063522, 2010, 1006.0699.

[34] Francis Bernardeau, Martin Crocce, and Emiliano Sefusatti. Multi-Point Propagators for Non-Gaussian Initial Conditions. *Phys. Rev.*, D82:083507, 2010, 1006.4656.

[35] Patrick Valageas and Takahiro Nishimichi. Combining perturbation theories with halo models. 2010, 1009.0597.

[36] Anna Elia, Suchita Kulkarni, Cristiano Porciani, Massimo Pietroni, and Sabino Matarrese. Modeling the clustering of dark-matter haloes in resummed perturbation theories. 2010, 1012.4833.

[37] Keisuke Izumi and Jiro Soda. Renormalized Newtonian Cosmic Evolution with Primordial Non-Gaussanity. *Phys. Rev.*, D76:083517, 2007, 0706.1604.

[38] R. Penco and D. Mauro. Perturbation theory via Feynman diagrams in classical mechanics. *Eur. J. Phys.*, 27:1241–1250, 2006, hep-th/0605061.

[39] Martin Crocce and Roman Scoccimarro. Memory of Initial Conditions in Gravitational Clustering. *Phys. Rev.*, D73:063520, 2006, astro-ph/0509419.

[40] F. R. Bouchet, R. Juszkiewicz, S. Colombi, and R. Pellat. Weakly nonlinear gravitational instability for arbitrary Omega. *Astrophys. J.*, 394:L5, 1992.

[41] Francis Bernardeau. Skewness and Kurtosis in large scale cosmic fields. *Astrophys. J.*, 433:1, 1994, astro-ph/9312026.

[42] Jordan Carlson, Martin White, and Nikhil Padmanabhan. A critical look at cosmological perturbation theory techniques. *Phys. Rev.*, D80:043531, 2009, 0905.0479.

[43] Beth A. Reid et al. Baryon Acoustic Oscillations in the Sloan Digital Sky Survey Data Release 7 Galaxy Sample. *Mon. Not. Roy. Astron. Soc.*, 401:2148–2168, 2010, 0907.1660.

[44] Eyal A. Kazin et al. The Baryonic Acoustic Feature and Large-Scale Clustering in the SDSS LRG Sample. *Astrophys. J.*, 710:1444–1461, 2010, 0908.2598.

[45] D. N. Spergel et al. Wilkinson Microwave Anisotropy Probe (WMAP) three year results: Implications for cosmology. *Astrophys. J. Suppl.*, 170:377, 2007, astro-ph/0603449.

[46] Takahiro Nishimichi et al. Modeling Nonlinear Evolution of Baryon Acoustic Oscillations: Convergence Regime of N-body Simulations and Analytic Models. 2008, 0810.0813.

[47] J. Lesgourgues, S. Matarrese, M. Pietroni, and A. Riotto. Non-linear Power Spectrum including Massive Neutrinos: the Time-RG Flow Approach. *JCAP*, 0906:017, 2009, 0901.4550.

[48] F. Saracco, M. Pietroni, N. Tetradis, V. Pettorino, and G. Robbers. Non-linear Matter Spectra in Coupled Quintessence. *Phys. Rev.*, D82:023528, 2010, 0911.5396.

[49] N. Brouzakis, V. Pettorino, N. Tetradis, and C. Wetterich. Nonlinear matter spectra in growing neutrino quintessence. 2010, 1012.5255.

[50] N. Brouzakis and N. Tetradis. Non-linear Matter Spectrum for a Variable Equation of State. *JCAP*, 1101:024, 2011, 1002.3277.

[51] Nicola Bartolo, J. P. Beltran Almeida, Sabino Matarrese, Massimo Pietroni, and Antonio Riotto. Signatures of Primordial non-Gaussianities in the Matter Power-Spectrum and Bispectrum: the Time-RG Approach. *JCAP*, 1003:011, 2010, 0912.4276.

[52] Antony Lewis, Anthony Challinor, and Anthony Lasenby. Efficient computation of CMB anisotropies in closed FRW models. *Astrophys. J.*, 538:473–476, 2000, astro-ph/9911177.

[53] R. J. Scherrer and E. Bertschinger. Statistics of primordial density perturbations from discrete seed masses. *Astrophys. J.*, 381:349–360, November 1991.

[54] Asantha Cooray and Ravi K. Sheth. Halo models of large scale structure. *Phys. Rept.*, 372:1–129, 2002, astro-ph/0206508.

[55] Daniel Baumann, Alberto Nicolis, Leonardo Senatore, and Matias Zaldarriaga. Cosmological Non-Linearities as an Effective Fluid. 2010, 1004.2488.